EEFIT PROJECT REPORT

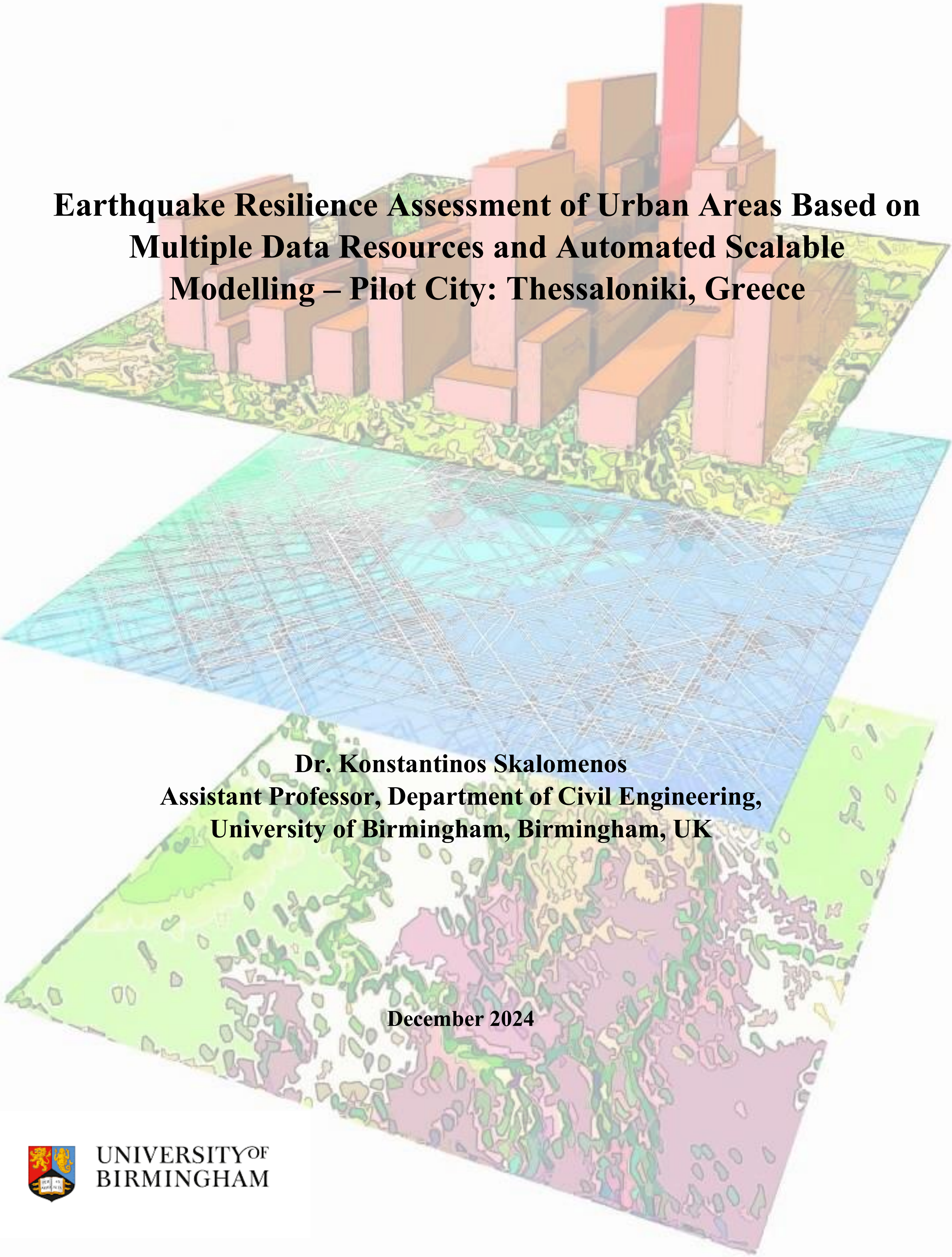

Earthquake Resilience Assessment of Urban Areas Based on Multiple Data Resources and Automated Scalable Modelling – Pilot City: Thessaloniki, Greece

Dr. Konstantinos Skalomenos
Assistant Professor, Department of Civil Engineering,
University of Birmingham, Birmingham, UK

December 2024

ACKNOWLEDGEMENTS

The author would like to thank his students for their commitment to their research work, fresh ideas and enthusiasm throughout the project. The author is also grateful to the project's international partners in Greece and China and to the funder of this research grant, the Earthquake Engineering Field Investigation Team (EEFIT), UK. The names and affiliations of those who were involved in the project and contributed to its completion are listed below:

MSc Graduates:

Mr. Panagiotis-Marios Stathis, School of Science and Technology, Hellenic Open University, Greece

Ms. Holta Shkurti, Department of Civil Engineering, University of Birmingham, UK

Mr. Rory Nicholls, Department of Civil Engineering, University of Birmingham, UK

Ms. Xiaori Zhou, Department of Civil Engineering, University of Birmingham, UK

Mr. Li Zeqin, Department of Civil Engineering, University of Birmingham, UK

International Partners:

Dr. Xuchuan Lin, Professor, Institute of Engineering Mechanics, China Earthquake Administration, Harbin, China

Dr. Nikolaos Theodoulidis, Research Director, Institute of Engineering Seismology and Earthquake Engineering - Earthquake Planning and Protection Organization of Greece (ITSAK – EPPO)

Dr. Vassilios Lekidis, Senior Researcher, Institute of Engineering Seismology and Earthquake Engineering - Earthquake Planning and Protection Organization of Greece (ITSAK – EPPO)

Dr. Konstantinos Morfidis, Researcher, Institute of Engineering Seismology and Earthquake Engineering - Earthquake Planning and Protection Organization of Greece (ITSAK – EPPO)

Funder:

Earthquake Engineering Field Investigation Team (EEFIT), The Institution of Structural Engineers, UK

CONTENTS

LIST OF FIGURES

LIST OF TABLES

ABSTRACT

This research programme analysed the seismic performance of an ageing building stock in central Thessaloniki, northern Greece, to improve understanding of expected earthquake damage at the city scale. A city-wide seismic simulation platform was developed for application to Greek cities. The platform generates a digital damage model of the target building stock through macroscopic nonlinear time-history analysis. A validated city-wide model of 1,252 buildings was developed and assessed under frequent, design-basis and rare earthquake scenarios. The calculated damage index for each building was visualised in a three-dimensional city model. For each scenario, the study estimated the loss of functionality in terms of structural damage and financial loss. Although the building stock performs satisfactorily under the design-basis scenario, extensive damage and an instantaneous functionality loss exceeding 50% are expected under the rare-event scenario. City-level resilience curves were developed to represent the initial functionality loss and the time required to restore pre-earthquake functionality. The time required to demolish unsafe buildings, clear construction and demolition waste, and complete repair and reconstruction was also estimated. Repair works can be completed in about two years for the frequent-event scenario, whereas the design-basis and rare-event scenarios require substantial mobilisation of labour and construction-sector capacity to avoid prolonged recovery. A pre-earthquake retrofitting programme was also evaluated and found to be financially viable when targeted at the most vulnerable buildings. The proposed methodology provides engineers and decision-makers with a practical framework for rapid city-scale assessment of ageing building stocks, helping them prioritise interventions that reduce damage and accelerate recovery.

Keywords

YouSimulator, urban seismic resilience, 3D physics-based numerical modelling, digital technologies, RC building stocks, resilience curves

1 Introduction

1.1 Background

Natural hazards have shaped human experience throughout history, and efforts to reduce their consequences have driven advances in engineering. A natural hazard becomes a disaster when it causes loss of life or serious disruption to communities, infrastructure and economic activity. In earthquake engineering, vulnerability describes the susceptibility of structures, infrastructure and communities to damage from seismic hazards.

Earthquakes are among the most destructive natural hazards, causing substantial loss of life and economic damage (House and Wallemacq, 2018). Their consequences depend on two broad groups of factors: earthquake-related characteristics, including geology, magnitude, epicentral distance and focal depth; and characteristics of the affected area, including building performance, population density and response capacity (Hansapinyo et al., 2020). Urbanisation can intensify these consequences by concentrating people and assets, particularly in seismically active regions. Seismic building performance and effective emergency-response measures are therefore central to urban resilience.

Given the potentially severe consequences of earthquakes, effective disaster-prevention and risk-reduction strategies are essential. Seismic simulation modelling (SSM) supports urban-resilience assessment by integrating geospatial information, building characteristics and ground-motion data in deterministic or probabilistic analyses (Hansapinyo et al., 2020; Cimellaro et al., 2017). The resulting city-scale simulations can identify vulnerable buildings and areas, support prioritised interventions, and help reduce functionality loss, recovery time and associated socioeconomic impacts.

This report employs the urban earthquake disaster simulator YouSimulator (Lin et al., 2019; Lin et al., 2020; Chen et al., 2022) to analyse the seismic performance of buildings in Thessaloniki, Greece, at the city scale. Thessaloniki has high seismic exposure and was struck by an Mw 6.5 earthquake in 1978, which has been the subject of extensive post-earthquake and microzonation studies (Panou et al., 2014). The predictions of YouSimulator can be assessed against empirical damage data and analytical studies reported by Kappos et al. (2013) and Panou et al. (2014). These databases can be updated and verified using geographic information system (GIS) tools, including ArcMap (ESRI, 2022), together with visual checks using Google Maps.

The proposed methodology quantifies the functional integrity of an urban building stock. YouSimulator generates a virtual damage model through macroscopic nonlinear time-history analysis using simplified multi-spring shear models. Each building is represented by a code-based trilinear capacity curve derived from its design characteristics. Damage data collected after the 1978 Thessaloniki earthquake are compared with the simulated results, and the model parameters can be adjusted where further calibration is required (Panou et al., 2014). A digital model of 1,252 buildings is then used to calculate the damage index of each building under frequent, design-basis and rare earthquake scenarios. ParaView (Squillacote et al., 2007) is used to visualise the resulting distribution of damage across the study area.

A city-wide generalised damage index is proposed to account for slightly, moderately and heavily damaged buildings, together with collapsed buildings. The report also estimates functionality loss, financial loss, repair and retrofitting costs, recovery time, construction and demolition waste, and debris-clearance time. These quantities are used to construct resilience curves that describe the response and recovery of the study-area building stock. The proposed virtual model provides engineers and decision-makers with a practical framework for rapid city-scale assessment, supporting the prioritisation of interventions that reduce damage and accelerate recovery.

1.2 Seismic vulnerability of the city of Thessaloniki

The need to limit and recover from the societal and economic damage caused by strong earthquakes has led to the development of methods that quantify seismic risk and support recovery planning.

According to Pitilakis (2010), reducing the vulnerability of infrastructure is one of the principal means of reducing seismic risk because vulnerability can be altered through improved design, construction, maintenance and retrofitting. Responsibility for these actions rests with the state and its competent authorities, including the Earthquake Planning and Protection Organization (EPPO) in Greece.

Makropoulos (2010) expresses seismic risk as a function of seismic hazard, vulnerability and the value of exposed assets. In urban environments, exposure is a broader and more useful metric because it includes population, resources at risk and asset value (Alexoudi et al., 2007; Proag, 2014; Banica et al., 2017). Seismic hazard is spatially variable and is governed by regional tectonics. Greece's geomorphology and complex seismotectonic setting make it one of Europe's most seismically active regions (Goldsworthy et al., 2002; Tsapanos, 2008). Costa et al. (2007) related the seismicity of the wider Thessaloniki region to the westward, counter-clockwise extrusion of the Anatolian block relative to Eurasia and the Aegean plate. Exposure continues to increase through population growth, urbanisation and economic interdependence. As Greece's second-largest city (ELSTAT, 2022b), Thessaloniki may therefore experience substantial societal and economic consequences from a major earthquake, including cascading effects on trade and infrastructure networks (Oliveira et al., 2014).

Vulnerability and its reduction are central to seismic-risk management and closely linked to resilience. Vulnerability studies identify the weaknesses and sensitivities of systems so that interventions can reduce functionality loss and recovery time (Makropoulos, 2010). Frerks et al. (2011) describe vulnerability as multifaceted, extending beyond physical and economic dimensions to include social, environmental and political factors; this broader view is also supported by Barbat et al. (2010) and Oliveira et al. (2014). Joshi et al. (2014) similarly interpret vulnerability as the susceptibility of a system, considering its physical, economic, social, environmental and political capacity to anticipate, cope with, resist and recover from a seismic event. Accordingly, vulnerability reduction is treated as a principal mechanism for reducing seismic risk in this report.

1.3 Seismic simulation modelling

In large urban centres, the exposure of buildings, transport and utility networks, and populations to seismic hazards can have major societal, environmental and economic consequences.

Over the past three decades, numerous numerical models and methods have been developed to simulate and estimate seismic losses in urban environments. These approaches can be divided broadly into data-driven models, which use existing damage databases, and physics-driven models, which simulate the structural response of buildings. Data-driven models use recorded earthquake damage and probabilistic methods to estimate losses under future scenarios. Physics-driven models address several limitations of these approaches, including the difficulty of assessing areas without strong-earthquake records and the dependence of building response on construction characteristics and ground-motion frequency content (Lu and Guan, 2017).

For these reasons, substantial progress has been made in physics-based simulation of buildings at the city scale. Current analytical approaches include capacity-spectrum methods (FEMA, 2022; Kappos et al., 2006) and multi-degree-of-freedom models subjected to nonlinear time-history analysis (Hori, 2011; Lu et al., 2014), as discussed below.

1.4 City simulation models using multi-degree-of-freedom oscillators

Inelastic dynamic time-history analysis using appropriately parameterised multi-degree-of-freedom (MDOF) models is one of the most reliable methods for evaluating building response at the city scale. Compared with equivalent single-degree-of-freedom capacity-spectrum methods, MDOF models can represent higher-mode effects and account for the frequency content and duration of seismic excitation. Their main disadvantage is computational demand: city-scale applications may require the analysis of thousands of buildings over tens of thousands of time steps.

Hori (2011) proposed an integrated system for dynamic simulation of buildings under seismic excitation. Subsequent studies developed simplified MDOF models that are less computationally demanding than detailed finite-element models while still providing reliable estimates of inter-storey drift ratio (IDR), a principal indicator of building damage (Xiong et al., 2016, 2017; Lin et al., 2019). One of the simplest and most robust approaches for buildings of up to approximately 10 storeys is the multi-storey shear-building model (Xiong et al., 2017; Lin et al., 2019). It can represent the inelastic behaviour of reinforced-concrete (RC) and load-bearing masonry buildings and estimate damage at individual storeys using mechanical parameters derived from analytical or experimental models for each building typology. The principal modelling assumptions are as follows:

1. The mass of each storey is lumped at floor level.

2. Buildings are represented as shear-type systems.

3. The model is most suitable for buildings that are regular in plan.

4. Storey mass and stiffness are assumed to be uniform over the building height.

5. The mechanical behaviour of each storey is represented by a trilinear backbone curve.

1.5 HAZUS methodology for seismic risk assessment

The HAZUS methodology (FEMA, 2022) integrates data and analytical procedures to estimate physical damage, operational losses and economic impacts caused by earthquakes. Development began in 1993, and the first version of the software was completed in 1997.

Although HAZUS was developed primarily for use in the United States, its underlying methodology can be applied elsewhere when adequate data are available to characterise local building vulnerability and seismic demand.

Estimating building damage requires information on ground motion and potential ground-failure mechanisms in the study area. HAZUS uses the resulting damage estimates to quantify direct physical and economic losses, repair time, casualties, displacement and short-term shelter demand.

In the HAZUS capacity-spectrum approach, building capacity curves are transformed into spectral coordinates and compared with the seismic demand spectrum. The intersection of capacity and demand provides an estimate of structural performance for the specified ground motion.

HAZUS classifies building components into three broad categories:

A. Structural components sensitive to inter-storey drift

B. Non-structural components sensitive to inter-storey drift

C. Non-structural components sensitive to acceleration

For each category, four damage states are defined:

i. Slight damage: Initial cracking occurs in the most vulnerable structural and non-structural components, together with minor acceleration-sensitive damage.
ii. Moderate damage: Cracking is evident in a substantial part of the structure, some members may have yielded, and significant repairs are required.
iii. Extensive damage: Several structural members have exhausted their resistance, partial collapse may occur, and repair costs are high.
iv. Complete damage: The structure has collapsed or is in an unstable condition and can no longer carry additional load; the damage is considered irreversible.

HAZUS defines the median and logarithmic dispersion of the damage-state distributions in terms of IDR for drift-sensitive components and spectral acceleration, Sa, for acceleration-sensitive components. Values are tabulated by building typology and seismic design level: pre-code, low-code, moderate-code and high-code.

1.6 Structure of the report

Chapter 1 reviews damage data from the 1978 Thessaloniki earthquake (Panou et al., 2014), mechanical characteristics of existing RC buildings in Greece (Kappos et al., 2006), the HAZUS methodology for vulnerability assessment (FEMA, 2022), and the concepts underlying seismic resilience curves (Bruneau et al., 2022).

Chapter 2 reviews the concept of urban resilience and presents a method for quantifying the instantaneous loss of functionality at the city scale. The method is illustrated using data from the Mw 6.1 Ludian earthquake in Yunnan Province, China (Shchukin and Skalomenos, 2022).

Chapters 3 and 4 describe the theoretical basis of YouSimulator (Lin et al., 2019, 2020; Chen et al., 2022) and the development of the city-scale model for Thessaloniki.

Chapter 5 presents the computational analyses used to develop and validate the virtual damage model for the RC building stock in central Thessaloniki.

Chapter 6 evaluates city-level losses in terms of lateral load-bearing capacity, repair and retrofitting costs, construction and demolition waste, and recovery time. These results are used to construct seismic resilience curves and assess the effects of the three earthquake scenarios on the resilience of the study-area building stock.

Finally, Chapters 7 and 8 present the conclusions and recommendations for future research, respectively.

2 Urban seismic resilience

This chapter reviews the concept of urban seismic resilience and the principal complexities identified in the literature. It presents a method for quantifying the instantaneous loss of functionality at the city scale and using this quantity to construct a resilience curve. The method is illustrated using data from the Mw 6.1 Ludian earthquake in Yunnan Province, China (Shchukin and Skalomenos, 2022).

2.1 Urban seismic resilience concept

According to Lu et al. (2014), a city is a complex system comprising many interacting subsystems. These include tangible assets, such as buildings, infrastructure, transport and utility networks, and intangible dimensions, such as social, economic and environmental functions. Describing the resilience of such a system with a single indicator is therefore challenging. Most quantitative studies focus on individual urban subsystems, such as buildings or networks, and on a single hazard type, such as earthquakes.

Bruneau et al. (2003) describe seismic resilience as the ability of a region or society to cope with seismic hazards and resist their disruptive effects. Although urban resilience has become an increasingly important concept, reviews by Meerow et al. (2016) and Amirzadeh et al. (2022) identify continuing ambiguity in definitions and assessment methods. Arendt et al. (2016) interpret resilience as the ability of a system to respond to and recover from a disaster, while Bruneau and Reinhorn (2006) broaden the concept to include reductions in structural damage, socioeconomic losses, casualties, failure probability and recovery time. In this report, vulnerability reduction is considered through two complementary strategies: prevention, which reduces the initial functionality loss, and recovery, which shortens the time required to restore functionality.

Prevention is achieved by addressing known weaknesses, particularly vulnerable buildings, because building robustness has a major influence on physical or “hard” resilience (Mastroberti et al., 2018; Bruneau et al., 2022). Recovery estimates are more uncertain because they depend on damage severity, societal behaviour, access to resources and governance constraints (Rofooei et al., 2021; Mastroberti et al., 2018). This report examines the relationship between building damage and functionality loss and provides simplified recovery estimates. More detailed future studies could use component-based methods such as FEMA P-58 (FEMA, 2018).

This report introduces a method for quantifying the instantaneous functionality loss of a building stock at the city scale and for using this quantity to construct a seismic resilience curve (Figure 1).

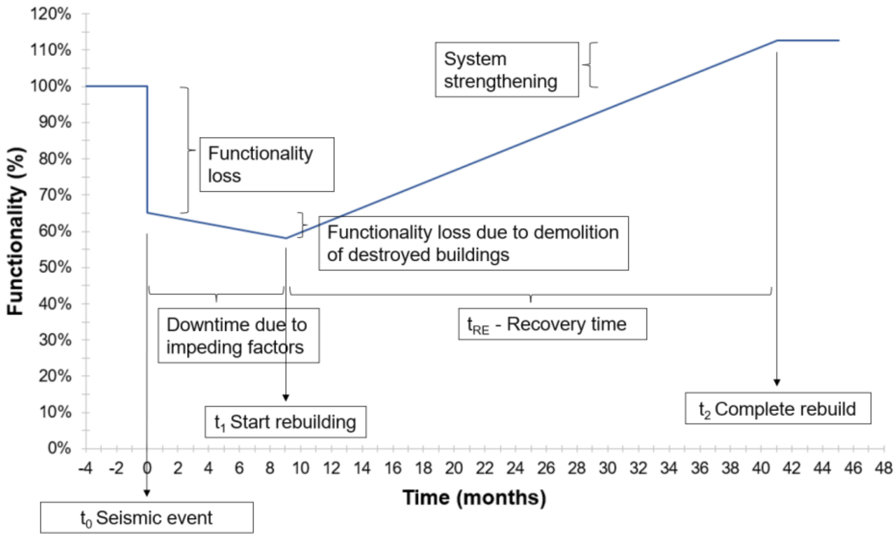

Figure 1: Generalised seismic resilience curve (adapted from Bruneau et al., 2022).

The area under the functionality curve between t0 and t2 represents the magnitude of resilience, R, and is mathematically expressed as:

$$R = \int_{t_0}^{t_2} [100 - Q(t)] \, dt$$

where Q(t) is the percentage functionality, ranging from 0% (total loss) to 100% (initial pre-earthquake functionality).

t_0 is the time at which the seismic event occurs and the sudden loss of functionality begins.

t_1 is the time at which repair and retrofitting activities begin.

t_2 is the time at which functionality has been restored to its target level, which may be lower than, equal to or higher than the pre-earthquake level.

t_{RE} is the total recovery time.

For an urban building stock, functionality loss can be represented in terms of reduced lateral load-bearing capacity or economic value, such as repair and retrofitting cost (Bruneau et al., 2022). Urban seismic resilience is therefore closely linked to building damage and vulnerability. Even when vulnerability is assessed reliably, however, the development of resilience curves involves substantial uncertainty because repair cost and duration depend on damage to both structural and non-structural components. Tools such as PACT and REDi, together with FEMA P-58 methodologies (FEMA, 2018; USRC, 2019), can estimate these effects for individual buildings, but aggregating thousands of building-level results into a city-scale recovery curve remains challenging.

Methods that account for available labour have been proposed to estimate city recovery time (Xiong et al., 2016), but many other factors can cause delays. These include restricted access caused by building collapse, debris clearance, damage to transport networks, interruptions to water and energy supplies, insufficient funding, decisions by building owners and the effectiveness of public administration.

The complexity of recovery is illustrated by Christchurch, New Zealand. Thirteen years after the Mw 6.3 earthquake of 2011, parts of the city had still not fully recovered to pre-earthquake functionality. Although critical infrastructure, including hospitals, utilities and road access, remained operational, severe damage to central-city buildings left the urban core largely non-functional for an extended period while damage assessment, demolition, safety measures and reconstruction were undertaken.

The disruption of central-city functionality caused broader delays in disaster management and led to demolition and reconstruction programmes lasting several years (Bruneau and MacRae, 2017). This example demonstrates that restoring transport, water, energy, telecommunications and health infrastructure is necessary but not sufficient for rapid recovery of overall urban functionality.

2.2 Seismic resilience curve estimation method at city level

Shchukin and Skalomenos (2022) collected data, with support from the Institute of Engineering Mechanics, China Earthquake Administration, for Longtoushan Township, which was severely affected by the Mw 6.1 Ludian earthquake of 3 August 2014 in Yunnan Province, China. The town comprised 192 buildings, predominantly low-quality load-bearing masonry structures with little or no seismic design. Approximately 60% of the total built-up area was destroyed.

Government data indicated that demolition of unsafe buildings and debris clearance took approximately six months, while repair and construction of replacement buildings were completed in about three years. These data were used to construct the observed resilience curve shown in Figure 2.

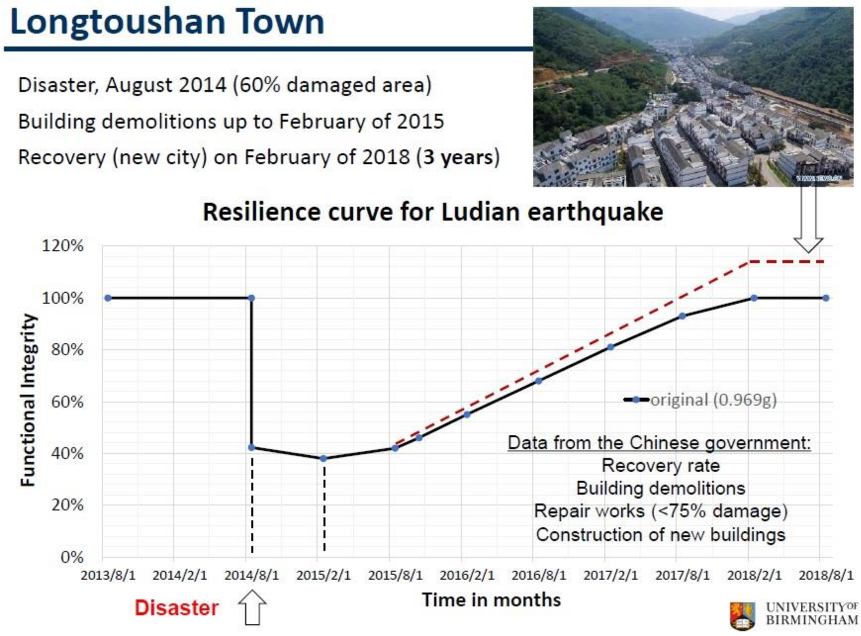

Figure 2: Observed seismic resilience curve for Longtoushan Township (Shchukin and Skalomenos, 2022).

Using YouSimulator, Shchukin and Skalomenos (2022) simulated the seismic response of the town's 192 buildings and performed incremental dynamic analysis (IDA) using 20 pairs of appropriately selected ground-motion records. Building damage indices and fragility curves were derived from the calculated inter-storey drift ratios and expressed in terms of peak ground acceleration (PGA) (Figure 3: Observed damage distribution (left) and derived fragility curves (right)).

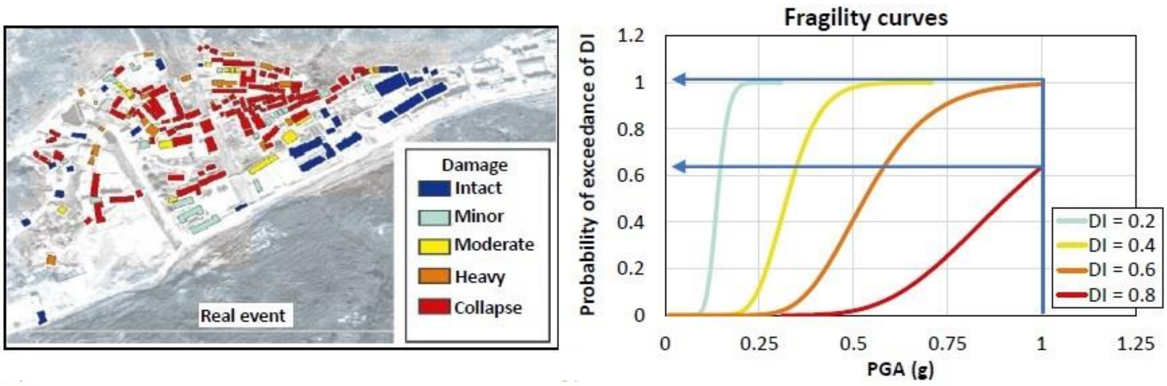

Figure 3: Observed damage distribution (left) and derived fragility curves (right) (Shchukin and Skalomenos, 2022).

The fragility curves were then used to construct seismic resilience curves for different levels of PGA. The analytical curve was compared with the observed resilience curve for the Ludian earthquake, for which the loss of city functionality was approximately 60% (Figure 4: Comparison of analytical and observed seismic resilience curves for the Ludian earthquake).

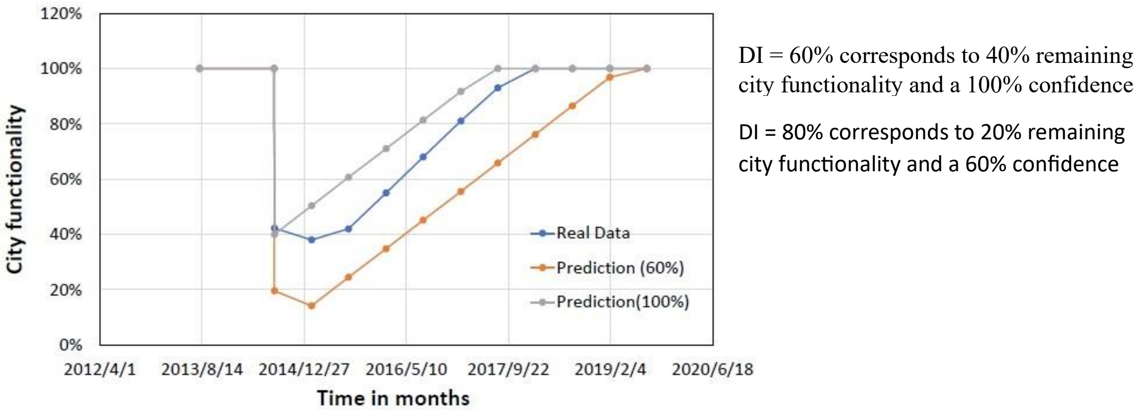

Figure 4: Comparison of analytical and observed seismic resilience curves for the Ludian earthquake (Shchukin and Skalomenos, 2022).

The curves showed satisfactory agreement, indicating that the methodology can estimate city-scale seismic resilience curves, with associated confidence intervals, for different seismic intensities (Figure 5: Estimated seismic resilience curves for Longtoushan Township at different seismic intensities (Shchukin and Skalomenos, 2022).).

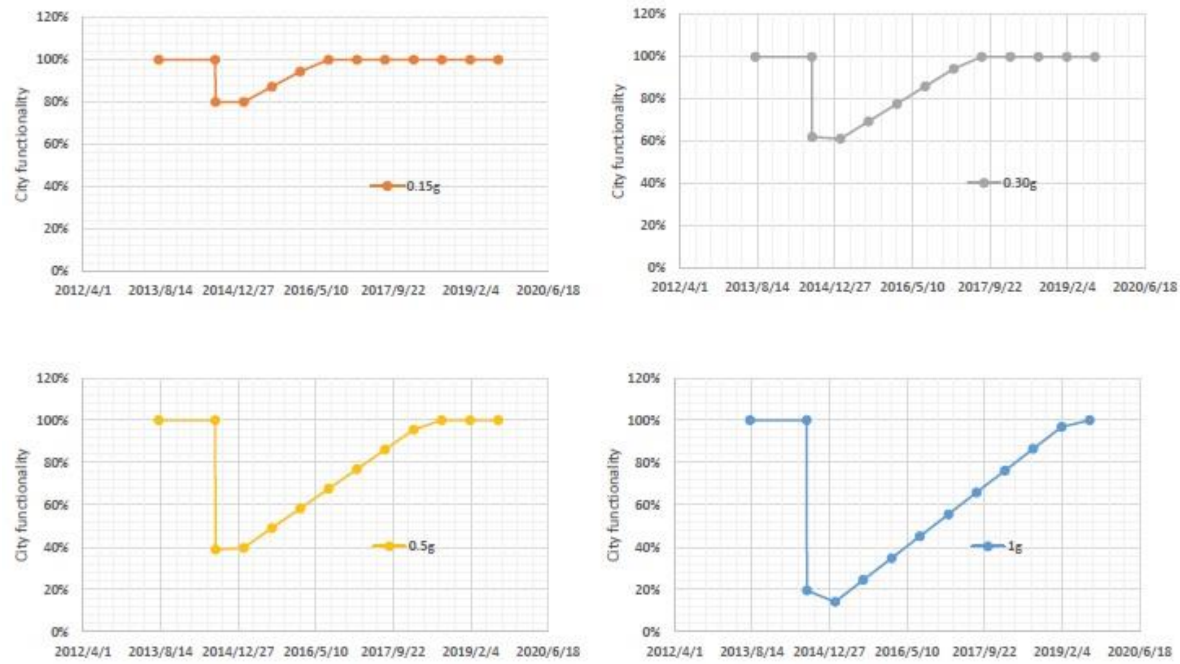

Figure 5: Estimated seismic resilience curves for Longtoushan Township at different seismic intensities (Shchukin and Skalomenos, 2022).

3 YouSimulator: a city-wide urban resilience assessment platform

Chapter 3 introduces YouSimulator, the city-scale seismic damage simulation software used in this study (Lin et al., 2019, 2020; Chen et al., 2022). The chapter outlines its theoretical basis, describes the input files required for nonlinear dynamic analyses, and presents the output formats and post-processing options.

3.1 Introduction to YouSimulator

YouSimulator comprises four functional modules: automated modelling of urban building stocks, seismic-response calculation, single- and multi-degree-of-freedom results analysis, and three-dimensional visualisation (Figure 6; Lin et al., 2019). Parallel computing and physics-based automated modelling enable nonlinear time-history analysis of large metropolitan building stocks. Although the modules operate independently, they exchange and update information through the data files.

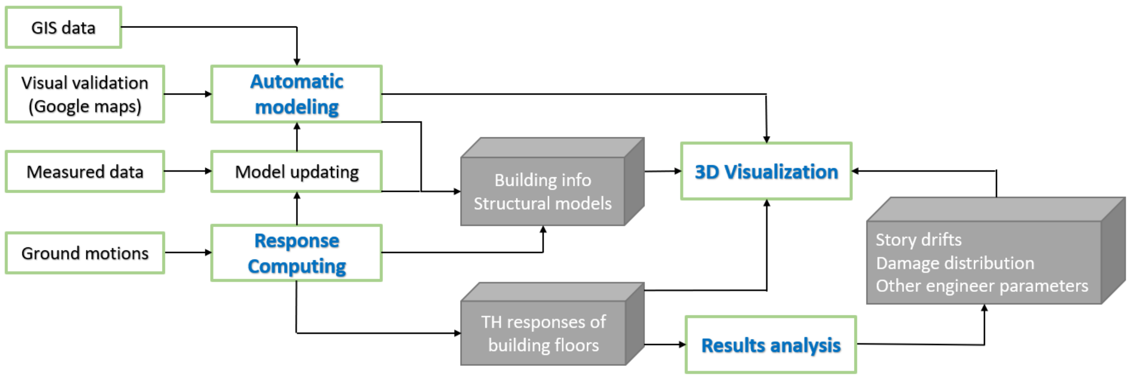

Figure 6: Flow diagram and principal modules of YouSimulator.

For automated modelling, the input files contain the information required to generate building polygons and calculate floor-plan areas. The data are obtained from geographic information system (GIS) databases and can be corrected or supplemented using drawings, on-site inspections or visual checks in Google Maps. Geographic coordinates, construction material, number and height of storeys, construction period and elevation complete the building-data profile.

During automated modelling, the software prepares the three-dimensional geometry and calculates the elastic parameters of the dynamic oscillators that represent the storey response (Figure 7). Parameters such as the fundamental period and building mass are calculated automatically. In its latest version, YouSimulator also applies the seismic design code corresponding to the construction period of each building when calculating design base shear, Vd.

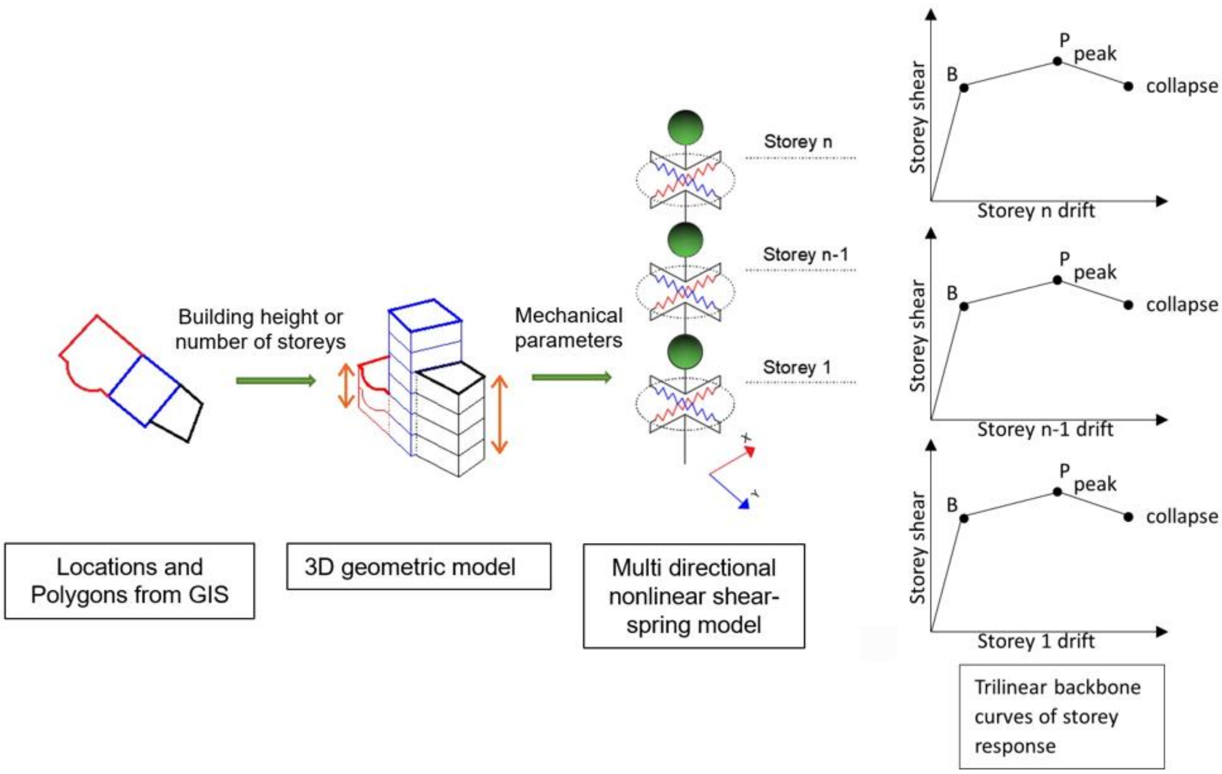

Figure 7: Schematic representation of the automated modelling procedure.

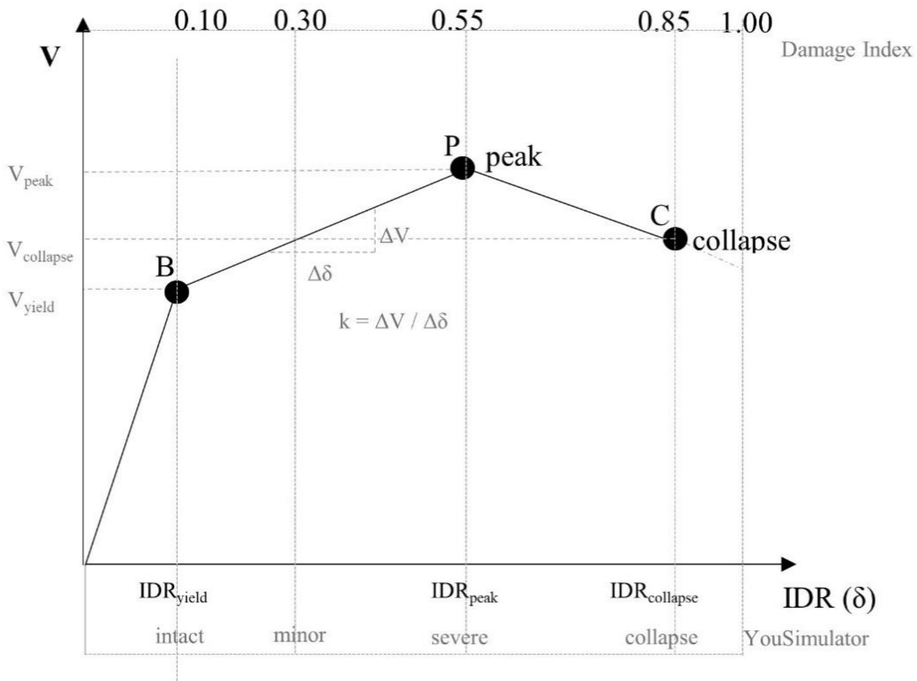

Figure 8: Trilinear skeleton curve of storey shear, V,

YouSimulator uses multiple shear springs (MSS) in the two principal directions (Wada and Hirose, 1989; Yamada et al., 2012). Each spring is described by a storey shear, V, versus inter-storey drift ratio, IDR, curve, which represents the storey capacity curve. The curve and its associated damage states are compatible with the general HAZUS methodology (FEMA, 2022).

The trilinear skeleton curve shown in Figure 8 is defined by three critical points used to calculate the damage index of each storey:

1. Yield point, B
2. Peak-strength point, P
3. Collapse point, C

The software estimates building response through inelastic dynamic time-history analysis under the imposed accelerograms. Each storey is represented by two independent shear springs arranged in mutually perpendicular directions, x and y, and each spring follows the corresponding capacity curve (Figure 7). Cyclic response is represented by the hysteretic model described by Steelman and Hajjar (2009).

The two horizontal response components are combined using the square root of the sum of the squares (SRSS). The final building damage state is governed by the maximum inter-storey drift ratio, IDRmax, calculated at any storey. YouSimulator assigns a damage index, DI, between 0 and 1. The capacity curve is divided into five regions representing increasing damage severity: intact, minor, moderate, severe and collapse (Table A1 in Appendix A).

For three-dimensional visualisation, YouSimulator exports VTK (Visualization Toolkit) files containing the building polygons and calculated damage results. These files can be processed using open-source visualisation software such as ParaView (Squillacote et al., 2007). Colour rendering of storey-level damage provides a detailed view of the spatial concentration of vulnerable buildings and storeys (Figure 9).

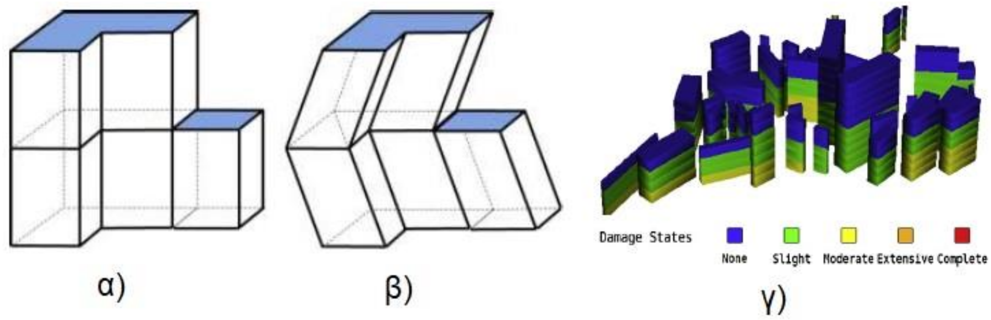

Figure 9: Three-dimensional visualisation of a structure: (a) undeformed; (b) deformed; and (c) damage-state colour rendering.

3.2 Definition of the shear-spring models

The multi-storey MDOF shear model used by YouSimulator can reproduce the inelastic behaviour of reinforced-concrete and load-bearing masonry buildings. Storey mass and stiffness are assumed to remain constant over the building height. The elastic properties are defined by the lateral stiffness, k0, and mass, m, of each storey. Equations (1) and (2) define the stiffness and mass matrices of the MDOF system.

$$[K] = k_0 \begin{bmatrix} 2 & -1 & & & \\ -1 & 2 & -1 & & \\ & -1 & \ddots & \ddots & \\ & & \ddots & 2 & -1 \\ & & & -1 & 1 \end{bmatrix} = k_0 [A] \tag{1}$$

$$[M] = m \begin{bmatrix} 1 & & & & \\ & 1 & & & \\ & & 1 & & \\ & & & \ddots & \\ & & & & 1 \end{bmatrix} = m[I] \tag{2}$$

The mass of each storey, m, is calculated using Equation (3) as the product of the floor area, A, obtained during automated modelling and the uniformly distributed seismic mass per unit floor area, mf.

$$m = m_f A \tag{3}$$

The mass per unit area, mf, is determined from the seismic combination of gravity loads specified by the relevant design code. Applying modal orthogonality gives Equation (4), which relates the lateral stiffness, k0, to the storey mass, m, and the fundamental period, T1, of the MDOF system:

$$k_0 = m\omega_1^2 \left(\frac{[\Phi_I]^T [I][\Phi_I]}{[\Phi_I]^T [A][\Phi_I]} \right) = \frac{4\pi^2 m}{T_1^2} \left(\frac{[\Phi_I]^T [I][\Phi_I]}{[\Phi_I]^T [A][\Phi_I]} \right) \tag{4}$$

where [Φ1] is the first-mode vector calculated for the building. The remaining variable required to determine k0 is the fundamental period, T1.

3.3 Defining MDOF curve parameters

3.3.1 Strength parameters

a. Design base shear, V_d

YouSimulator uses the code-based design base shear, Vd (Figure 8), as the reference design strength of a building. For each country, Vd is calculated automatically from the seismic zone and the seismic design code corresponding to the building's construction period. For example, YouSimulator can calculate Vd using modern seismic codes in accordance with Equation (5):

$$V_d = M \cdot \Phi_d(\mathrm{T}) \tag{5}$$

b. Yielding shear, $V_{yield,i}$

The software calculates the yield shear of each storey, $V_{yield,i}$ (Figure 8), which is generally greater than the design shear, $V_{d,i}$, using Equation (6).

$$V_{yield,i} = \Omega_1 \cdot V_{d,i} \tag{6}$$

The overstrength factor, Ω1, is influenced by several factors, including the actual strengths of construction materials. For RC buildings, an important contribution arises from masonry infill walls, which are generally not included explicitly in the original structural design.

c. Peak shear, $V_{peak,\,i}$

The peak shear, $Vpeak_{,i}$ (Figure 8), is the maximum storey shear attained in the inelastic range. RC buildings can develop additional strength through reinforcement strain hardening, concrete contribution and structural redundancy; consequently, $Vpeak_{,i}$ exceeds the yield shear, $Vyield_{,i}$. This increase is represented by the factor Ω2 in Equation (7).

$$V_{peak,i} = \Omega_2 \cdot V_{yield,i} \tag{7}$$

The coefficient Ω2 is specified by the user as a representative value for each building typology. It may be obtained from statistical analysis of pushover curves or from values recommended by relevant guidance, such as FEMA (2022), using Equation (8).

$$\Omega_2 = \frac{SA_u}{SA_y} = \frac{V_{peak,i}}{V_{yield,i}} \tag{8}$$

d. Collapse shear, $V_{collapse,\,i}$

RC buildings generally possess reserves of ductility. After reaching peak shear, a storey can continue to resist load while developing large deformations, with constant or decreasing strength, until collapse. The ultimate storey shear, $Vcollapse_{,i}$ (Figure 8), is specified by the user and may be taken as equal to or lower than $Vpeak_{,i}$. In this study, it is taken as 80% of Vpeak,i:

$$V_{collapse,i} = 0.80 \cdot V_{peak,i} \tag{9}$$

3.3.2 Deformation parameters

a. Yield deformation, $IDRyield_{,i}$ ($\delta yield_{,i}$/Hi)

The response remains elastic up to the yield point, $Vyield_{,i}$, with stiffness k0. The yield inter-storey drift ratio, $IDRyield_{,i,}$ defined as the relative floor displacement, $\delta yield_{,i,}$ divided by storey height, Hi, is calculated using Equation (10).

$$IDR_{yield,i} = V_{yield,i} / k_0 \tag{10}$$

b. Peak deformation, $IDRpeak_{,i}$ ($\delta peak_{,i}$/Hi)

The peak inter-storey drift ratio, $IDRpeak_{,i}$ (Figure 8), is calculated using the post-yield stiffness, ksec, in Equation (11):

$$IDR_{peak,i} = V_{peak,i} / k_{sec} \tag{11}$$

where the post-yield stiffness is given by Equation (12):

$$k_{sec} = n \cdot k_0 \tag{12}$$

where n is the elastic-stiffness reduction factor. It may be obtained from reinforced-concrete design guidance (ACI, 2011) or calculated from the HAZUS capacity points (FEMA, 2022) using Equation (13):

$$n = \frac{SA_u - SA_y}{SD_u - SD_y} \cdot \frac{SD_y}{SA_y} = \frac{V_{peak} - V_{yield}}{IDR_{peak} - IDR_{yield}} \cdot \frac{IDR_{yield}}{V_{yield}} \tag{13}$$

where (SDy, SAy) and (SDu, SAu) correspond to the yield point (IDRyield,i, Vyield,i) and the peak point (IDRpeak,i, Vpeak,i) of the trilinear curve.

c. Collapse deformation, IDRcollapse$_{,i}$ (δcollapse$_{,i}$/Hi)

The collapse inter-storey drift ratio, IDRcollapse$_{,i}$ (Figure 8), is specified by the user for each building typology. HAZUS (FEMA, 2022), for example, provides landmark collapse-drift values for different building typologies.

3.3.3 Hysteretic behaviour

When shear deformations dominate the cyclic response, hysteretic behaviour can be represented by the simplified model of Steelman and Hajjar (2009). Figure 10 illustrates the response of a representative storey under seismic loading, and Figure 11 shows the hysteretic model adopted in this version of YouSimulator.

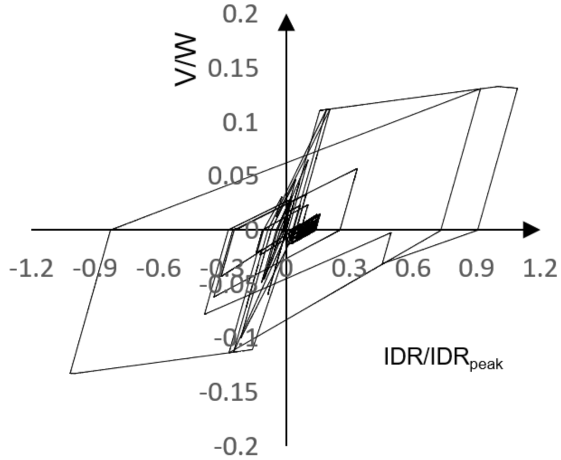

Figure 10: Storey behaviour under seismic loading.

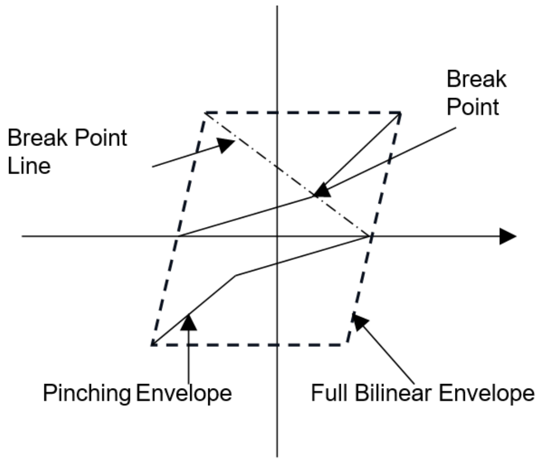

Figure 11: Hysteretic model adopted in YouSimulator (Lu et al., 2014).

The model depends on parameter τ, which represents the magnitude of hysteresis and is defined by Equation (14).

$$\tau = \frac{A_p}{A_b} \tag{14}$$

where:
Ap and Ab are the areas enclosed by the degradation curve and the trilinear backbone curve, respectively, under cyclic loading.

For a specified construction type and excitation duration, τ can be obtained from HAZUS guidance (FEMA, 2022) or other relevant sources.

3.4 Input files

YouSimulator uses plain-text input files (.txt) containing the geometric and technical information required to generate each building model. Plain-text files are also used to provide ground-motion records in the two horizontal directions, x and y.

Examples of a building input file and a ground-motion input file are presented in Figures A1 and A2 of Appendix A. The principal input parameters are summarised in Table 1.

Table 1: Parameters used in the input files.

I	Serial number of the building
H	Total building height (m)
A	Floor surface (m^2)
sType	Structural type (1 = timber, 2 = steel, 3 = RC, 4 = reinforced masonry, 5 = other)
NS	Number of storeys
SH	Storey height (m)
BY	Building's construction year
GMSF	Ground-motion scale factors in the x and y directions
SMF	Strength modification factor (overstrength ratio $\Omega 1 = Vy/Vd$)
MT1	Measured fundamental period of the building T_1 Initial value is "0" which means that T_1 is calculated automatically
BH	Building altitude (m)
Country code	Country code used to select the corresponding design parameters China - 0
T_1	First characteristic period of the response spectrum
T_2	Second characteristic period of the response spectrum
Accel	Reference peak ground acceleration for the seismic design
q	Behaviour factor
θ	Foundation influence coefficient

γ_I	Building importance factor
ND	Number of points (vectors)
H	Building height
{Coordinates of N^{th} polygon}	Coordinates of the Nth point of the building footprint polygon
0	"0" means that the floor plan of the building does not enclose

3.5 Output files

YouSimulator exports plain-text result files (.txt), which can be viewed and edited directly, and VTK files (.vtk), which can be visualised in three dimensions using software such as ParaView (Squillacote et al., 2007).

3.5.1 Plain text result files

YouSimulator saves analysis results in plain-text files within the “Results” and “ShearDrift” folders. For each analysis time step, dt, the displacement, velocity, acceleration, inter-storey drift ratio and corresponding storey shear are recorded for each storey in both horizontal directions.

The software can also compile the principal results for each building into summary lists. These include the maximum inter-storey drift ratio, IDRmax, floor area, number of storeys and construction year, and are stored as plain-text files in the “DataList” folder.

3.5.2 Three-dimensional result files

The software creates VTK files containing the floor polygons of each building together with displacement and damage-index results for each time step. These files enable time-dependent three-dimensional visualisation and further post-processing in ParaView or equivalent software.

4 Development of the Thessaloniki city model

A sample of 1,252 reinforced-concrete (RC) buildings in central Thessaloniki was selected using ArcMap (ESRI, 2022) and GIS data. Building input files were generated using data from the Hellenic Statistical Authority (ELSTAT, 2022a). The buildings were classified by height, structural system and construction period. Greek seismic codes were compared by construction era, and the corresponding design shear was calculated. Building ductility and damage-state thresholds were derived using HAZUS guidance (FEMA, 2022) and trilinear capacity curves. Finally, the buildings were assigned to three macroseismic-intensity zones on the basis of the spatial distribution of damage observed during the 20 June 1978 Thessaloniki earthquake.

4.1 Selection of buildings

The selected buildings are located in one of the most densely built-up areas of central Thessaloniki (Figure 12: Study area (left) and reported damage to 3,707 RC buildings during the 20 June 1978 Thessaloniki earthquake (right), based on Panou et al. (2014).), where the stock is dominated by mid- and high-rise RC buildings constructed before 1985. The area is considered representative of the city centre and is particularly suitable for this study because it combines an ageing, potentially vulnerable building stock with detailed records of damage from the 20 June 1978 earthquake.

Figure 12: Study area (left) and reported damage to 3,707 RC buildings during the 20 June 1978 Thessaloniki earthquake (right), based on Panou et al. (2014).

The building inventory was developed in collaboration with University of Birmingham students (Nicholls, 2022; Zeqin, 2020; Xiaorui, 2022). Building blocks and footprint coordinates were extracted from GIS files using ArcMap (ESRI, 2022). ELSTAT data (2022a) were then used to identify the buildings and add technical attributes. The inventory was visually checked using Google Maps, and data were corrected or supplemented where necessary. This procedure produced a database of 1,252 RC buildings.

4.2 Building classification

The buildings are classified according to their principal technical and geometric characteristics: number of storeys, construction year and structural system. The classification follows the

RISK-UE methodology (Mouroux and Brun, 2006), which has been adopted widely in seismic-vulnerability studies, including Kappos et al. (2006).

The 1,252 RC buildings are classified using the following characteristics:

- Height: low-rise (1–3 storeys), mid-rise (4–7 storeys) and high-rise (8 or more storeys)
- Structural system: moment-resisting frames or dual systems comprising frames and RC walls
- Infill arrangement: regular infill over the height or an open ground storey (pilotis)
- Seismic design code in force at the time of construction:
  - ✓ Before 1959: no seismic code (N, no/pre-code)
  - ✓ 1959–1985: Greek Seismic Code of 1959, RD ’59 (L, low-code)
  - ✓ 1985–1995: Supplementary Clauses of the Greek Seismic Code of 1984, which became mandatory in 1985 (M, moderate-code)
  - ✓ After 1995: modern seismic regulations, including NEAK (1992), EAK/2000 (1999) and Eurocode 8 (CEN, 2004) (H, high-code)

Certain reasonable assumptions have been made to facilitate this categorization, which are based on practical knowledge of construction periods and seismic design codes in Greece, as discussed in the following paragraph. These assumptions are outlined below:

- RC buildings in Greece, and more broadly in south-eastern Europe, typically have robust masonry infill walls, particularly in perimeter frames. The 1,252 buildings are therefore classified as either regularly infilled buildings or buildings with an open ground storey (pilotis).

- Information on the presence of RC walls was not available. Consequently, mid- and high-rise buildings of four or more storeys constructed after 1985 (approximately 4% of the sample) were assumed to use dual frame–wall systems. This assumption reflects the requirements and common practice of more recent Greek regulations. The effect of an open ground storey was disregarded for these dual-system buildings (Kappos et al., 2006). Following the 1978 earthquake, adding RC walls and well-reinforced stair cores also became common practice in northern Greece.

- Older regulations, including RD ’59, also recommended RC wall elements in high-rise buildings. Elevator-shaft walls could sometimes act as structural walls, although they were not always adequately designed. Because wall information was unavailable, buildings in the older construction categories were conservatively modelled as frame systems.

The building nomenclature follows the form RCi.xy, where i identifies the structural system, x the height category and y the seismic design level (Table 2). For example, RC3.1ML denotes a regularly infilled, mid-rise, low-code building.

Table 2: Building classification and associated seismic design codes.

Building characteristic	Classification	Denotation	Category distinction	Seismic design code
Structural system	Concrete frames	RC3.1 RC3.2 RC4.2	Regularly infilled frame Irregular infill (pilotis) Regularly infilled dual system	
Construction period	No/Pre-Code Low-Code Moderate-Code High-Code	N L M H	Before 1959 1959–1985 1985–1995 1995–present	No seismic code 1959 seismic code 1984 supplementary clauses NEAK–EAK/2000–Eurocode 8
Height (storeys)	Low-rise Medium-rise High-rise	L M H	1–3 4–7 8+	

4.2.1 Classification by construction period

Building seismic performance depends strongly on the regulations in force at the time of construction. The design-strength provisions of older regulations and the subsequent introduction of ductility requirements reflect the evolution of earthquake-engineering knowledge and practice.

The first national Greek seismic code was introduced in 1959 and is commonly referred to as RD ’59. It was followed by the 1984 Supplementary Clauses, NEAK (1992), EAK/2000 (1999) and Eurocode 8 (CEN, 2004), together with the Greek National Annex.

The principal characteristics and evolution of these Greek seismic regulations are summarised below (Kappos et al., 2006).

❖ **Period before 1959 (no/pre-code)**

- RC buildings had little or no seismic design and generally poor detailing of critical elements.
- Their strength was assumed to be 20% lower than that of low-code buildings (Kappos et al., 2006), with the same displacement-ductility factor, because ductility was not considered explicitly in Greek seismic design before the 1985 revision.
- Foreign regulations, often of German origin, were sometimes applied; analysis and design used the allowable-stress method and generally considered gravity loads only.
- No explicit seismic calculation was required.
- Buildings were generally frame structures without RC walls.
- Beam–column framing was typically dense.
- Masonry infills were generally dense and well constructed, with cross-beams and careful wedging beneath the beams.

- The limited seismic resistance of flexible frame systems was mitigated to some extent by dense and robust masonry infills.

❖ **Greek Seismic Code of 1959, RD ’59 (low-code)**

- RC buildings had a low level of seismic design, broadly comparable with other pre-1980 southern-European codes.
- Multi-storey frames were divided into a series of equivalent single-storey frames using the “Exact Greek Method”.
- Each storey was represented by a model with columns fixed at the top and bottom.
- The structural model was shear-type.
- Seismic forces were distributed uniformly over the building height.
- The design force was calculated as a percentage of total building weight using the seismic coefficient, ε.
- The force was independent of the fundamental vibration period.
- Design *was based* on the allowable-stress method.
- Wall design and shear checks were limited.
- Frame–wall interaction was generally ignored.
- Seismic coefficients depended on regional seismicity and soil category.

❖ **Supplementary Clauses of the Greek Seismic Code of 1984 (moderate-code)**

- RC buildings achieved a moderate level of seismic design, broadly comparable with post-1980 southern-European codes, and more rational detailing of RC members was introduced.
- Buildings with more than three storeys were required to be analysed using a multi-storey frame model.
- A building-importance factor was introduced.
- A triangular distribution of base shear over the building height was introduced.
- Control of horizontal displacement became mandatory.
- Additional design checks and construction provisions for RC members, frame joints and infill walls were introduced to improve ductility in critical regions.
- Second-order effects caused by horizontal seismic displacement had to be checked.
- Capacity design was required when the permissible limits were exceeded.

❖ **NEAK (1992), EAK/2000 (1999) and Eurocode 8 (CEN, 2004) (high-code)**

- RC buildings achieved a high level of seismic design and ductile detailing under a modern generation of seismic codes.
- Dynamic seismic analysis, particularly response-spectrum analysis, was introduced for all structures.
- Design acceleration replaced the earlier seismic coefficient, ε, and the country was divided into seismic zones.
- A full three-dimensional structural model became mandatory.
- Structural regularity criteria were introduced for response-spectrum analysis.
- The simplified spectral method used a triangular distribution of base shear over the building height.

- Capacity checks for beams, columns and walls were based on the actual section resistance.
- NEAK was issued in 1992 and became mandatory in 1995.
- Eurocode 8 and EAK/2000 have applied in parallel since 2014.
- Eurocode 8 follows a philosophy similar to EAK/2000 but includes soil-dependent spectral amplification and does not include the favourable foundation influence coefficient used in EAK/2000, resulting in a less favourable design spectrum in some cases.

4.3 Building design strength

Building design strength depends on the seismic regulations in force at the time of construction and on the seismicity assigned to the site. YouSimulator calculates the design base shear, Vd, for each Thessaloniki building using the relevant historical regulation, as summarised below.

❖ **RD ’59 (low-code) and the 1984 Supplementary Clauses (moderate-code)**

Under these regulations, Thessaloniki was assigned to seismic-risk zone II. Assuming the medium soil category in Table 3 gives a seismic coefficient ε = 0.08. The design base shear, Vd, for both regulations is calculated using Equation (15):

$$V_d = 0.08 \cdot W \tag{15}$$

where W is the total building weight.

Table 3: Seismic zones and coefficients under RD ’59 and the 1984 Supplementary Clauses.

Zone	***Seismic factor, ε* (a/g) *(hard→ soft soil)***		
I	0.04	0.06	0.08
II	0.06	0.08	0.12
III	0.08	0.12	0.16

❖ **NEAK (1992), EAK/2000 (1999) and Eurocode 8 (CEN, 2004) (high-code)**

Modern Greek regulations introduced response spectra and a substantially different seismic-design philosophy. Thessaloniki is classified in seismic zone I with reference design ground acceleration agR = 0.16g. A behaviour factor q = 3.5 is adopted for the RC buildings; none of the 1,252 buildings in the sample was designed directly to Eurocode 8. Using Equation (16) and ground type B under EAK/2000, the design base shear, Vd, is calculated as follows:

$$V_d = M \cdot \Phi_d(T) = \begin{Bmatrix} \gamma_I \cdot 0.16g \cdot M\left[1 + \frac{T}{T_1}\left(\frac{n \cdot \theta \cdot \beta_0}{3.5} - 1\right)\right] \; for\; 0 \le T < T_1 \\ \gamma_I \cdot 0.16g \cdot M \frac{n \cdot \theta \cdot \beta_0}{3.5} \; for\; T_1 \le T < T_2 \\ \gamma_I \cdot 0.16g \cdot M \frac{n \cdot \theta \cdot \beta_0}{3.5}\left[\frac{T_2}{T}\right]^{2/3} \; for\; T_2 < T_1 \end{Bmatrix} \tag{16}$$

where T and M are the fundamental period and mass of the building, respectively, as calculated by

YouSimulator;
γI is the building-importance factor specified in the input file;
T1 = 0.15 s and T2 = 0.60 s are the characteristic periods for ground type B;
β0 = 2.5 is the spectral amplification factor;
η = 1.0 is the damping correction factor for ξ = 5%; and
θ = 1.0 is the foundation influence coefficient (θ = 0.90 for a basement).

The design spectra of the Greek seismic regulations integrated into YouSimulator are shown in Figure A3 of Appendix A.

❖ **Period before 1959 (No/pre-code)**

Buildings constructed before 1959 were not designed explicitly for seismic loading. Kappos et al. (2006) found that their strength can be approximated as 80% of the strength of buildings designed to RD ’59. Their design base shear, Vd, is therefore calculated as follows:

$$V_d = 0.80 \cdot 0.08 \cdot M \Rightarrow V_d = 0.064M \tag{17}$$

4.3.1 RC-building overstrength factors in Greece

The yield shear of a building, $V_{yield,i}$ (Figure 8), is generally greater than the design shear, $V_{d,i}$. YouSimulator accounts for this difference through Equation (18).

$$V_{yield,i} = \Omega_1 \cdot V_{d,i} \tag{18}$$

The overstrength coefficient, Ω1, represents the reserve strength of a building beyond its nominal design resistance. Determining Ω1 requires nonlinear analysis of representative structural models.

Kappos et al. (2006) and Kappos (2013) reported nonlinear static analyses of RC building typologies similar to those used here. The overstrength coefficient Ω1 is derived from the pushover curve and the actual yield point, enabling calculation of Vyield.

Table 4 gives representative yield and ultimate points from pushover analyses of mid-rise buildings. The source studies used ε = 0.08 for buildings designed to RD ’59 or the 1984 Supplementary Clauses, and ag = 0.16g with q = 3.5 for the modern-code typologies. The Ω1 values adopted for the full sample are presented in Table A2 of Appendix A.

Table 4: Ω_1 coefficients as derived from pushover curves for mid-rise buildings (Kappos et al., 2006).

Regulation	Height	Frame Type	Code	Ω_1
	Medium Rise	Infilled	RC3.1MN	1.729
		Pilotis	RC3.2MN	1.281
	Medium Rise	Infilled	RC3.1ML	1.733
		Pilotis	RC3.2ML	1.283

	Medium Rise	Infilled	RC3.1MM	1.713
		Pilotis	RC3.2MM	1.266
		Infilled	RC4.2MM	2.121
	Medium Rise	Infilled	RC3.1MH	2.351
		Pilotis	RC3.2MH	2.071
		Infilled	RC4.2MH	2.100

The peak-to-yield shear ratio, Ω2, is introduced as a single representative value for each building typology (Figure 8):

$$\Omega_2 = \frac{V_{peak,i}}{V_{yield,i}} = 1.20 \tag{19}$$

Finally, the ultimate storey shear, Vcollapse,i, is calculated using Equation (20) as 80% of the peak shear, Vpeak,i (Figure 8).

$$V_{collapse,i} = 0.80 \cdot V_{peak,i} \tag{20}$$

4.4 Building fundamental eigenperiod

The fundamental period is either calculated automatically by YouSimulator or specified by the user. In this report, Equation (21), recommended by KAN.EPE (OASP, 2022), is used when more precise measured data are unavailable; the expression was derived from statistical analysis of existing RC buildings in Greece.

$$T_1 = 0.052 H^{0.90} \tag{21}$$

4.5 Building ductility by HAZUS and damage states

HAZUS guidance (FEMA, 2022) is used to define building ductility and structural damage states. For drift-sensitive structural components, HAZUS provides inter-storey drift ratio thresholds at which a building transitions from one damage state to the next. Median IDR thresholds are tabulated by building typology, height and design level: pre-code, low-code, moderate-code and high-code.

In this study, low levels of damage are represented using a force-based criterion, while more severe damage is governed by deformation demand (Lu et al., 2014).

HAZUS tables (FEMA, 2022; Table A3 in Appendix A) provide IDR thresholds for different building typologies and design levels. Buildings are also categorised by height as low-rise (1–3 storeys), mid-rise (4–7 storeys) and high-rise (8 or more storeys).

The trilinear curves are defined by yield, peak and collapse points. Figure 13: Adopted trilinear curves for RC3.1 mid-rise buildings. shows normalised curves for a representative mid-rise building in the pre-code, low-code, moderate-code and high-code categories. Lateral strength is normalised by the corresponding pre-code value. HAZUS guidance (FEMA-NIBS, 2003) provides values for IDRextensive, taken here at peak strength, and IDRcollapse. YouSimulator uses IDR values normalised by the pre-code values, IDRpre. For low-rise buildings, the adopted ratios are 1.25 for low-code, 1.93 for moderate-code and 2.50 for high-code buildings. Collapse strength is taken as 80% of peak strength.

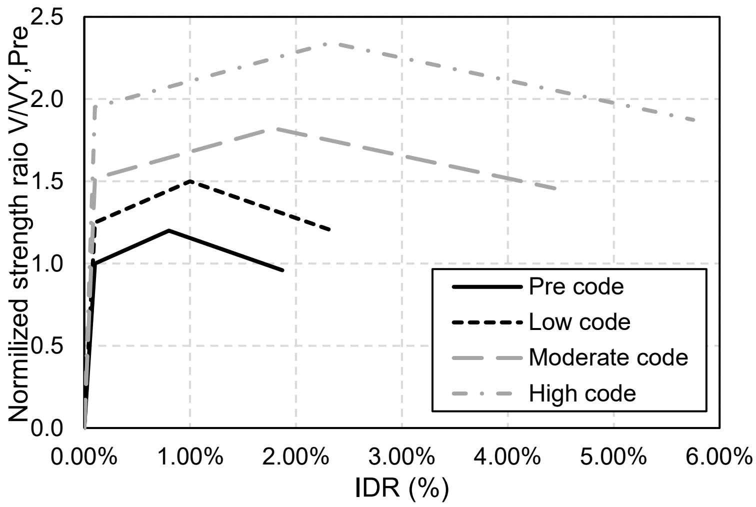

Figure 13: Adopted trilinear curves for RC3.1 mid-rise buildings.

Table 5 summarises the IDR values used to define the capacity curves, and Table 6 presents the IDR values for each design era normalised by the corresponding pre-code values.

Table 5: Adopted IDR values.

Seismic design level	Low-rise		Mid-rise		High-rise	
	Extensive	**Collapse**	**Extensive**	**Collapse**	**Extensive**	**Collapse**
Pre-code	0.0120	0.0280	0.0080	0.0187	0.0060	0.0140
Low-code	0.0150	0.0350	0.0100	0.0234	0.0075	0.0175
Moderate-code	0.0232	0.0540	0.0179	0.0444	0.0135	0.0328
High-code	0.0300	0.0700	0.0233	0.0575	0.0175	0.0425

Table 6: Normalised IDR ratios.

Ductility	Low-rise	Mid-rise	High-rise
IDR_{Pre} / IDR_{Pre}	1.00	1.00	1.00
IDR_{Low} / IDR_{Pre}	1.25	1.25	1.25
$IDR_{Moderate} / IDR_{Pre}$	1.93	2.25*	2.34*
IDR_{High} / IDR_{Pre}	2.50	2.92*	3.04*

*Values differ from 1.93 and 2.50 because the assumed structural typology changes from a frame to a dual frame–wall system.

YouSimulator calculates the damage index of each building from its force–deformation response history. Figure 14 shows the damage-state ranges DS1–DS5, corresponding to no damage, minor damage, moderate damage, severe damage and collapse. The limits are aligned with the European Macroseismic Scale (EMS-98; Grünthal, 1998) and are broadly consistent with HAZUS (FEMA, 2022). The damage index represents structural strength loss; the software also calculates acceleration and velocity at each storey, which can support assessment of non-structural damage.

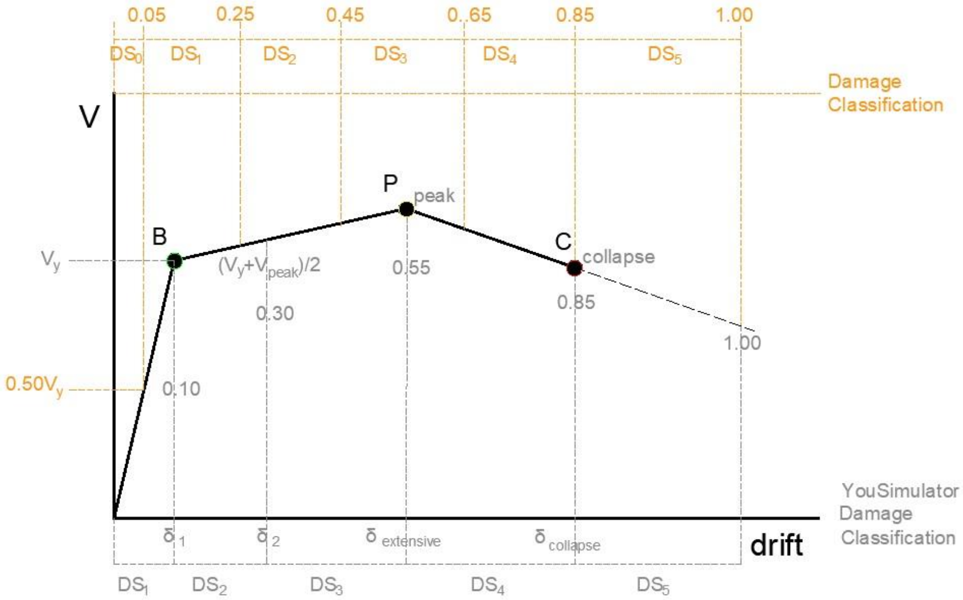

Figure 14: Definition of the damage index. The orange line is based on EMS-98 damage states (Panou et al., 2014), and the grey line shows the default YouSimulator classification.

Equation (22) defines the damage index calculated by YouSimulator, while Table 7 describes the corresponding EMS-98 damage states.

$$
\begin{aligned}
&DI=0.10*(D/D_y) \text{ when } 0 < D \leq D_y \\
&DI=0.10+0.20*(D-Dy)/((Dc-Dy)/6) \text{ when } Dy < D \leq Dy+(Dc-Dy)/6 \\
&DI=0.30+0.25*(D-Dy-(Dc-Dy)/6)/((Dc-Dy)/3) \text{ when } Dy+(Dc-Dy)/6 < D \leq Dy+(Dc-Dy)/2 \\
&DI=0.55+0.30*(D-Dy-(Dc-Dy)/2)/((Dc-Dy)/2) \text{ when } Dy+(Dc-Dy)/2 < D \leq Dc \\
&DI=0.85+0.15*(1-D_c/D) \text{ when } D \geq D_c
\end{aligned}
\tag{22}
$$

where DI is the damage index calculated by YouSimulator; D is the maximum IDR; and Dy and Dc are the IDRs at the yield and collapse points, respectively.

Table 7: Damage-state definitions based on Panou et al. (2014).

DS0 [0–0.05]	• No damage
DS1 [0.05–0.25]	• Infill wall detachment from the surrounding frame
DS2 [0.25–0.45]	• Infill wall cracking • Beam damage (all types) • Column cracking due to bending moments at joints • RC walls (cracks due to slippage of the base)
DS3 [0.45–0.65]	• Infill wall collapse • Columns (concrete crushing at joints due to compressive stresses)

	• RC walls (yielding of reinforcement due to bending moments, concrete crushing due to compressive stresses, failure of coupling beams)
DS4 [0.65–0.85]	• Columns (shear failure / short columns) • RC walls (shear failure)
DS5 [0.85–1.00]	• Complete or partial collapse of the structure

4.6 Profile of the building sample

Before presenting the analytical results, this section summarises the principal characteristics of the 1,252 RC buildings. Figure 15 shows the number of buildings by height category and seismic design level.

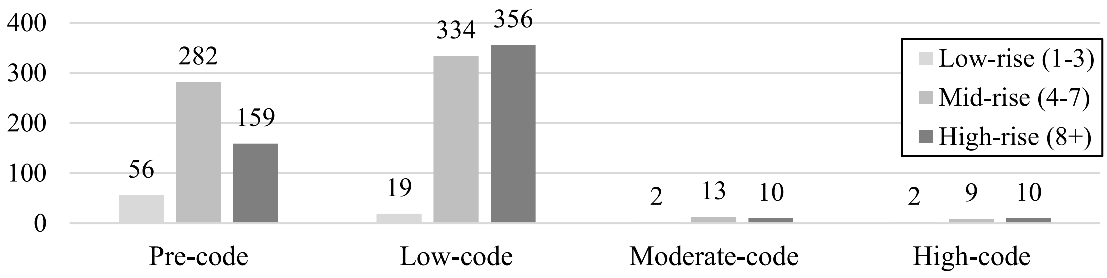

Figure 15: Distribution of the building sample by height and seismic design level.

Figure 16 shows the proportions of buildings by design era and height category. Only 3.7% of the sample was constructed after 1985, while 93.7% comprises mid- and high-rise buildings. This combination of age and height contributes to the seismic vulnerability of central Thessaloniki.

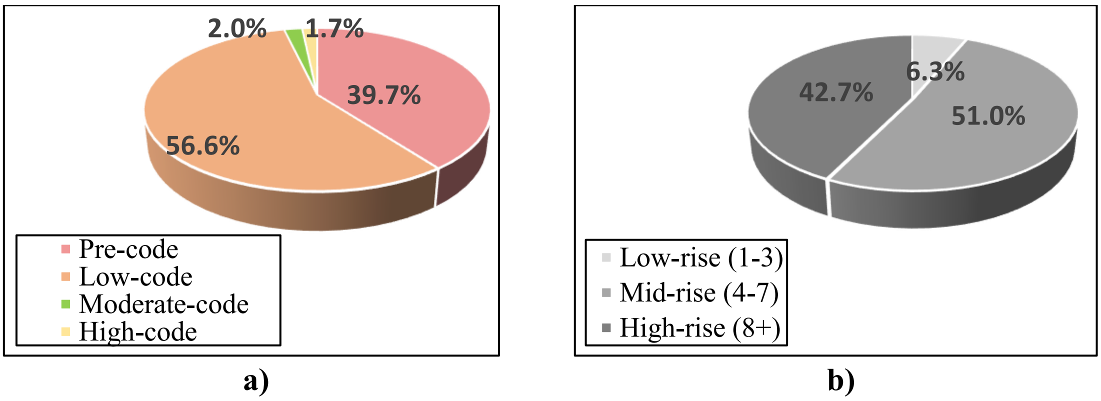

Figure 16: Distribution of the building sample by (a) seismic-code era and (b) height

Figure 17 summarises building-footprint area using four area classes. Most buildings (721 of 1,252) have footprints between 200 and 400 m². A small number have footprints greater than 600 m² and may comprise more than one structurally independent building separated by joints.

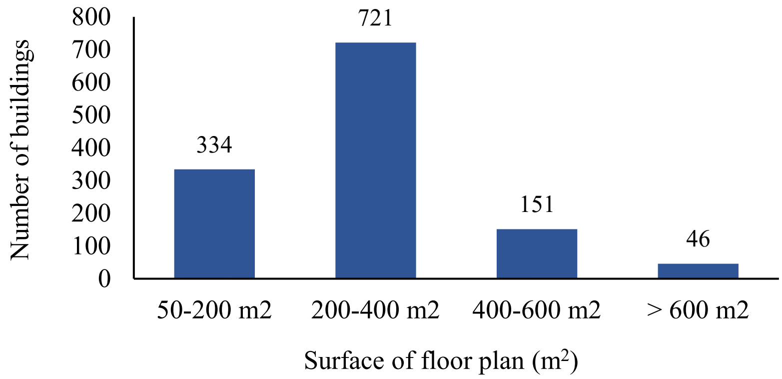

Figure 17: Distribution of the building sample by footprint area.

4.7 Microzonation effect

The RC building stock was divided into location-based groups so that spatial variations in ground-motion amplification could be represented. The 1978 earthquake record was scaled for the three macroseismic-intensity zones shown in Figure 18. Koliopoulos et al. (1998) related macroseismic intensity, I, to PGA for shallow Greek earthquakes as follows:

$$\ln(PGA) = 0.74I + 0.03 \quad (23)$$

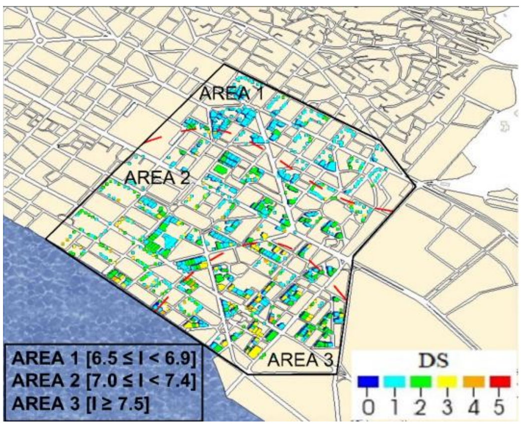

Figure 18: Macroseismic-intensity zones and EMS-98 damage states in the study area.

The Thessaloniki record had PGA = 149 cm/s² (0.15g), corresponding to AREA 1 in Figure 18 and I = 6.7. Using the lower-bound intensities reported for AREAS 2 and 3, I = 7.0 and 7.5, respectively, gives ground-motion scale factors of 1.24 and 1.80.

5 City-scale nonlinear time-history analysis results

The city model developed in Chapter 4 is subjected to nonlinear dynamic time-history analysis. First, the model is analysed using the Mw 6.5 record from the 20 June 1978 Thessaloniki earthquake, and predicted damage states are compared with observed damage for 345 identified buildings. The validated model is then analysed under frequent, design-basis and rare earthquake scenarios with return periods TRC = 70, 475 and 2,475 years, respectively, as defined by KAN.EPE (OASP, 2022). Twenty pairs of compatible ground-motion records are scaled to the corresponding target spectra and used in the analyses.

5.1 Model verification

The Thessaloniki city model is first subjected to the two horizontal components of the recorded 20 June 1978 earthquake (ITSAK, 2023). The event occurred at 23:03 local time, had moment magnitude Mw 6.5, lasted approximately 10 s and had a focal depth of about 8–10 km. Its maximum reported intensity was VIII on the Modified Mercalli scale. It was the first major earthquake to affect a modern Greek city: 49 people died, more than 220 were injured and many thousands were displaced. Figure 19 shows the two acceleration components and compares their response spectrum with the Eurocode 8 elastic spectrum. Figure 20 shows the normalised base-shear–storey-drift response of representative six-storey pre-code and moderate-code RC3.1 buildings. The moderate-code building develops greater lateral strength and lower drift demand than the pre-code building.

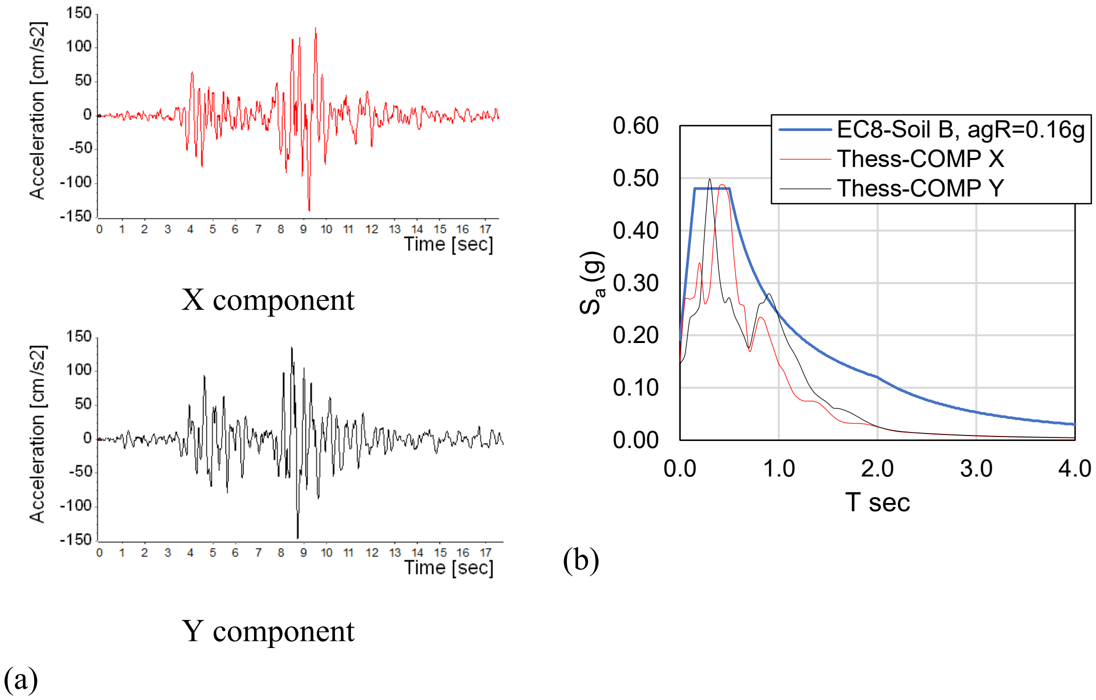

Figure 19: (a) Recorded ground-motion components and (b) comparison of the record response spectrum with the Eurocode 8-1 elastic spectrum (CEN, 2004).

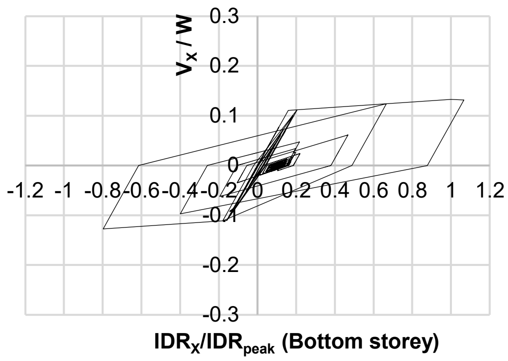

(a)

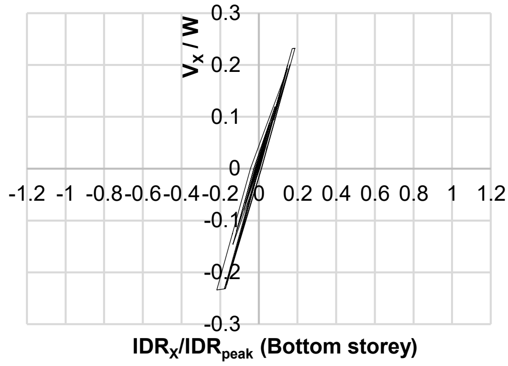

(b)

Figure 20: Base-shear–storey-drift response of (a) six-storey pre-code RC3.1 building and (b) six-storey moderate-code RC3.1 building.

5.2 Comparison of simulated and observed damage states

The simulated and observed damage states of 345 buildings were compared to validate the physics-based city model (Figure 21). Building-specific trilinear curves were calibrated through inverse nonlinear time-history analysis to reduce differences between the simulated and observed damage. Table 8 summarises the difference between predicted and observed damage states: 36.8% matched exactly, 59.1% were within ±one damage state, 3.8% differed by ±two states and 0.3% differed by three states. YouSimulator slightly overestimated lower damage states and generally underestimated higher damage states by approximately one level. Figure 23 presents a three-dimensional visualisation of the calculated damage.

(a)

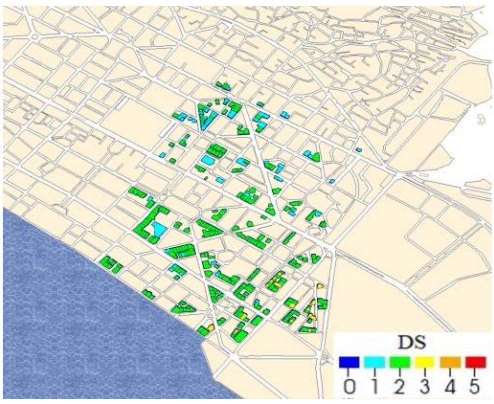

(b)

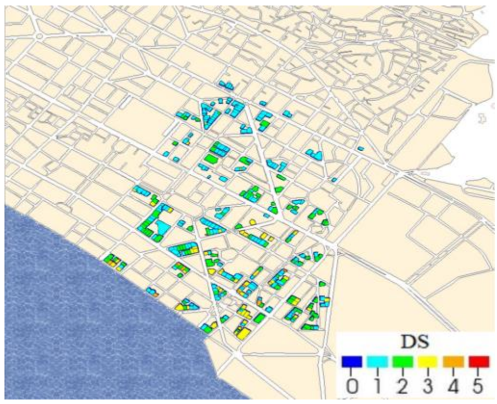

Figure 21: (a) Simulated and (b) observed damage states for the 345 validation buildings.

Table 8: Difference between simulated and observed damage states.

Damage-state difference	Number of buildings	Percentage of buildings
0	127	36.8%
-1	147	42.6%
-2	3	0.9%
1	57	16.5%
2	10	2.9%
3	1	0.3%

(a) 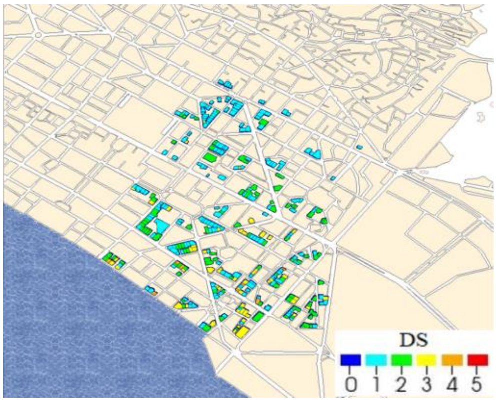

(b) 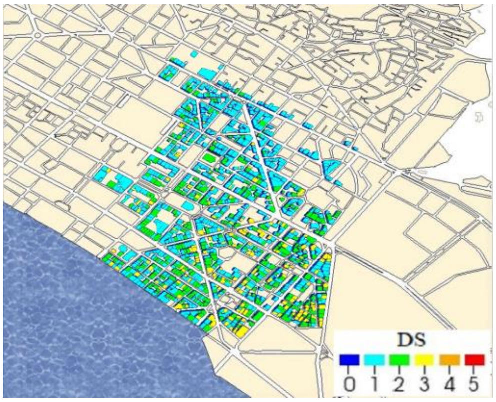

Figure 22: (a) Observed damage states for the 345 validation buildings and (b) simulated damage states for all 1,252 buildings.

Figure 22: (a) Observed damage states for the 345 validation buildings and (b) simulated damage states for all 1,252 buildings. presents the simulated damage distribution for the 1978 Thessaloniki earthquake. The three-dimensional representation in Figure 23 demonstrates that YouSimulator calculates damage at individual storeys, unlike vulnerability methods based on equivalent single-degree-of-freedom models.

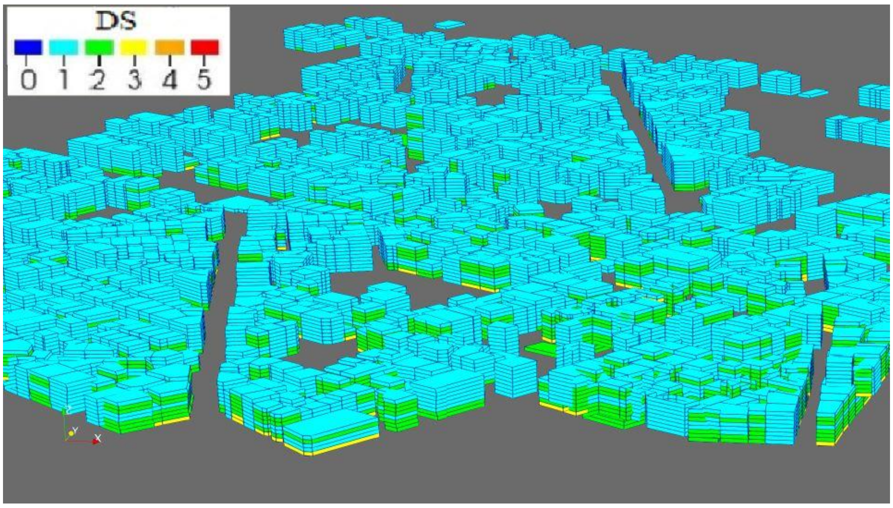

Figure 23: Three-dimensional representation of storey-level building damage in central Thessaloniki.

5.3 City-model analyses for three seismic-intensity scenarios

Following validation, the 1,252-building model is analysed under three earthquake scenarios. Twenty pairs of far-field ground motions are selected from the PEER database (PEER, 2023). The records were obtained on sites with Vs,30 between 360 and 800 m/s, corresponding to ground type B under Eurocode 8, and have magnitudes between 5.8 and 7.5; pulse-like records are excluded. Their geometric-mean spectrum is matched to the Eurocode 8 design spectrum for agR = 0.16g and ground type B. Scale factors of 0.45, 1.00 and 1.80 are applied for the frequent, design-basis and rare scenarios with return periods of 70, 475 and 2,475 years, respectively, following KAN.EPE (OASP, 2022). Location-dependent amplification factors for AREAS 1–3 are then applied to account for the microzonation model described in Figure 18.

5.3.1 Design spectra under KAN.EPE

The seismic assessment of the 1,252 RC buildings follows KAN.EPE (OASP, 2022). The relationship between return period, probability of exceedance and reduced reference ground acceleration is given in Table 9: Relationship between return period and horizontal ground acceleration..

Table 9: Relationship between return period and horizontal ground acceleration.

Return period (years)	Probability of exceeding seismic action within a nominal lifetime of 50 years	$\alpha g/\alpha g_{,ref}$
2475	**2%**	**1.80**
975	5%	1.30
475	**10%**	**1.00**
225	20%	0.75
135	30%	0.60

70	**50%**	**0.45**
40	70%	0.35
20	90%	0.25
< 20	> 90%	< 0.25

Figure 24 shows the elastic spectra adopted for the three earthquake scenarios, all for ground type B under Eurocode 8 (CEN, 2004).

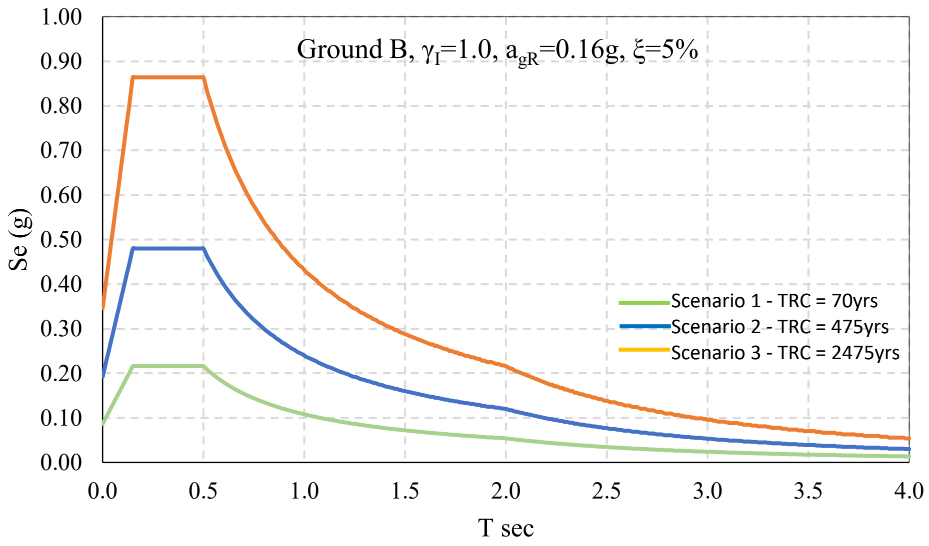

Figure 24: Elastic spectra for the three earthquake scenarios under Eurocode 8 and KAN.EPE.

KAN.EPE (OASP, 2022) adopts Eurocode 8 and its Greek National Annex. Thessaloniki is in seismic zone Z1 with reference ground acceleration αgR = 0.16g. The design-basis spectrum corresponds to TRC = 475 years and a scale factor of 1.00. The rare and frequent spectra use factors of 1.80 and 0.45 for TRC = 2,475 and 70 years, respectively (Table 9).

5.3.2 Selection of accelerograms from PEER

The three elastic spectra were used as target spectra in the PEER Ground Motion Database (PEER, 2023) to select 20 compatible pairs of records. The database provides records from earthquakes worldwide and tools for filtering and spectral matching.

For the design-basis scenario, 20 pairs of natural records were selected so that the combined spectrum of the two horizontal components was compatible with the target spectrum. Compatibility was assessed using the SRSS combination of the two component spectra.

The selected records are listed in Table 10: Twenty ground-motion records selected to match the Eurocode 8 design-basis spectrum.. The same records were scaled to the frequent and rare target spectra using the PEER tools. Scaling was necessary because a set of 20 unscaled records matching the rare-event spectrum was not available. The same approach was applied to the frequent-event scenario for consistency. The assigned return periods describe the target spectra rather than the return period of each individual record at every location; a site-specific probabilistic hazard analysis would be required for a more rigorous treatment of spatially variable exceedance probabilities.

Table 10: Twenty ground-motion records selected to match the Eurocode 8 design-basis spectrum.

ID	Earthquake Name	Year	Station Name	M_w	R_{rup} (km)	Vs,30 (m/s)
1	San Fernando	1971	Lake Hughes #1	6.61	27.4	425.34
2	San Fernando	1971	Palmdale Fire Station	6.61	28.99	452.86
3	San Fernando	1971	Pasadena - CIT Athenaeum	6.61	25.47	415.13
4	Santa Barbara	1978	Santa Barbara Courthouse	5.92	12.16	514.99
5	Norcia_ Italy	1979	Cascia	5.9	4.64	585.04
6	Imperial Valley-06	1979	Cerro Prieto	6.53	15.19	471.53
7	Livermore-01	1980	Del Valle Dam (Toe)	5.8	24.95	403.37
8	Livermore-01	1980	San Ramon - Eastman Kodak	5.8	17.24	377.51
9	Mammoth Lakes-03	1980	Convict Creek	5.91	12.43	382.12
10	Irpinia_ Italy-01	1980	Brienza	6.9	22.56	561.04
11	Irpinia_ Italy-01	1980	Calitri	6.9	17.64	455.93
12	Irpinia_ Italy-01	1980	Rionero In Vulture	6.9	30.07	574.88
13	Irpinia_ Italy-02	1980	Calitri	6.2	8.83	455.93
14	Irpinia_ Italy-02	1980	Rionero In Vulture	6.2	22.69	574.88
15	Corinth_ Greece	1981	Corinth	6.6	10.27	361.4
16	Coalinga-01	1983	Parkfield - Cholame 4W	6.36	46.35	410.4
17	Coalinga-01	1983	Parkfield - Fault Zone 16	6.36	27.67	384.26
18	Coalinga-01	1983	Parkfield - Gold Hill 3W	6.36	39.12	510.92
19	Coalinga-01	1983	Parkfield - Stone Corral 3E	6.36	34	565.08
20	Coalinga-01	1983	Parkfield - Vineyard Cany 1E	6.36	26.38	381.27

Table 11 summarises the scale factors applied to the 20 ground-motion pairs for the three earthquake scenarios.

Table 11: Scale factors applied to the 20 ground-motion pairs.

ID	**Scaling factors**			**ID**	**Scaling factors**		
	Design earthquake, TRC = 475 years	Frequent earthquake, TRC = 70 years	Rare earthquake, TRC = 2,475 years		Design earthquake, TRC = 475 years	Frequent earthquake, TRC = 70 years	Rare earthquake, TRC = 2,475 years
1	1.000	0.519	2.076	**11**	1.000	0.412	1.647
2	1.000	0.485	1.939	**12**	1.000	0.648	2.590
3	1.000	0.602	2.407	**13**	1.000	0.379	1.516
4	1.000	0.503	2.011	**14**	1.000	0.601	2.404
5	1.000	0.449	1.797	**15**	1.000	0.276	1.105

6	1.000	0.343	1.373	**16**	1.000	0.573	2.291
7	1.000	0.463	1.851	**17**	1.000	0.448	1.793
8	1.000	0.627	2.507	**18**	1.000	0.568	2.270
9	1.000	0.335	1.338	**19**	1.000	0.633	2.531
10	1.000	0.371	1.486	**20**	1.000	0.367	1.467

Figure 25: Comparison of the target spectra with the mean elastic spectra of the 20 selected record pairs for the three earthquake scenarios (logarithmic axes). compares the mean spectra of the 20 selected record pairs with the corresponding PEER target spectra on logarithmic axes. Agreement is particularly good over the period range 0.1–1.5 s, which is most relevant to the RC building stock.

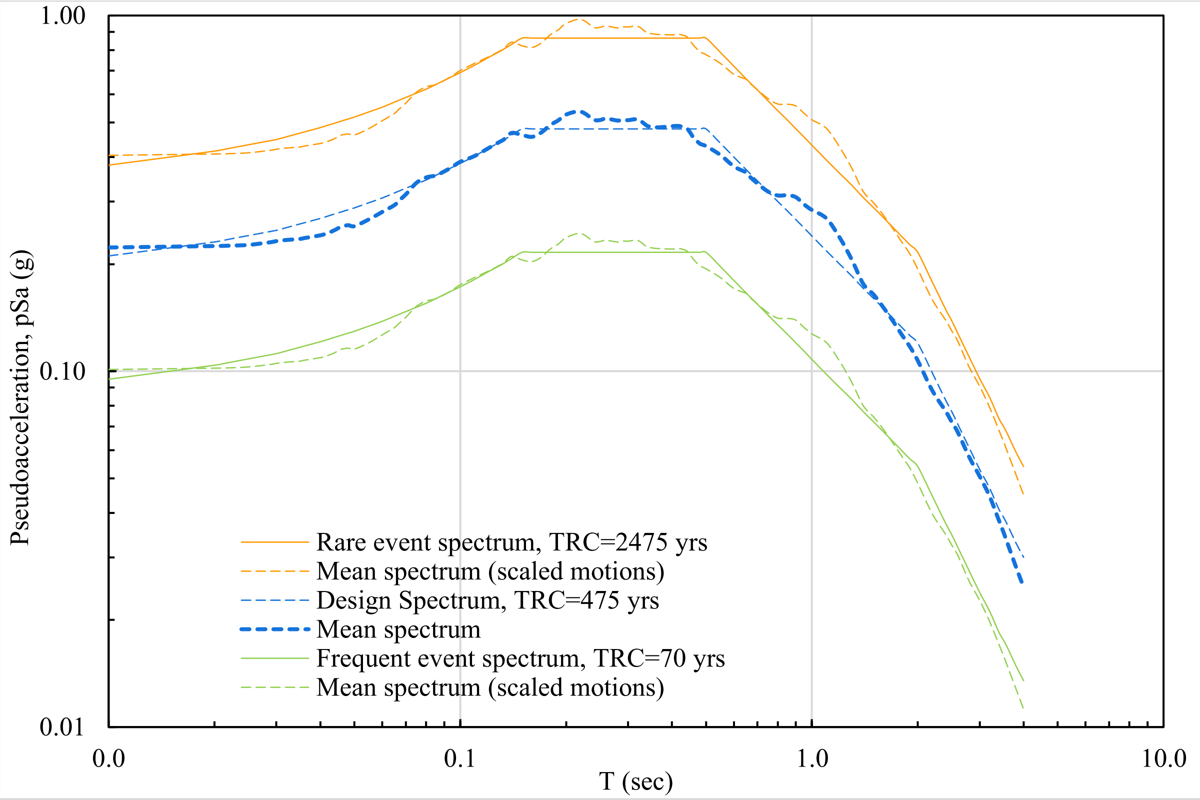

Figure 25: Comparison of the target spectra with the mean elastic spectra of the 20 selected record pairs for the three earthquake scenarios (logarithmic axes).

5.4 Nonlinear time-history analysis results

This section presents and discusses the nonlinear time-history analysis results for the 1,252 buildings in central Thessaloniki.

5.4.1 Seismic Scenario 1: TRC = 70 years

T_{RC} = 70 yrs (mean)
Probability of exceedance: 50%

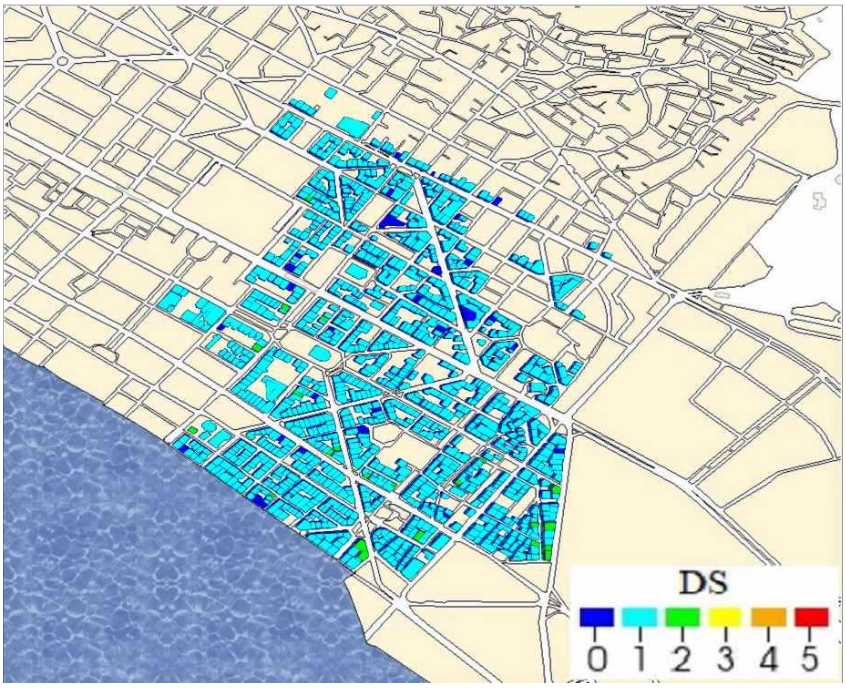

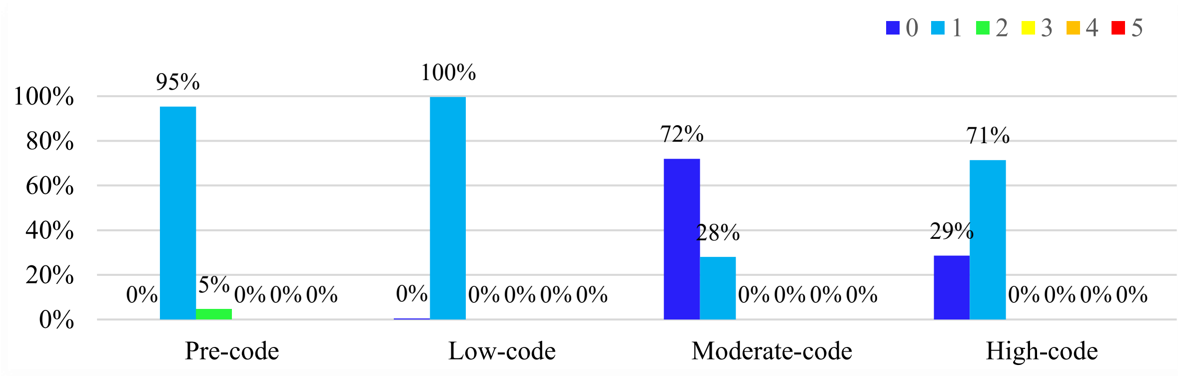

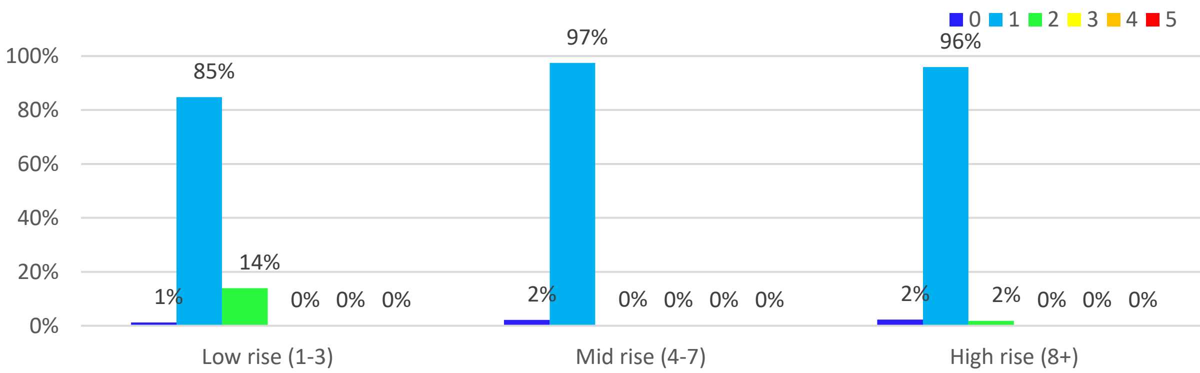

Figure 26: Graphical representation of damage to buildings in the centre of Thessaloniki for the "frequent" seismic event (above). Percentage distribution of damage by regulation level (middle) and by building height (bottom) for the "frequent" seismic event (mean).

T_{RC} = 70 yrs (mean - standard deviation)
Probability of exceedance: 84%

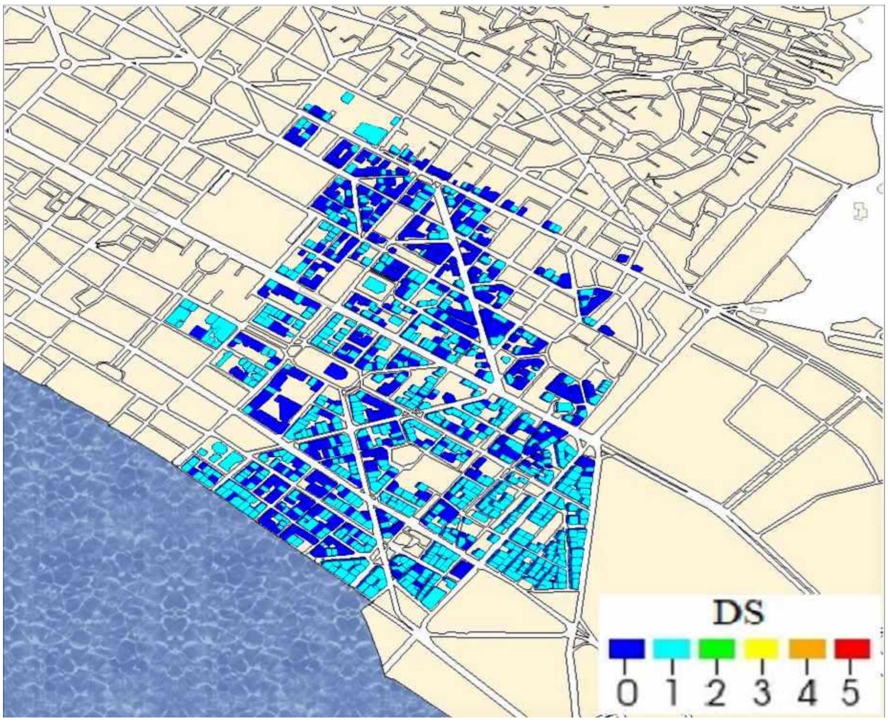

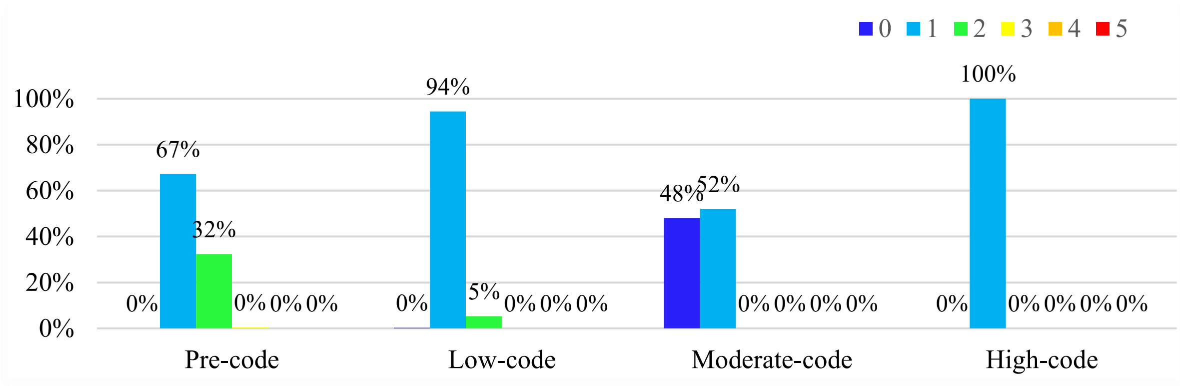

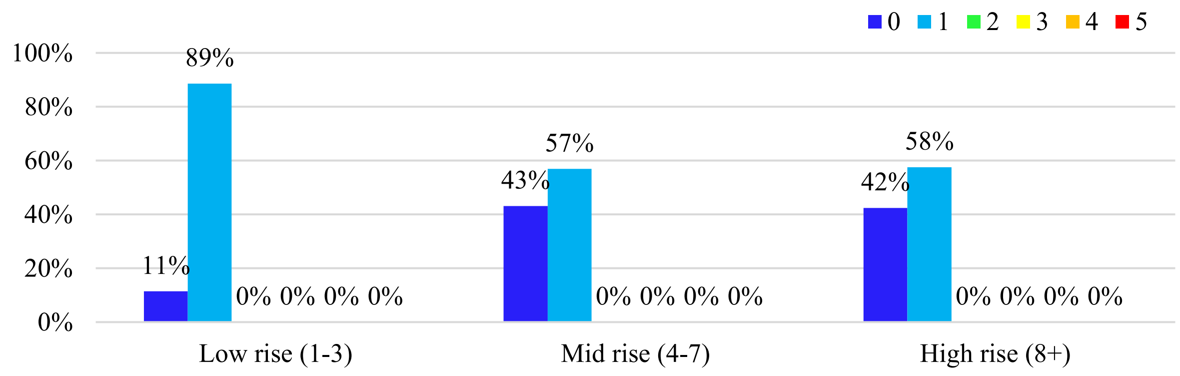

Figure 27: Graphical representation of damage to buildings in the centre of Thessaloniki for the "frequent" seismic event (above). Percentage distribution of damage by regulation level (middle) and by building height (bottom) for the "frequent" seismic event (mean-stdv).

TRC = 70 yrs (mean + standard deviation)
Probability of exceedance: 16%

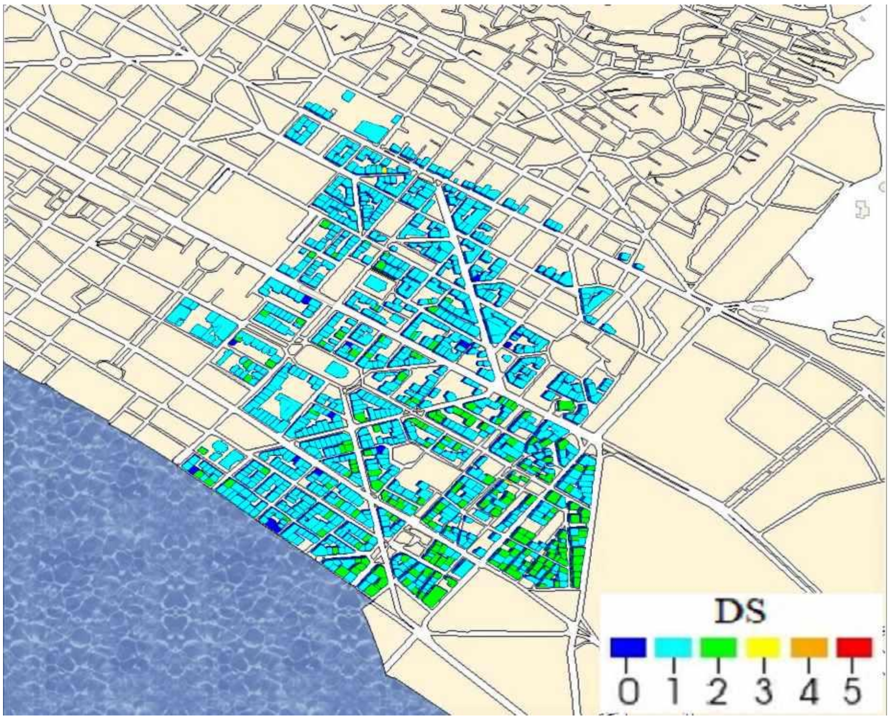

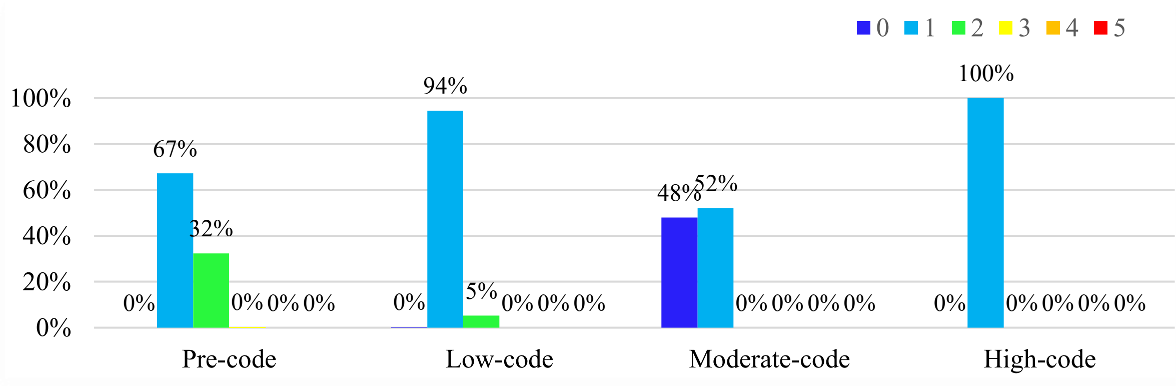

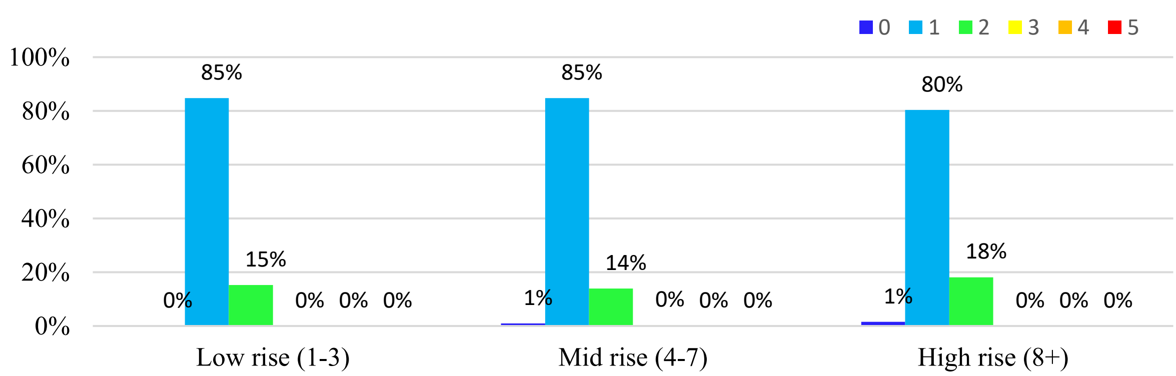

Figure 28: Graphical representation of damage to buildings in the centre of Thessaloniki for the "frequent" seismic event (above). Percentage distribution of damage by regulation level (middle) and by building height (bottom) for the "frequent" seismic event (mean+stdv).

Scenario 1 – Frequent earthquake with return period TRC = 70 years

- In the median case (Figure 26), performance is very good across the study area. By design level, only 5% of pre-code buildings reach DS2; all remaining buildings are in DS0 or DS1. By height, 14% of low-rise and 2% of high-rise buildings reach DS2, while the remainder are in DS0 or DS1.

- In the lower-bound case (mean - standard deviation; Figure 27), damage remains concentrated in pre-code buildings, 32% of which reach DS2. All other buildings are in DS0 or DS1.

- In the adverse case (mean + standard deviation; Figure 28), 32% of pre-code and 5% of low-code buildings reach DS2; all remaining buildings are in DS0 or DS1. By height, 15% of low-rise, 14% of mid-rise and 18% of high-rise buildings reach DS2.

5.4.2 Seismic Scenario 2: TRC = 475 years

T_{RC} = 475 yrs (mean)
Probability of exceedance: 50%

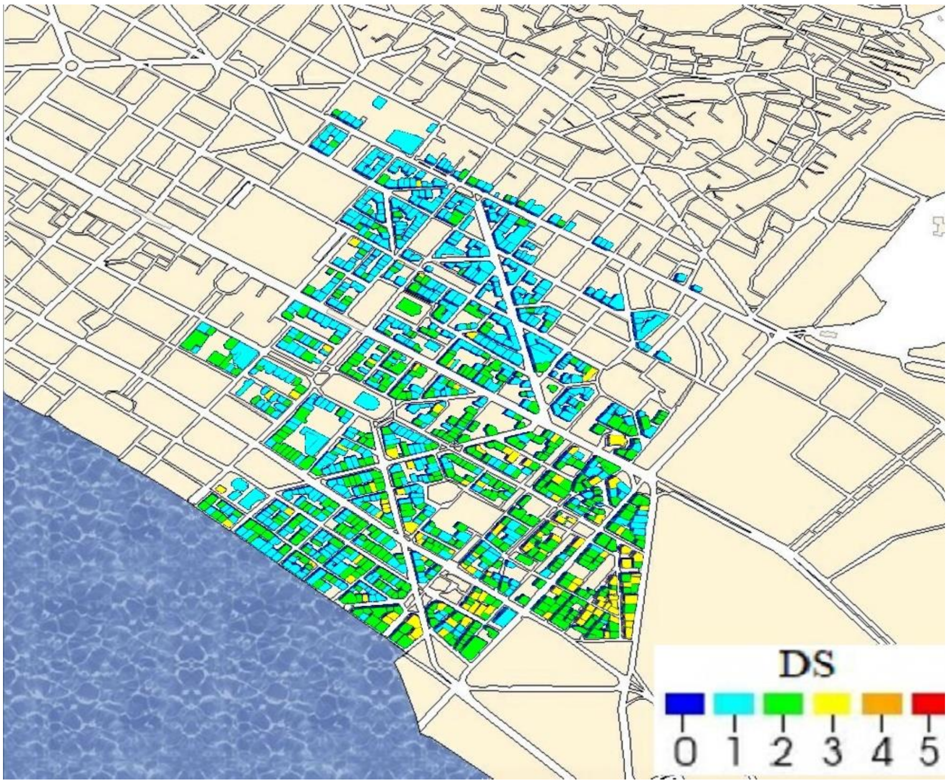

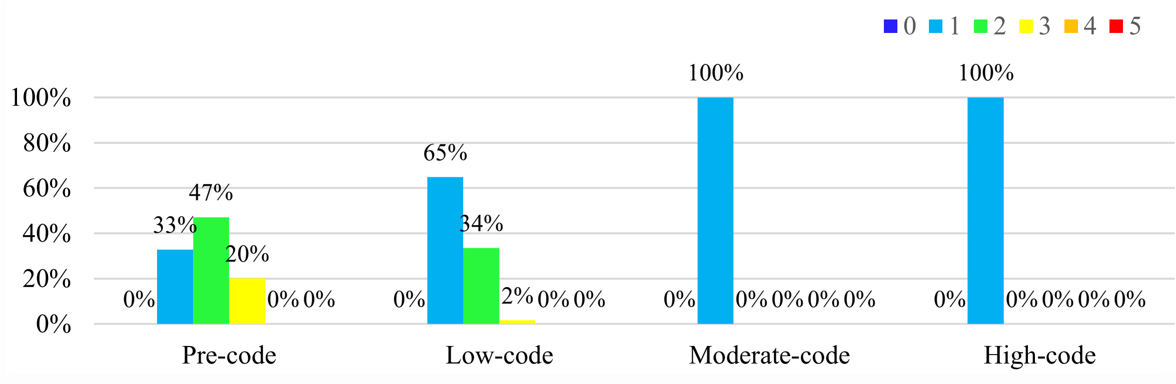

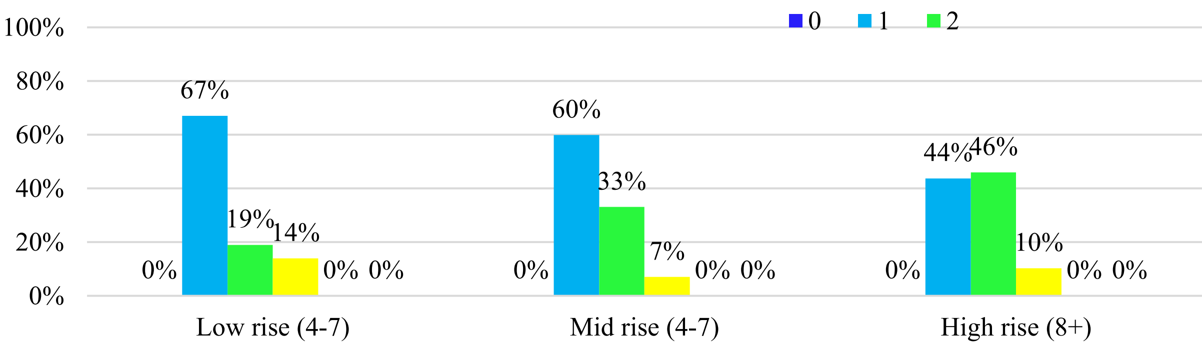

Figure 29: Damage map (top) and percentage distribution by seismic design level (middle) and building height (bottom) for the design-basis event (mean).

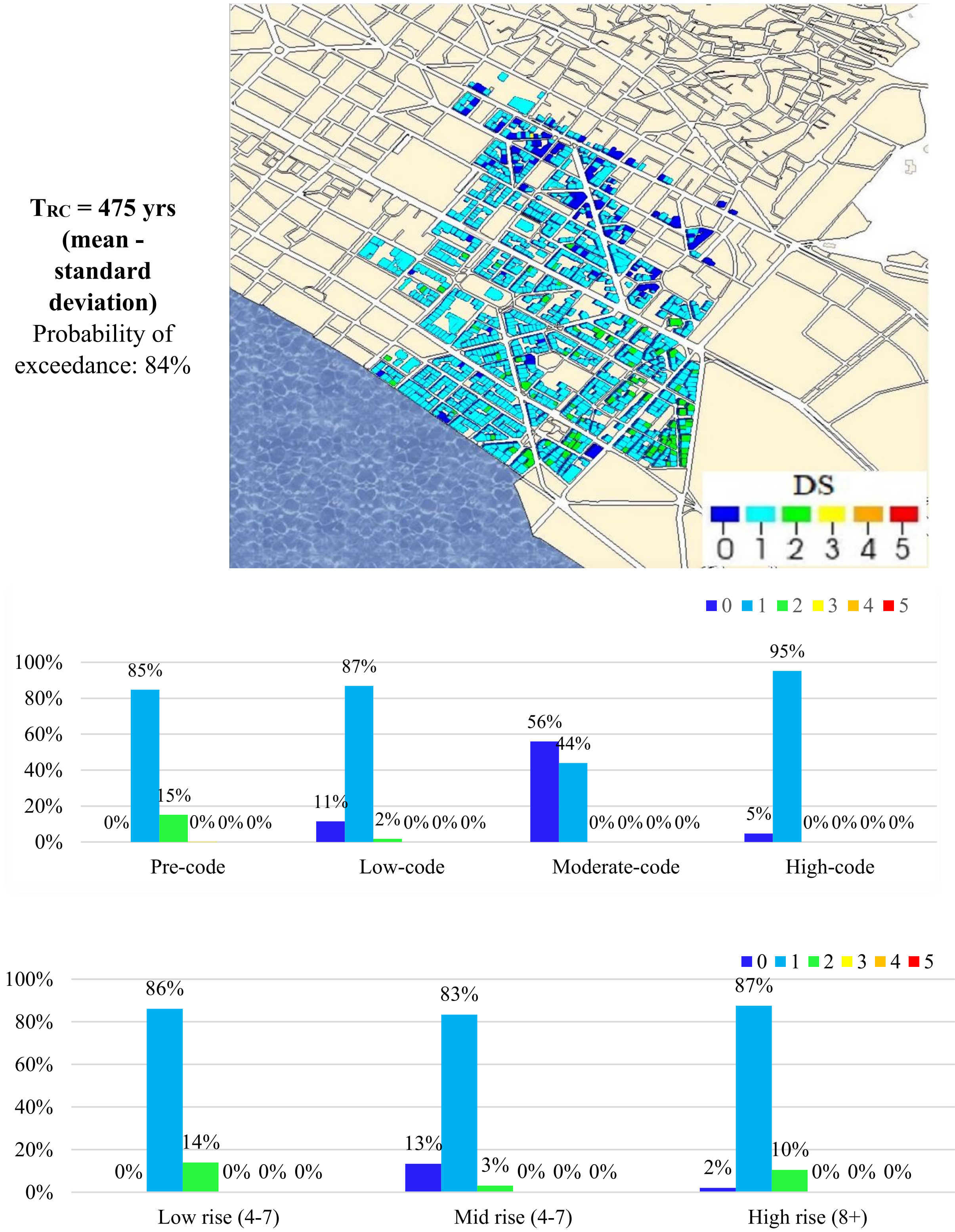

Figure 30: Damage map (top) and percentage distribution by seismic design level (middle) and building height (bottom) for the design-basis event (mean - standard deviation).

T_{RC} = 475 yrs (mean + standard deviation)
Probability of exceedance: 16%

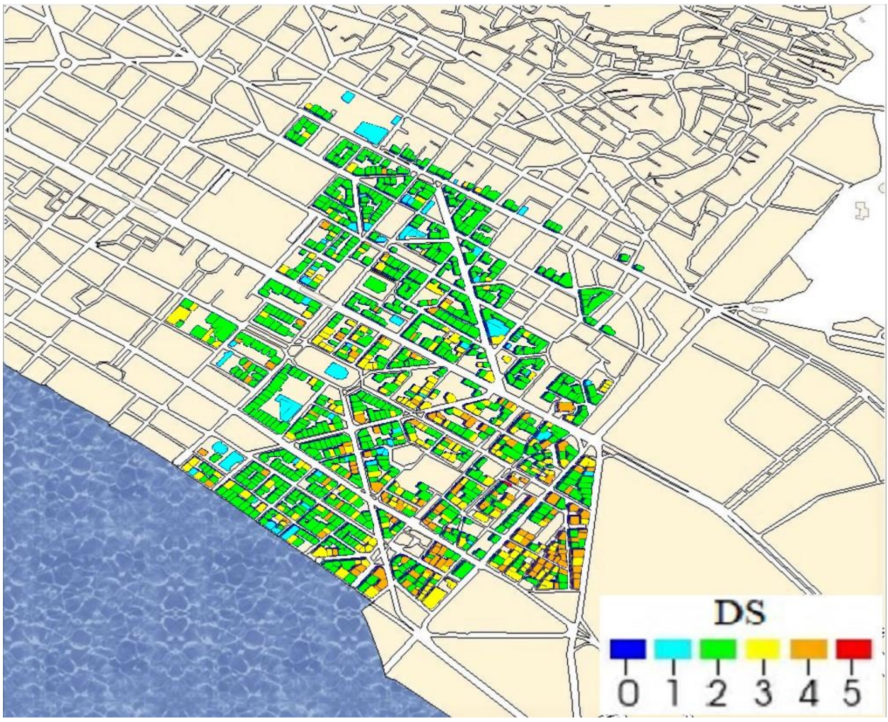

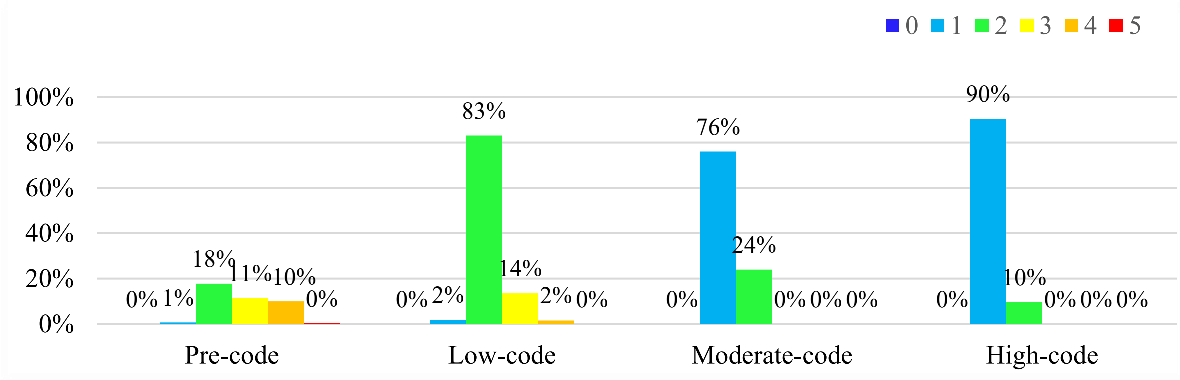

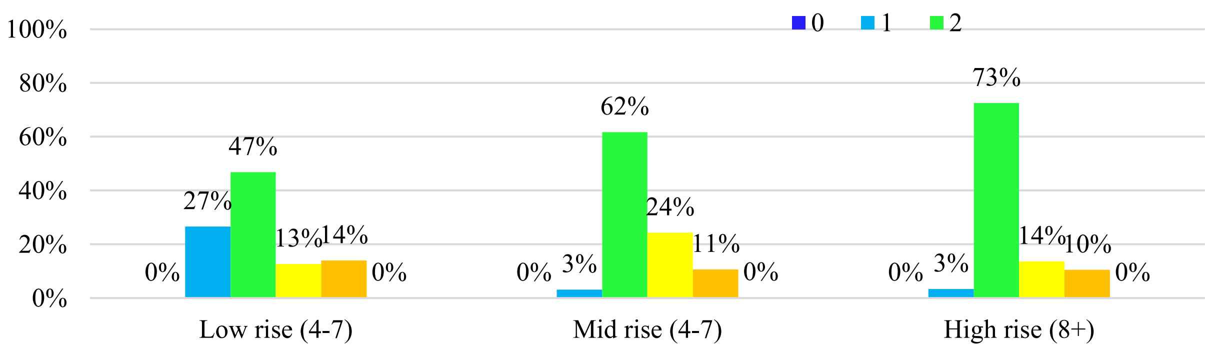

Figure 31: Damage map (top) and percentage distribution by seismic design level (middle) and building height (bottom) for the design-basis event (mean + standard deviation).

Scenario 2 – Design-basis earthquake with return period TRC = 475 years

- In the median case (Figure 29: Damage map (top) and percentage distribution by seismic design level (middle) and building height (bottom) for the design-basis event (mean).), 20% of pre-code and 2% of low-code buildings reach DS3. A further 47% of pre-code and 34% of low-code buildings reach DS2; the remaining buildings are in DS1. By height, DS3 affects 14% of low-rise, 7% of mid-rise and 10% of high-rise buildings, while DS2 affects 19%, 33% and 46%, respectively.

- In the lower-bound case (mean - standard deviation; Figure 30), 15% of pre-code and 2% of low-code buildings reach DS2, while the remaining buildings are in DS0 or DS1. By height, DS2 affects 14% of low-rise, 3% of mid-rise and 10% of high-rise buildings.

- In the adverse case (mean + standard deviation; Figure 31: Damage map (top) and percentage distribution by seismic design level (middle) and building height (bottom) for the design-basis event (mean + standard deviation).), DS4 affects 10% of pre-code and 2% of low-code buildings. DS3 affects 11% and 14%, respectively. DS2 affects 18% of pre-code, 83% of low-code, 24% of moderate-code and 10% of high-code buildings; the remaining buildings are in DS1. By height, DS4 affects 14% of low-rise, 11% of mid-rise and 10% of high-rise buildings; DS3 affects 13%, 24% and 14%; and DS2 affects 47%, 62% and 73%, respectively.

5.4.3 Seismic Scenario 3: TRC = 2,475 years

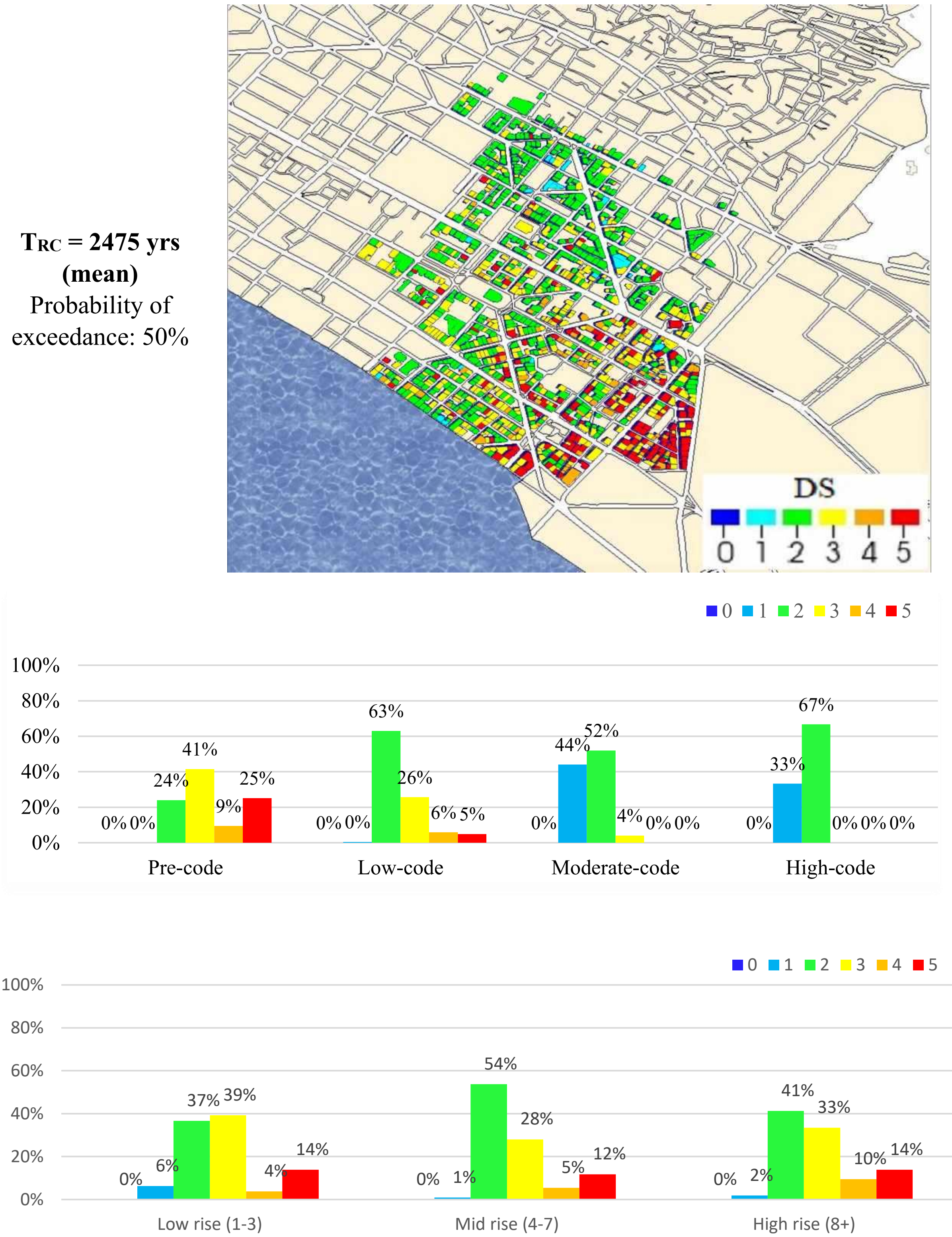

Figure 32: Graphical representation of damage to buildings in the centre of Thessaloniki for the rare seismic event (above). Percentage distribution of damage by regulation level (middle) and by building height (bottom) for the rare seismic event (mean).

T_{RC} = 2475 yrs (mean - standard deviation)
Probability of exceedance: 84%

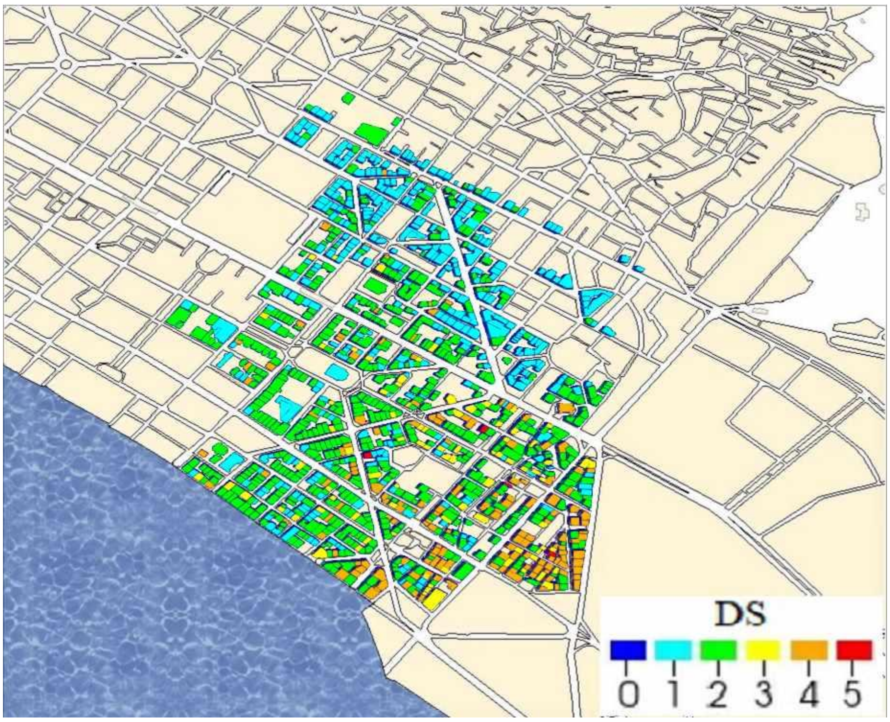

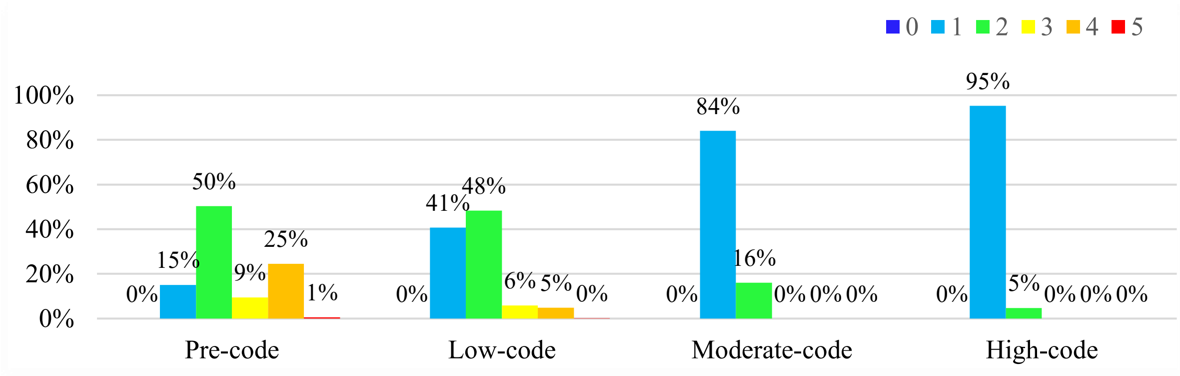

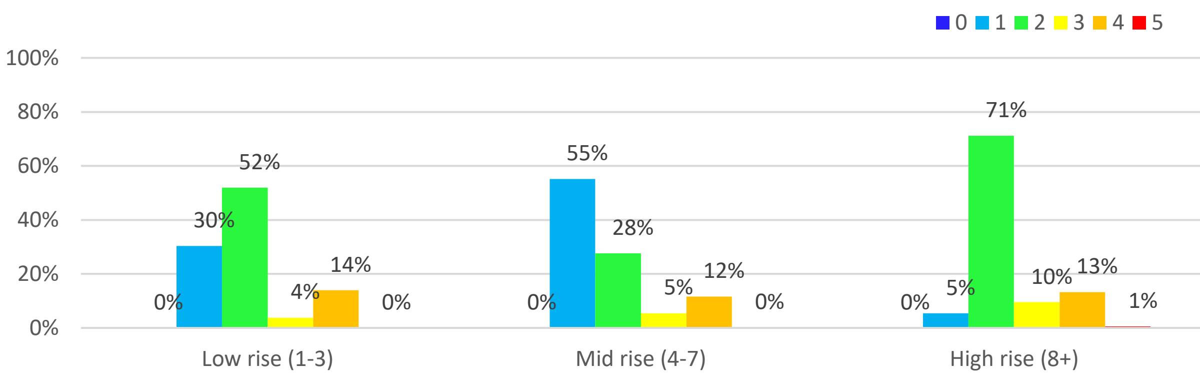

Figure 33: Graphical representation of damage to buildings in the centre of Thessaloniki for the rare seismic event (above). Percentage distribution of damage by regulation level (middle) and by building height (bottom) for the rare seismic event (mean-stdv).

T_{RC} = 2475 yrs (mean + standard deviation)
Probability of exceedance: 16%

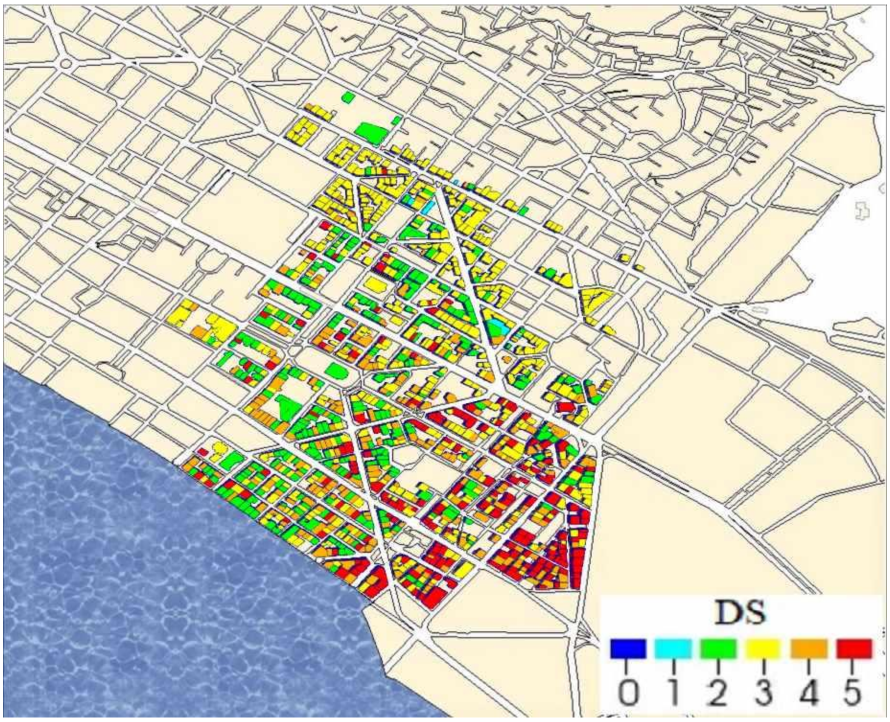

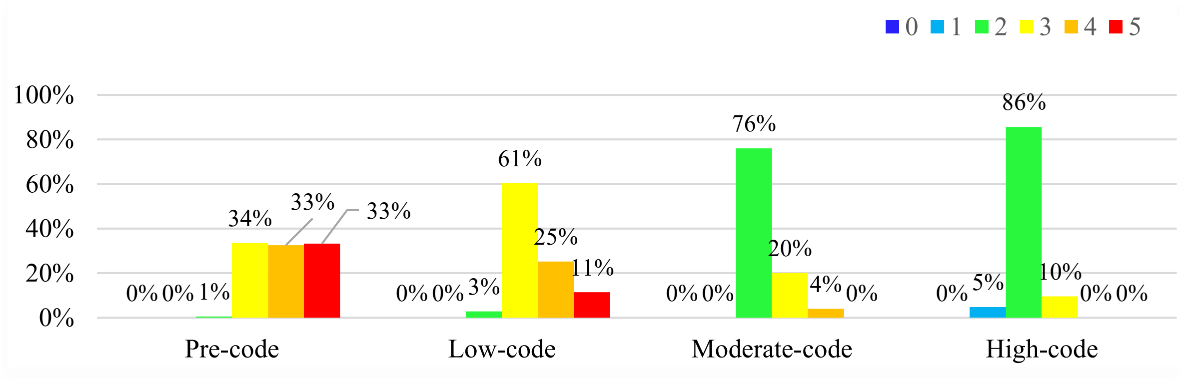

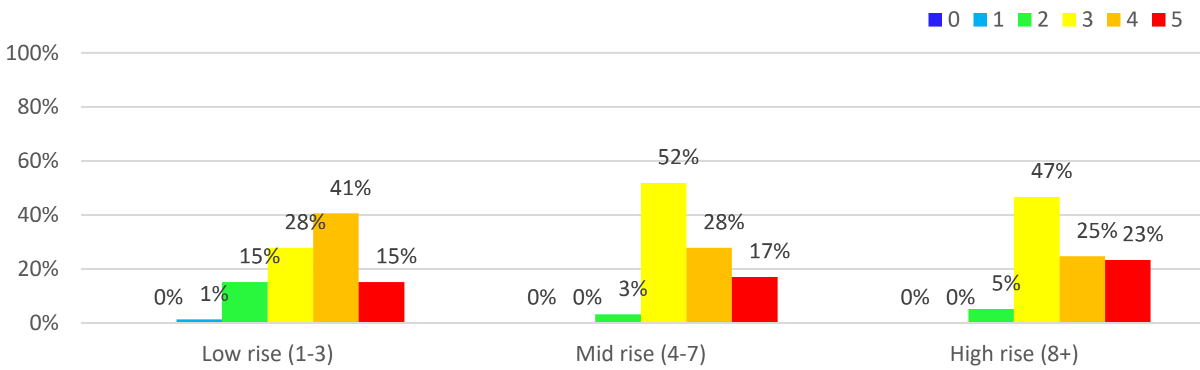

Figure 34: Graphical representation of damage to buildings in the centre of Thessaloniki for the rare seismic event (above). Percentage distribution of damage by regulation level (middle) and by building height (bottom) for the rare seismic event (mean+stdv).

Scenario 3 – Rare earthquake with return period TRC = 2,475 years

- In the median case (Figure 32), DS5 affects 25% of pre-code and 5% of low-code buildings; DS4 affects 9% and 6%, respectively; and DS3 affects 41% of pre-code, 26% of low-code and 4% of moderate-code buildings. DS2 affects 24% of pre-code, 63% of low-code, 52% of moderate-code and 67% of high-code buildings. By height, DS5 affects 14% of low-rise, 12% of mid-rise and 14% of high-rise buildings; DS4 affects 4%, 5% and 10%; DS3 affects 39%, 28% and 33%; and DS2 affects 37%, 54% and 41%, respectively.

- In the lower-bound case (mean - standard deviation; Figure 33), DS5 affects 1% of pre-code and 0.5% of low-code buildings; DS4 affects 25% and 5%; and DS3 affects 9% and 6%, respectively. DS2 affects 50% of pre-code, 48% of low-code, 16% of moderate-code and 5% of high-code buildings. By height, DS5 affects 0.5% of mid-rise and 1% of high-rise buildings; DS4 affects 14% of low-rise, 12% of mid-rise and 13% of high-rise buildings; DS3 affects 4%, 5% and 10%; and DS2 affects 52%, 28% and 71%, respectively.

- In the adverse case (mean + standard deviation; Figure 34), DS5 affects 33% of pre-code and 11% of low-code buildings. DS4 affects 33% of pre-code, 25% of low-code and 4% of moderate-code buildings. DS3 affects 34% of pre-code, 61% of low-code, 20% of moderate-code and 10% of high-code buildings. DS2 affects 1%, 3%, 76% and 86%, respectively. By height, DS5 affects 15% of low-rise, 17% of mid-rise and 23% of high-rise buildings; DS4 affects 41%, 28% and 25%; DS3 affects 15%, 52% and 47%; and DS2 affects 15%, 3% and 5%, respectively.

5.5 Results summary

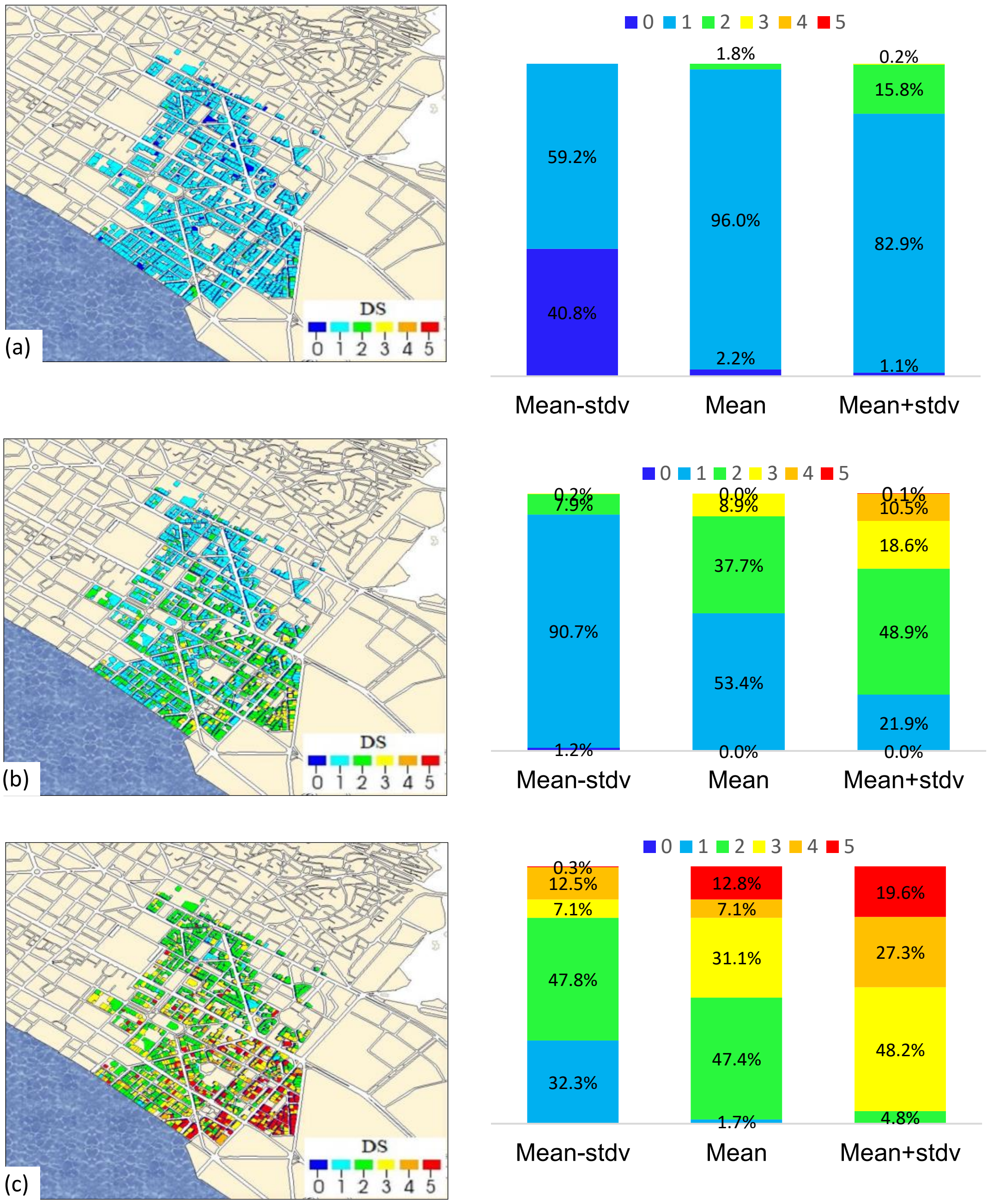

Figure 35: Damage maps for the (a) frequent, (b) design-basis and (c) rare earthquake scenarios.

Scenario 1 – Frequent earthquake with return period of T_{RC} = 70 years (Figure 35a)

- The RC buildings in central Thessaloniki perform very well, irrespective of seismic design level.
- In the median case, maximum damage is limited to DS2 in only 1.8% of buildings, while 96.0% experience slight damage, DS1.

- In the adverse case (mean + standard deviation), performance remains satisfactory. Only 0.1% of buildings reach the maximum damage level observed in this scenario; 53.0% are in DS1 and 40.7% remain in DS0.

Scenario 2 – Design-basis earthquake with return period TRC = 475 years (Figure 35b)

- The RC buildings perform satisfactorily under the design-basis earthquake, with no collapse in the median case and only isolated collapse in the adverse case.
- In the median case, the maximum damage is DS3, affecting 8.9% of buildings and concentrated primarily in pre-code buildings.
- In the adverse case, with a 16% probability of exceedance, only 0.1% of buildings collapse (DS5), while 10.5% reach DS4. Severe damage is concentrated in pre-code and low-code buildings, with pre-code buildings performing worst. Mid-rise buildings are slightly more susceptible than the other height classes.
- The highest damage levels occur along the south-eastern boundary of the study area, within macroseismic-intensity zone 3.

Scenario 3 – Rare earthquake with return period TRC = 2,475 years (Figure 35c)

- The building stock is highly vulnerable under the rare-event scenario, and the resulting losses indicate that the study area would not recover satisfactorily without substantial external resources.
- In the median case, 12.8% of buildings collapse (DS5), while a further 38.2% reach DS3 or DS4. Consequently, approximately 51% of the RC building stock becomes immediately non-functional.
- In the adverse case, with a 16% probability of exceedance, 19.8% of buildings collapse, 27.3% reach DS4 and 48.2% reach DS3. Almost the entire sample, particularly the pre-code and low-code stock, becomes non-functional.
- Moderate- and high-code buildings perform best: approximately 80% reach DS2 and the remaining 20% reach DS3.
- Mid- and high-rise buildings are slightly more susceptible to very heavy damage or collapse (DS4 and DS5).
- The highest damage levels are concentrated along the south-eastern boundary and coastal zone, mainly within macroseismic-intensity AREAS 2 and 3. Extensive collapse could block roads and impede movement of emergency-response and debris-clearance teams. An emergency plan should therefore distribute response resources across more than one operational centre.

5.6 Building damage using the colour card method

To present damage in a form familiar to Greek engineers, the EMS-98 damage states for the 1,252 buildings are converted to the green, yellow and red post-earthquake card categories. The correspondence follows Smerzini and Pitilakis (2018):

- ❖ GREEN: DS0 + DS1 + 30% of DS2
- ❖ YELLOW: 70% of DS2 + 50% of DS3
- ❖ RED: 50% of DS3 + DS4 + DS5

Table 12 presents the resulting card-category distribution for the three earthquake scenarios.

Table 12: Distribution of building damage using the card method for the three seismic scenarios.

Colour indication	**Scenario 1 TRC = 70 years**	**Scenario 2 TRC = 475 years**	**Scenario 3 TRC = 2,475 years**
	(mean)	**(mean)**	**(mean)**
GREEN	98.71%	64.74%	15.89%
YELLOW	1.29%	30.82%	48.69%
RED	0.00%	4.43%	35.42%

6 Earthquake resilience curves at the city scale

This chapter assesses losses in terms of lateral load-bearing capacity and repair and retrofitting costs for the three earthquake scenarios analysed in Chapter 5. It also estimates the time required to clear construction and demolition waste and to repair, retrofit or replace damaged buildings. These quantities are used to construct seismic resilience curves for the sample of 1,252 RC buildings.

6.1 Losses at city level

YouSimulator calculates the maximum building damage index, DI, for each scenario: frequent, design-basis and rare earthquakes with return periods TRC = 70, 475 and 2,475 years, respectively.

The remaining lateral load-bearing capacity, SI, of the 1,252 RC buildings is calculated using Equation (24).

$$SI(\%) = 100 \cdot (1 - \Delta SI) = 100 \cdot \left(1 - \left(\sum_{i=1}^{n} A_i \cdot DI_i \Big/ \sum_{i=1}^{n} A_i\right)\right) \quad (24)$$

where n = 1,252 is the number of RC buildings;

Ai is the footprint area of building i; and

DIi is the maximum damage index of building i.

Table 15 summarises functionality loss in terms of damaged footprint area, normalised by the total footprint area of the building stock. Losses are minor under the frequent scenario and minor to moderate under the design-basis scenario, but exceed 50% under the median rare-event scenario. The high losses reflect the predominance of pre-code and low-code buildings in the study area.

Table 13: Predicted functionality loss for the sample of 1,252 buildings.

	mean-stdv	**mean**	**mean+stdv**
	Remaining *SI* % (Losses Δ*SI* %)	Remaining *SI* % (Losses Δ*SI* %)	Remaining *SI* % (Losses Δ*SI* %)
Scenario T_{RC} = 70 yrs	94.2% (5.8%)	88.1% (11.9%)	81.7% (18.3%)
Scenario 2 T_{RC} = 475 yrs	87.8% (12.2%)	73.4% (26.6%)	58.9% (41.1%)
Scenario 3 T_{RC} = 2475 yrs	64.4% (35.6%)	46.7% (53.3%)	32.2% (67.8%)

6.2 Improvement of city functionality after repair and retrofitting

Modern intervention regulations, including KAN.EPE (OASP, 2022), distinguish between repair, which restores earthquake damage, and retrofitting, which increases seismic resistance and improves performance. KAN.EPE adopts performance level B1 (Life Protection) as the principal assessment objective for ordinary RC buildings under the design earthquake. This is broadly consistent with the life-safety objective of EAK/2000 and Eurocode 8 for new buildings. The post-intervention lateral load-bearing capacity of the 1,252-building sample is estimated by re-analysing the models under the assumptions listed below.

<u>Repair and retrofitting assumptions</u>

1. Pre-code buildings with very heavy damage, DS4, are assumed to be impractical to retrofit to KAN.EPE performance level B1 and are therefore demolished. These buildings are denoted DEM.
2. Buildings in DS0 and DS1 undergo repair only, without substantial strengthening, consistent with the cost model of Del Vecchio et al. (2020).
3. Buildings in DS5 are assumed to have collapsed and are replaced.
4. Buildings in DS2, DS3 and DS4, except the pre-code DS4 buildings identified above, are retrofitted to performance level B1 and are represented as high-code buildings in the post-intervention analyses.

Retrofitting produces new total lateral load-bearing-capacity indices, SInew, relative to the pre-earthquake capacity of the 1,252-building sample. Table 16 presents the percentage increase, ΔSI+, calculated using Equation (25).

$$\Delta SI^{+}(\%) = 100\left(\frac{SI_{new}}{SI} - 1\right) \quad (25)$$

Table 14: Percentage increase in lateral load-bearing capacity after intervention, ΔSI+.

	mean-stdv	**mean**	**mean+stdv**
	Increase ΔSI^{+}	Increase ΔSI^{+}	Increase ΔSI^{+}
Scenario 1 **T_{RC} = 70 yrs**	0%	0.3%	3.1%
Scenario 2 **T_{RC} = 475 yrs**	1.8%	11.9%	27.9%
Scenario 3 **T_{RC} = 2475 yrs**	23.0%	46.5%	73.6%

6.3 Repair and retrofitting costs

Repair and retrofitting costs are estimated using Del Vecchio et al. (2020), who compiled observed intervention costs for 120 RC buildings damaged during the 2009 Mw 6.3 L'Aquila earthquake in central Italy and related them to EMS-98 damage states.

The L'Aquila RC building stock is broadly comparable with common Greek construction, comprising frame and dual frame–wall systems with masonry infills (Figure 36).

Figure 36: Typical RC buildings damaged during the L'Aquila earthquake, Italy. Masonry infills are visible within the RC frames.

The repair and retrofitting methods represented in the source data are relatively recent, and Italian intervention regulations are aligned with Eurocode 8 Part 3 (Cosenza et al., 2018). The reported ratio of intervention cost to replacement cost is therefore considered suitable for an approximate application to Thessaloniki.

Del Vecchio et al. (2020) calculated total repair and retrofitting cost, REC, by summing all work required to return a building to service, expressed in €/m². For L'Aquila, the replacement cost, RECC, was €1,213.4/m². Normalised cost ratios are transferred to the Thessaloniki case.

Figure 37: Ratio of repair and retrofitting cost to replacement cost by damage state. shows the ratio of repair and retrofitting cost, REC, to replacement cost, RECC, for each damage state.

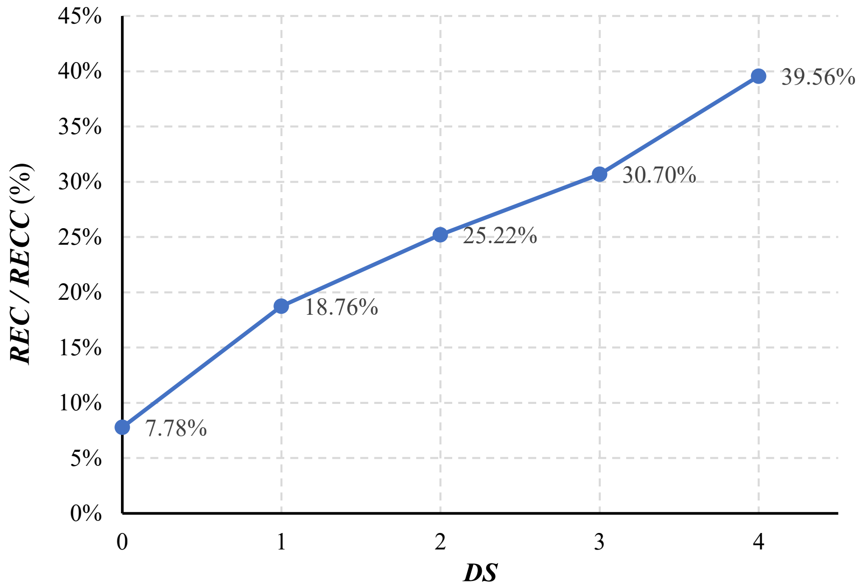

Figure 37: Ratio of repair and retrofitting cost to replacement cost by damage state.

Buildings classified as DS0 can still incur material costs because of damage to non-structural components, such as stairs, finishes and roofs, even when structural retrofitting is not required.

6.3.1 Estimation of repair and retrofitting costs for the Thessaloniki buildings

The total repair and retrofitting cost of the 1,252 buildings is estimated using Equation (26). The total intervention cost, ΣREC, is normalised by the total replacement cost, ΣRECC, of the sample.

$$\frac{\sum REC}{\sum RECC} = \frac{\left[0.0778\sum A_i^{DS0} + 0.1876\sum A_i^{DS1} + 0.2522\sum A_i^{DS2} + 0.3070\sum A_i^{DS3}\right]\times RECC}{\sum_1^N A_i \times RECC} + \frac{\left[0.3956\sum A_i^{DS4} + \sum A_i^{DEM} + \sum A_i^{DS5}\right]\times RECC}{\sum_1^N A_i \times RECC} \quad (26)$$

where:

ΣREC is the total repair and retrofitting cost;

ΣRECC is the total replacement cost;

N = 1,252 is the number of buildings in the study area; and

A_i^{DS}, the total area of the building, i, with damage level, DS [from 0-5] or DEM (m^2)

For comparison with recent Greek retrofit programmes (Moscholios et al., 2019), a pre-pandemic RC replacement cost of RECC = €1,100/m² is adopted. Table 17 presents the resulting costs for the median and confidence-bound cases.

Table 15: Repair and retrofitting costs for each earthquake scenario.

	mean-stdv		mean		mean+stdv	
	ΣREC / ΣRECC (%)	ΣREC (€)	ΣREC / ΣRECC (%)	ΣREC (€)	ΣREC / ΣRECC (%)	ΣREC (€)
Scenario 1 T_{RC} = 70 yrs	10.7%	289,315,792	18.5%	499,422,538	19.7%	530,713,364
Scenario 2 T_{RC} = 475 yrs	18.4%	495,238,397	22.4%	604,546,154	33.1%	892,167,563
Scenario 3 T_{RC} = 2475 yrs	31.3%	845,131,744	40.1%	1,082,804,813	52.7%	1,421,494,058

Repair costs remain substantial even under the frequent scenario. A loss of 11.9% in lateral load-bearing capacity corresponds to intervention costs equal to 18.5% of replacement cost. As damage becomes more severe, the cost ratio does not increase proportionally until collapse and demolition become significant; for the median rare-event scenario, a 53.3% capacity loss corresponds to intervention costs equal to 40.1% of replacement cost.

6.3.2 Pre-earthquake city-wide retrofit programme under KAN.EPE

Moscholios et al. (2019) reported cost data from the design of interventions to existing RC buildings under KAN.EPE. The ten buildings had poor structural characteristics and high importance classes, and the interventions were designed to achieve performance level B1, Life Protection.

Tender budgets before discount were used to calculate intervention cost per square metre of total floor area. The estimated range was €65–445/m², with a median of €156/m².

Because the interventions were designed under KAN.EPE and the costs represent relatively recent pre-pandemic prices, they are used to estimate a hypothetical programme for all pre-1985 RC buildings. These buildings comprise 96.3% of the sample and fall within the pre-code and low-code categories; assessment under KAN.EPE would be expected to identify substantial strengthening demand.

Using the median retrofit cost STRC = €156/m² and the total floor area of the pre-code and low-code buildings, the total median pre-earthquake retrofitting cost, ΣSTRC, is calculated using Equation (27):

$$\sum STRC = 156 \times \left(\sum A_i^{Pre\text{-}code} + \sum A_i^{Low\text{-}code} \right) \tag{27}$$

giving the following median total retrofit cost:

$$\sum STRC = 371{,}874{,}887 \text{ €}$$

To compare the alternatives, post-earthquake repair and retrofitting costs for the strengthened stock must also be included.

The design-basis and rare scenarios were therefore re-analysed after assigning the strengthened pre-code and low-code buildings to performance level B1 and modelling them as high-code buildings. This provides an approximate assessment of the benefits of a stock-wide pre-earthquake retrofit programme.

Table 16: Cost comparison for seismic Scenarios 2 and 3. presents median results with and without pre-earthquake retrofitting. Capacity losses, ΔSI and ΔSI*, and post-earthquake intervention costs, ΣREC and ΣREC*, are compared. The final column gives the combined pre-earthquake and post-earthquake cost, ΣSTRC + ΣREC*.

Table 16: Cost comparison for seismic Scenarios 2 and 3.

	Without pre-earthquake retrofitting (mean)		**With pre-earthquake retrofitting (mean)**		**Pre-earthquake retrofit cost ΣSTRC (€) (mean)**	**Total cost ΣSTRC + ΣREC* (€) (mean)**
	Losses ΔSI (%)	Repair Cost Σ*REC* (€)	Losses ΔSI* (%)	Repair Cost Σ*REC** (€)		
Scenario 2 T_{RC} = 475 yrs	26.6%	604,546,154	17.5%	405,118,724	371,874,887	776,993,611
Scenario 3 T_{RC}=2475 yrs	53.3%	1,082,804,813	31.7%	650,985,404	371,874,887	1,022,860,291

For Scenario 2, the combined cost ΣSTRC + ΣREC* exceeds the post-earthquake intervention cost ΣREC without pre-earthquake retrofitting.

$$\sum STRC + \sum REC^* = 776{,}993{,}611\,€ > \sum REC = 604{,}546{,}154\ €$$

Given the satisfactory performance of the stock under the design-basis earthquake, a uniform pre-earthquake retrofit programme for all old buildings is not economically favourable under Scenario 2.

For Scenario 3, however, the combined cost ΣSTRC + ΣREC* is slightly lower than the post-earthquake intervention cost ΣREC without pre-earthquake retrofitting.

$$\sum STRC + \sum REC^* = 1{,}022{,}860{,}291\,€ < \sum REC = 1{,}082{,}804{,}813\ €$$

Avoiding widespread collapse, casualties, displacement and prolonged interruption of economic activity provides additional benefits that are not captured fully by the direct cost comparison. A targeted or broader pre-earthquake retrofit programme is therefore more strongly justified for the rare-event scenario.

6.4 Estimation of total repair time of the city

Following Del Vecchio et al. (2020), interventions are divided into simple repairs for DS0–DS1 and repair plus retrofitting for DS2–DS4. Based on consultation with engineers experienced in repair and retrofitting, the duration of substantial interventions is taken as approximately two-thirds of the time required for full replacement, TREC. Simple repairs for DS0–DS1 are taken as one-tenth of full replacement time.

Table 19 presents construction activity in the Region of Central Macedonia for 2022. Table 20 estimates the 2022 regional construction workforce using detailed 2011 census data and national employment statistics.

Table 17: Construction activity data for the year 2022 (ELSTAT, 2022b).

Construction of the Region of Central Macedonia ***Period: 01/2022–12/2022***	
New-build floor area (m²)	622,816
Added floor area (m²)	235,140
Total floor area (m²/year)	**857,956**
Total floor area (m²/month)	**71,496**

Table 18: Available labour.

Sector	ELSTAT's latest detailed census (2023a) of the labour force in Greece (2011 census)		Employment data for the year 2022 (ELSTAT, 2023b)	
	Workforce Nationwide	Workforce Central Macedonia Region	Workforce Nationwide	Workforce Central Macedonia Region
Construction (general)	**254,081**	**34,191**	**197,247**	26,543
Building construction	**124,776**	**15,910**	96,866	**12,351**

❖ Values in bold are taken directly from official statistics for 2011 and 2022. Values in red are the estimated 2022 regional figures obtained by scaling the latest detailed 2011 census data for the labour force and construction sector.

The construction productivity derived from Tables 19 and 20 is:

Pw = 71,496/12,351 = 5.78 m²/month/person

An initial workforce of 1,500 employees is assumed for recovery of the city centre under each scenario. This represents approximately 12% of the construction workforce in Central Macedonia.

The total building-restoration time, STREC, is calculated using Equation (28):

$$\Sigma T_{REC} = \frac{\left[0.1\left(\Sigma A_i^{DS_0} + \Sigma A_i^{DS_1}\right) + 0.66\left(\Sigma A_i^{DS_2} + \Sigma A_i^{DS_3} + \Sigma A_i^{DS_4}\right) + \left(\Sigma A_i^{DEM} + \Sigma A_i^{DS_5}\right)\right]}{(P_w \times N)} \quad (28)$$

where:

ΣTREC is the total restoration time for central Thessaloniki (months);

Pw = 5.78 m²/month/person is the construction productivity derived from 2022 ELSTAT data;

N is the number of workers employed in repair and retrofitting; and

A_i^{DS} , the total area of the building, i, with damage level, DS [from 0-5] or DEM (m^2)

Important note:
The 1,252-building sample cannot be assumed to represent the entire Municipality of Thessaloniki, which contains 24,173 buildings (ELSTAT, 2022a). Building typologies and macroseismic-intensity zones vary across the municipality, so direct extrapolation would be unjustified. Generalisation beyond the study area, or beyond the 3,707-building damage database shown in Figure 12, requires development of a municipality-wide model. The purpose of this report is to establish and demonstrate the methodology.

6.4.1 Time required to clear construction and demolition waste from the city centre

City recovery after a major earthquake is affected by many interacting factors that can delay the start of repair and retrofitting. These include blocked access caused by collapse, the time required to clear construction and demolition waste (CDW), damage to transport and utility networks, funding constraints and the effectiveness of public administration.

The delay before reconstruction is estimated indirectly from the annual CDW-processing capacity of waste-management facilities in Central Macedonia.

Kourmousis (2014) used on-site measurements from 30 construction sites to estimate waste-density factors and annual CDW generation by region for 1997–2012. The resulting model was used to determine the processing capacity required for rational regional CDW management.

Using ELSTAT construction-activity data for 1997–2009, Kourmousis (2014) estimated that Central Macedonia required capacity for 438,000 tonnes of CDW per year under normal operation, assumed to use 50% of the available days. For emergency planning, the present study assumes that facilities could operate at full capacity, giving 876,000 tonnes per year.

The study estimated the average CDW volume generated by demolition of an existing RC building as:

CDW volume, CDWV = 0.80 m^3/m^2

and the average density as:

CDW density, CDWD = 1.6 t/m^3

Table 21 lists buildings classified as collapsed (DS5) or designated for demolition (DEM). The total footprint area of these buildings is converted to CDW volume and mass using CDWV and CDWD. This mass is then compared with the assumed annual processing capacity for Central Macedonia.

For an approximate upper-bound estimate, the damage distribution in the 1,252-building sample is extrapolated to the 3,707 RC buildings in the database of Panou et al. (2014) using the factor 3,707/1,252 = 2.96. This extrapolation is used only for the CDW estimates and should not be interpreted as a municipality-wide prediction.

Table 19: Estimated minimum CDW-management time for the three earthquake scenarios.

	Scenario 1 TRC = 70 years		**Scenario 2 TRC = 475 years**		**Scenario 3 TRC = 2,475 years**	
	mean	**mean + standard deviation**	**mean**	**mean + standard deviation**	**mean**	**mean + standard deviation**
Building collapses	0	0	0	1	96	246
Demolished buildings (DEM)	0	0	0	124	46	162
CDW-generating building area (m^2)	0	0	0	227,108	420,062	731,535
CDW volume (m^3)	0	0	0	181,686	336,050	585,228
CDW mass (t)	0	0	0	290,698	537,680	936,364
Maximum annual CDW-management capacity (t/year)	876,000	876,000	876,000	876,000	876,000	876,000
Required CDW-management time after ×2.96 scaling (years)	0	0	0	0.98	1.82	3.16

Estimated delay, TD (months)	0	0	0	11.8	21.8	38

6.5 Resilience curves

The parameters summarised in Tables 15, 16 and 21 are used to construct seismic resilience curves for the study-area building stock. Equation (28) gives the repair and retrofitting time, TREC, for the 1,252 buildings. Figure 38 first presents all scenarios for a workforce of 1,500. Additional curves for Scenarios 2 and 3 use 2,500 workers, based on the assumption described below.

Under Scenarios 2 and 3, extraordinary reconstruction demand is assumed to mobilise 50% of the national construction workforce in proportion to the study-area share of the municipal building stock:

$(1{,}252/24{,}173) \times 0.50 \times 96{,}866 \approx 2{,}500$ workers

Resilience curves are presented for the median case only.

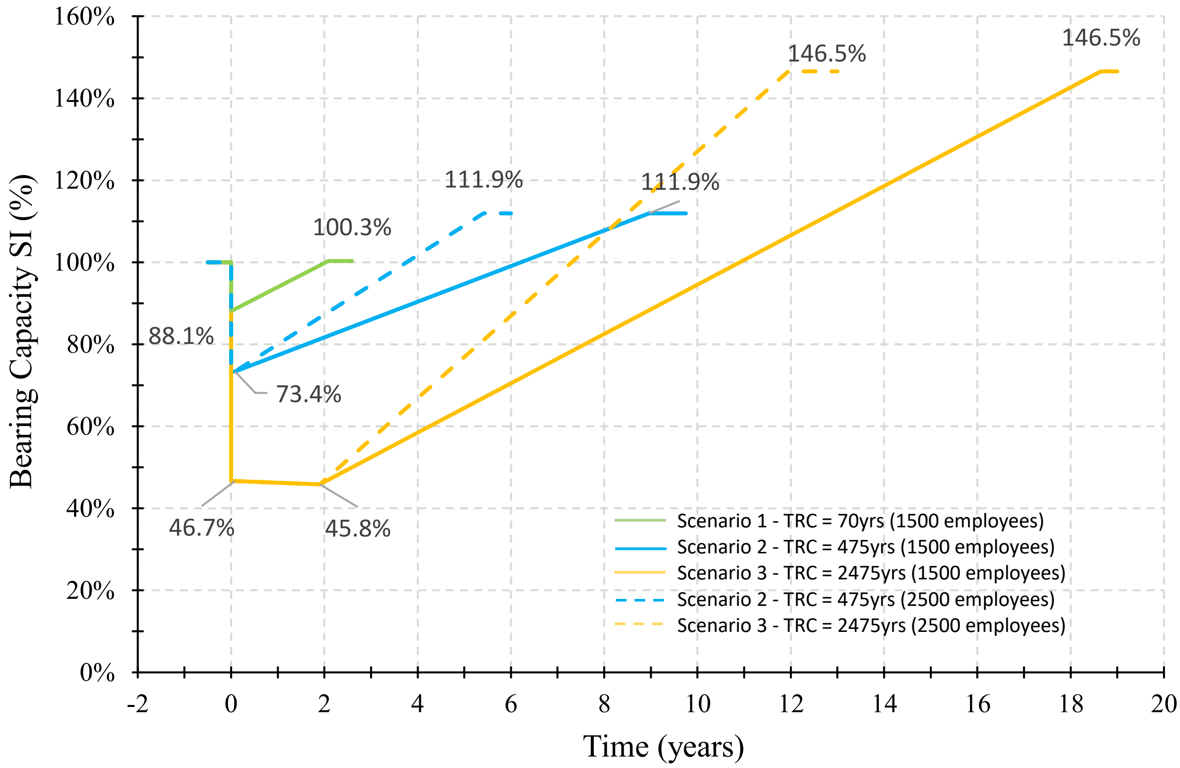

Figure 38: Resilience curves for the three earthquake scenarios based on median SI values.

Figure 38 shows that workforce availability has a major influence on recovery time. The 1,500-worker case represents approximately 12% of the regional construction workforce. Increasing the workforce to 2,500 for Scenarios 2 and 3, approximately 20% of the regional total, substantially shortens the recovery period, as shown by the dashed curves.

6.6 Results summary

<u>Scenario 1 – Frequent earthquake with return period TRC = 70 years</u>

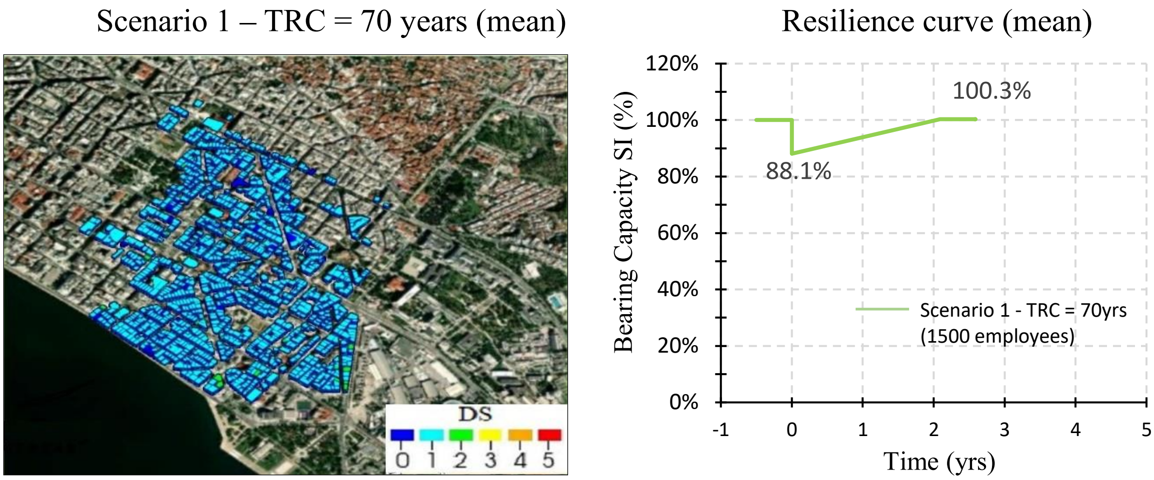

Figure 39: Building damage map and seismic resilience curve of the centre of Thessaloniki – Scenario 1 (mean).

- The RC building stock in central Thessaloniki performs satisfactorily under the frequent scenario, irrespective of seismic design level.
- In the median case, the instantaneous loss of lateral load-bearing capacity is 11.9%.
- A workforce of 1,500 can complete the repair works in approximately two years. Despite the generally light damage, the median repair cost is substantial at 18.5% of replacement cost, compared with an 11.9% loss of capacity.
- Post-repair capacity increases by only 0.3% relative to the pre-earthquake condition.
- Repair cost is significant even under the frequent scenario because non-structural damage contributes to intervention cost. As structural damage increases, the cost ratio does not rise proportionally until collapse and demolition become important.

Scenario 2 – Design-basis earthquake with return period TRC = 475 years

Scenario 2 – TRC = 475 years (mean) | Resilience curve (mean)

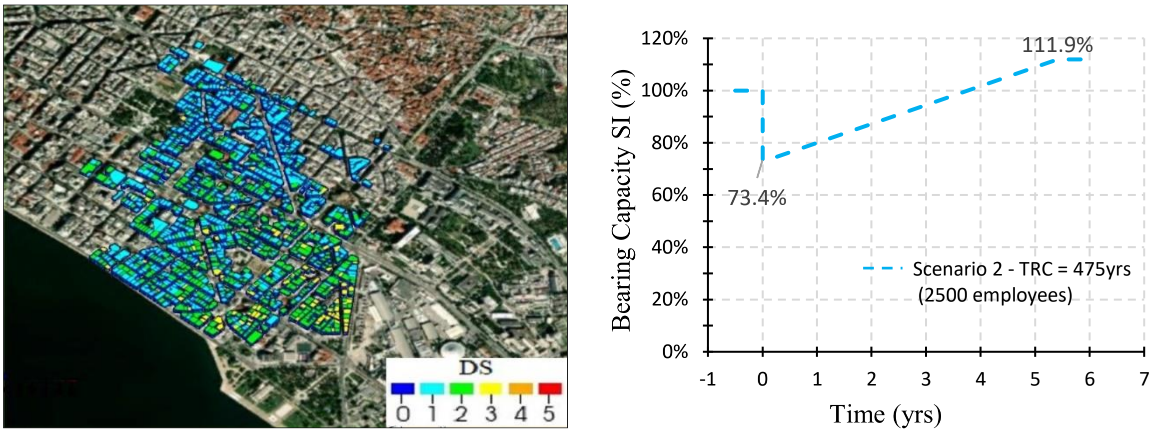

Figure 40: Building damage map and seismic resilience curve for central Thessaloniki – Scenario 2 (mean).

- The RC building stock performs satisfactorily under the design-basis scenario, with no collapse in the median case.
- In the median case, the instantaneous loss of lateral load-bearing capacity is 26.6%.
- The greatest damage occurs along the south-eastern boundary of the study area, within macroseismic-intensity zone 3.
- A workforce of 2,500 can complete the intervention works in approximately five years. The median repair and retrofitting cost is 22.4% of replacement cost.
- Post-intervention lateral load-bearing capacity increases by 11.9% relative to the pre-earthquake condition.
- In the adverse case (mean + standard deviation), approximately 290,698 tonnes of CDW are generated, requiring an estimated 11.8 months to manage under the stated capacity assumptions.
- A universal pre-earthquake retrofit programme for all pre-1985 RC buildings is not economically favourable under Scenario 2. A targeted programme focused on the most vulnerable buildings is more appropriate.

$$\sum STRC + \sum REC^* = 776{,}993{,}611\,€ > \sum REC = 604{,}546{,}154\ €$$

<u>Scenario 3 – Rare earthquake with return period TRC = 2,475 years</u>

Scenario 3 – TRC = 2,475 years (mean)

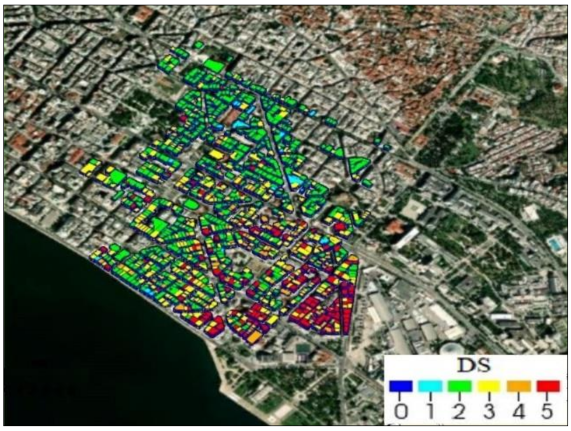

Resilience curve (mean)

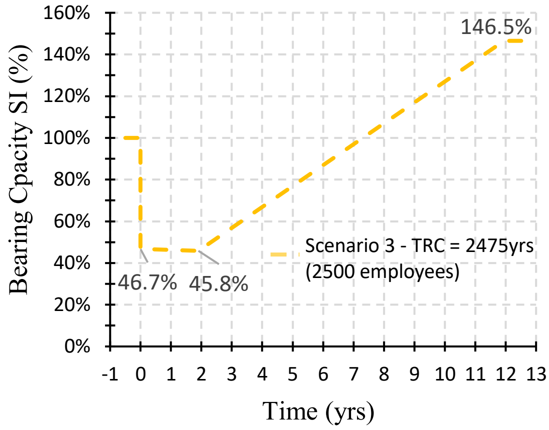

Figure 41: Building damage map and seismic resilience curve of the centre of Thessaloniki – Scenario 3 (mean).

- The RC building stock is highly vulnerable under the rare-event scenario. The greatest damage is concentrated along the south-eastern boundary and coastal zone of the study area.
- In the median case, the instantaneous loss of lateral load-bearing capacity is 53.3%.
- A workforce of 2,500 can complete recovery works in approximately 12 years. The median repair and retrofitting cost is 40.1% of replacement cost.
- The assumed CDW-management capacity in Central Macedonia is insufficient for the rare-event scenario.
- Post-intervention lateral load-bearing capacity increases by 46.5% relative to the pre-earthquake condition.
- In the adverse case, approximately 936,364 tonnes of CDW are generated, requiring an estimated 38 months to manage. In the median case, the corresponding values are 537,680 tonnes and 21.8 months.
- The delay between the earthquake and completion of debris clearance is potentially substantial. Additional temporary storage and processing areas would be required under the rare-event scenario.
- A pre-earthquake retrofit programme for the pre-1985 RC stock is a credible risk-reduction strategy for the rare-event scenario and is also favourable in the direct cost comparison presented here.

$$\sum STRC + \sum REC^* = 1{,}022{,}860{,}291 € < \sum REC = 1{,}082{,}804{,}813 \; €$$

7 Conclusions

The principal conclusions of the study are as follows:

- YouSimulator was adapted for application to Greek cities and used to develop a validated city-scale model of 1,252 RC buildings. The framework combines automated modelling, nonlinear time-history analysis, a generalised damage index, three-dimensional visualisation and recovery metrics to support rapid prioritisation of risk-reduction measures.
- Under the frequent scenario (TRC = 70 years), the median loss of lateral load-bearing capacity is 11.9%, while repair cost is 18.5% of replacement cost.
- Under the design-basis scenario (TRC = 475 years), the median analysis predicts no collapse, but the 26.6% loss of lateral load-bearing capacity is significant.
- Under the rare scenario (TRC = 2,475 years), more than 50% of lateral load-bearing capacity is lost in the median case. Widespread severe damage, collapse and demolition extend recovery to approximately 12 years, compared with about five years for the design-basis scenario.
- With 1,500 workers, repair after the frequent scenario takes approximately two years. With 2,500 workers, recovery takes approximately five years for the design-basis scenario and 12 years for the rare scenario. Median intervention costs are 18.5%, 22.4% and 40.1% of replacement cost for the frequent, design-basis and rare scenarios, respectively.
- Retrofitting all pre-1985 RC buildings is not economically favourable under Scenario 2, because the direct benefits do not offset the programme cost. A targeted programme should therefore prioritise the most vulnerable buildings. For the rare-event scenario, broader retrofitting is more favourable and can substantially reduce collapse risk and post-earthquake losses.
- In adverse cases, estimated CDW generation reaches 290,698 tonnes in Scenario 2 and 936,364 tonnes in Scenario 3. Under the assumed processing capacity, management would take approximately 11.8 and 38 months, respectively. Additional temporary storage and processing capacity would be required to avoid prolonged delays.
- Damage is particularly severe along the south-eastern boundary and coastal areas. Concentrated collapse could divide the study area, restrict east–west access, hinder rescue operations and delay debris removal.

Additional conclusions on the seismic performance of the central Thessaloniki RC building stock are as follows:

- Vulnerability is concentrated in the pre-code and low-code buildings constructed before 1985, which together represent 96.3% of the sample.
- Mid- and high-rise buildings are slightly more susceptible to severe and very severe damage than low-rise buildings.
- Many pre-1959 buildings reaching DS4 under the design-basis or rare scenarios are likely to require demolition. Retrofitting damaged buildings to the KAN.EPE B1 performance level would substantially reduce the vulnerability of the post-earthquake building stock.
- Damage depends strongly on building age and macroseismic-intensity zone. Extrapolating the results directly to the whole municipality would therefore be overly conservative and potentially misleading. Any municipality-wide application should represent spatial variations in site response explicitly.
- Expected structural losses are minor under the frequent scenario and minor to moderate under the design-basis scenario, but extensive under the rare scenario, for which the median instantaneous functionality loss exceeds 50%.

8 Future research recommendations

Some recommendations for future research are as follows:

- The present dynamic city model represents 1,252 RC buildings in central Thessaloniki. Future work should extend the inventory to the whole municipality and include other construction types, particularly load-bearing masonry.
- The software can scale ground motions for incremental dynamic analysis, enabling development of fragility curves for regional building typologies.
- A municipality-wide model could be linked to real-time ground-motion data on an operational platform. Subject to data availability and validation, civil-protection services could then obtain rapid estimates of damage distribution after a strong earthquake and use them to coordinate response resources.
- Comparable models should be developed for other Greek cities, particularly where observed damage databases are available for calibration and validation.

9 References

ACI (2011). *Building code requirements for structural concrete and commentary, (ACI 318-11/318R-11)*. American Concrete Institute, Farmington Hills, Michigan.

Alexoudi, M., Anastasiadis, A., Argyroudis, S. A., Kakderi, K. and Pitilakis, K. (2007). Seismic zonation, vulnerability assessment and loss scenarios in Thessaloniki. In: *2nd Japan–Greece Workshop on Seismic Design, Observation and Retrofit of Foundations*. Available at: https://www.researchgate.net/publication/281838152_Seismic_zonation_vulnerability_assessment_and_loss_scenarios_in_Thessaloniki (accessed 14 September 2022).

Amirzadeh, M., Sobhaninia, S. and Sharifi, A. (2022). Urban resilience: A vague or an evolutionary concept? *Sustainable Cities and Society*, 81, 103853. https://doi.org/10.1016/j.scs.2022.103853.

Applied Technology Council (1996). ATC-40: Seismic evaluation and retrofit of concrete buildings, Rep. SSC 96-01, CSSC-ATC, Redwood City, Calif.

Arendt, L., Cimellaro, G. P., Reinhorn, A. M. and Renschler, C. (2016). PEOPLES: A framework for evaluating resilience. *Journal of Structural Engineering*, 142(10), 04016063. https://doi.org/10.1061/(ASCE)ST.1943-541X.0001514.

Bai, X., Dou, Y., Daniell, J., He, C., Huang, Q., Robinson, D.T., Shi, P., Xu, F., Yan, J., Zhao, B. and Zhang, Q. (2021), A Global Analysis of the Relationship Between Urbanization and Fatalities in Earthquake-Prone Areas, *International Journal of Disaster Risk Science*, 12(6), pp.805–820. doi:10.1007/s13753-021-00385-z.

Barbat, A. H., Carreño, M. L., Pujades, L. G., Lantada, N., Cardona, O. D. and Marulanda, M. C. (2010). Seismic vulnerability and risk evaluation methods for urban areas: A review with application to a pilot area. *Structure and Infrastructure Engineering*, 6(1–2), 17–38. https://doi.org/10.1080/15732470802663763.

Banica, A., Rosu, L., Muntele, I. and Grozavu, A. (2017). Towards Urban Resilience: A Multi-Criteria Analysis of Seismic Vulnerability in Iasi City (Romania). *Sustainability*, 9(2), p.270. doi:10.3390/su9020270.

Blaikie, P., Cannon, T., Davis, I. and Wisner, B. (2004). *At Risk: Natural Hazards, People's Vulnerability and Disasters,* 2nd ed. London: Routledge.

Bruneau, M. and Reinhorn, A. (2006), Overview of the Resilience Concept, In: *8th U.S. National Conference on Earthquake Engineering*.

Bruneau, M., & MacRae, G. (2017). Reconstructing Christchurch: A seismic shift in building structural systems. *The Quake Centre, University of Canterbury.*

Bruneau, M., Elhami-Khorasani, N. and Salado Castillo, J. G. (2022). Functionality measures for quantification of building seismic resilience index. *Engineering Structures*, 253, 113800. https://doi.org/10.1016/j.engstruct.2021.113800.

Chen, X., Zhang, L., Lin, X., Skalomenos, K. A. and Chen, Z. (2024). A clustering-based analysis method for simulating seismic damage of buildings in large cities. *Engineering Structures,* 307, 117860. https://doi.org/10.1016/j.engstruct.2024.117860.

Chen X, Jiang L, Skalomenos KA, Lin X, Zhu B (2022), Investigation on the seismic performance of single-span R/C frame school buildings retrofitted with wing walls under different seismic intensities, *Structures*, 44, 1945-1961, https://doi.org/10.1016/j.istruc.2022.08.113

Chen X, Zhang Y, Wang Z, Yu J, Skalomenos KA, Xu O (2022), Shaking table tests on a 5-storey unreinforced masonry structure strengthened by ultra-high ductile cementitious composites, *Journal of Building Engineering*, 104635, https://doi.org/10.1016/j.jobe.2022.104635

Chen, X., Lin, X., Zhang, L. and Skalomenos, K. A. (2022). Method for rapidly generating urban damage scenarios under non-uniform ground-motion input based on matching algorithms and time-history analyses. *Soil Dynamics and Earthquake Engineering,* 152, 107055. https://doi.org/10.1016/j.soildyn.2021.107055.

Cimellaro, G.P., Domaneschi, M., Mahin, S. and Scutiero, G. (2017), Exploring Simulation Tools For Urban Seismic Analysis And Resilience Assessment, *Proceedings of the 6th International Conference on Computational Methods in Structural Dynamics and Earthquake Engineering (COMPDYN 2015)*. doi:10.7712/120117.5549.18264.

Cosenza E, Del Vecchio C, Di Ludovico M, et al. (2018) The Italian Guidelines for seismic risk classification of constructions: Technical principles and validation. *Bulletin of Earthquake Engineering* 16: 5905–5935

Costa, G., Moratto, L., Suhadolc, P., and Triantafyllidis, P. (2007). Source Modeling of the Kozani and Arnea 1995 Events with Strong Motion Estimates for the City of Thessaloniki. *Journal of Earthquake Engineering*, 11(4), pp.560–581. doi:10.1080/13632460601188035

Del Vecchio, C., Di Ludovico, M. and Prota, A. (2020). Repair costs of reinforced-concrete building components: From actual data analysis to calibrated consequence functions. *Earthquake Spectra*, *36*(1), 353–377.

CEN (2004). EN 1998-1:2004+A1:2013, *Eurocode 8: Design of Structures for Earthquake Resistance – Part 1: General Rules, Seismic Actions and Rules for* Buildings. Brussels: European Committee for Standardization.

ESRI (2022). *ArcMap Resources for ArcGIS Desktop | Download & Documentation*. https://www.esri.com/en-us/arcgis/products/arcgis-desktop/resources

FEMA (2018). *Seismic Performance Assessment of Buildings, Volume 1: Methodology, FEMA P-58-1, 2nd ed*. Washington, DC: Federal Emergency Management Agency.
Available at: https://femap58.atcouncil.org/

FEMA (2022). *Hazus Earthquake Model Technical Manual* (Hazus-5.1), Federal Emergency Management Agency (July 2022) https://www.fema.gov/sites/default/files/documents/fema_hazus-earthquake-model-technical-manual-5-1.pdf

Frerks, G., Warner, J. and Weijs, B. (2011), The politics of vulnerability and resilience, *Ambiente & Sociedade*, 14(2), pp.105–122. doi:10.1590/s1414-753x2011000200008.

Giannaraki G. (2018). Seismic risk assessment in the city of Aegion through stochastic simulation of
strong ground motion (Master's thesis). Retrieved from: https://www.researchgate.net/profile/Georgia-Giannaraki/publication/329400856_Seismic_risk_assessment_in_the_city_of_Aigion_with_stochastic_simulation_of_strong_ground_motion_NKUA_in_Greek.pdf

Goldsworthy, M., Haines, J. and Jackson, J. (2002). The continuity of active fault systems in Greece. *Geophysical Journal International,* 148(3), 596–618.

Greek Anti-Seismic Regulation, EAK/2000 (1999). Official Gazette 2184/B'20.12.1999, Approval of the Greek Anti-Seismic Regulation.

Retrieved from: https://elinyae.gr/sites/default/files/2019-07/b2184_1999.1129186130082.pdf

Grünthal, G. (ed.) (1998). European Macroseismic Scale 1998 (EMS-98). Cahiers du Centre Européen de Géodynamique et de Séismologie, 15. Luxembourg: Centre Européen de Géodynamique et de Séismologie. https://doi.org/10.2312/EMS-98.full.en.

Hansapinyo, C., Latcharote, P. and Limkatanyu, S. (2020). Seismic Building Damage Prediction From GIS-Based Building Data Using Artificial Intelligence System. *Frontiers in Built Environment,* 6. doi:10.3389/fbuil.2020.576919.

Hellenic Statistical Authority [ELSTAT] (2022a). Characteristics of houses - households / 2011. Retrieved from: https://www.statistics.gr/el/statistics/-/publication/SAM05/2011.

Hellenic Statistical Authority [ELSTAT] (2022b). Building activity. Retrieved from: https://www.statistics.gr/en/statistics/-/publication/SOP03/2022-M12

Hellenic Statistical Authority [ELSTAT] (2023a). Economic characteristics. Retrieved from: https://www.statistics.gr/el/statistics/-/publication/SAM04/2011

Hellenic Statistical Authority [ELSTAT] (2023b). Employment. Retrieved from: https://www.statistics.gr/el/statistics/-/publication/SEL21/-

Hori, M. (2011). *Introduction To Computational Earthquake Engineering (2nd Edition)*. World Scientific.

House, R. and Wallemacq, P. (2018). *Economic losses, poverty & disasters: 1998-2017*. https://www.undrr.org/publication/economic-losses-poverty-disasters-1998-2017.

ITSAK (2023). GIS Hellenic Accelerograms Database - GHEAD v1.0. Retrieved from: http://ghead.itsak.gr/

Joshi, P.K., Priyanka, N. and Sinha, N. (2014). Using Spatial Multi-Criteria Analysis and Ranking Tool (SMART) in earthquake risk assessment: a case study of Delhi region, India. *Geomatics, Natural Hazards and Risk*, 7(2), pp.680–701. doi:10.1080/19475705.2014.945100.

KAN.EPE. (2022) Code of Structural Interventions. 3rd Edition. Athens: Earthquake Planning and Protection Organization. Available at: https://ecpfe.oasp.gr

Kappos, A. J. (2013). Seismic Vulnerability and Loss Assessment for Buildings in Greece. In: Gueguen, P. (Ed.), *Seismic Vulnerability of Structures*. (pp. 111-159). Wiley-ISTE. ISBN 1118603966. doi: 10.1002/9781118603925.ch3.

Kappos, A.J., Panagopoulos, G., Panagiotopoulos, C. and Penelis, G. (2006). A hybrid method for the vulnerability assessment of R/C and URM buildings. *Bulletin of Earthquake Engineering*, 4(4), pp.391–413. doi:10.1007/s10518-006-9023-0.

Koliopoulos, P. K., Margaris, B. N., & Klimis, N. S. (1998). Duration and energy characteristics of Greek strong motion records. *Journal of Earthquake Engineering*, 2(3), 391-417.

Kourmousis, F. M. (2014). Development of construction and demolition waste management units (PhD thesis). Available from: DSpace, NTUA. Retrieved from: http://dspace.lib.ntua.gr/xmlui/handle/123456789/38956

Le Grand, H. and Oreskes, N. (2018). Plate Tectonics: An Insider's History of the Modern Theory of the Earth. Boca Raton, FL: CRC Press.

Lin, X., Chen, X., Wang, F., He, X., Zhang, L. and Skalomenos, K. A. (2020). Real-time physics-based regional earthquake-disaster simulation using structural-monitoring data. In: *Proceedings of the 17th World Conference on Earthquake Engineering*, Sendai, Japan, 13–18 September 2020.

Lin, X., Wang, K., Skalomenos, K. A. and Zhang, L. (2019). Development of a simulation platform to model, assess and visualise earthquake disasters at the city scale. In: *Proceedings of the 2nd International Conference on Natural Hazards and Infrastructure*, Chania, Greece, 23–26 June 2019.

Lu, X., & Guan, H. (2017). *Earthquake disaster simulation of civil infrastructures*. Singapore: Springer.

Lu, X., Han, B., Hori, M., Xiong, C., & Xu, Z. (2014). A coarse-grained parallel approach for seismic damage simulations of urban areas based on refined models and GPU/CPU cooperative computing. *Advances in Engineering Software*, *70*, 90-103.

Lucantoni, A., Bosi, V., Bramerini, F., De Marco, R., Lo Presti, T., Naso, G. and Sabetta, F. (2001). Il rischio sismico in Italia. *Ingegneria Sismica*, 1, 5–36.

Makropoulos, K.C. (2010). Earthquakes and preventive measures. *Bulletin of the Geological Society of Greece*, 43(1), p.216. doi:10.12681/bgsg.11175.

Mastroberti, M., Mitidieri, L., Tataranna, S. and Vona, M. (2018), New resilience model of communities based on numerical evaluation and observed post seismic reconstruction process, *International Journal of Disaster Risk Reduction*, 28, pp.602–609. doi:10.1016/j.ijdrr.2018.01.010.

Meerow S, Newell JP and Stults M (2016). Defining urban resilience: A review. *Landscape and Urban Planning*, 147: 38-49. doi:10.1016/j.landurbplan.2015.11.011.

Moscholios, P., Vlahakis, G., Karagiannakis, Z., Bardakis, B. (2019). Economics of Modern Interventions (EN1998-3, KAN.EPE.). In the 4th Panel. Syn. of Anti-Seismic Technology & Technical Seismology, Athens September 5-7, 2019. ETAM/TEE.

Mouroux, P., & Brun, B. L. (2006). Presentation of RISK-UE project. *Bulletin of Earthquake Engineering*, *4*, 323-339.

New Greek Anti-Seismic Regulation, NEAK (1992). Official Gazette 613/B`12.10.1992, Approval of the Greek Anti-Seismic Regulation. Retrieved from: https://elinyae.gr/sites/default/files/2020-02/613%CE%92_1992.pdf

Nicholls, R., (2022), Macroscopic Analysis of Seismic Building Performance in the City of Thessaloniki, MSc dissertation, University of Birmingham.

OASP (1997). Instructions and Forms for Direct Primary Post-earthquake Inspection of Buildings for Use. Athens: Ministry for the Environment, Physical Planning and Public Works.

OASP (2001). Recommendations for Pre-earthquake and Post-earthquake Interventions in Buildings. Athens: Ministry for the Environment, Physical Planning and Public Works. Available at: https://www.oasp.gr/sites/default/files/Recommendations%20for%20foreshock%20and%20aftershock%20Interventions%20in%20buildings.pdf

Organization for Earthquake Planning and Protection (OASP) (2022). "Regulation of Interventions (KAN.EPE.)", 3rd Revision.

Oliveira, C.S., Ferreira, M.A. and Mota Sa, F. (2014). Earthquake Risk Reduction: From Scenario Simulators Including Systemic Interdependency to Impact Indicators. In: *Perspectives on European Engineering and Seismology Volume 1*. London: Springer Open, pp.309–330.

Pacific Earthquake Engineering Research Center, PEER (2023). *Ground Motion Database*. https://ngawest2.berkeley.edu/.

Panou, A.A., Hatzidimitriou, P.M., Theodoulidis, N., Styliandis, K.C., Triantafyllidis, P. and Zacharopoulos, S. (2014). Comparison of damage data from questionnaires and field survey: the case of the June 20, 1978 Thessaloniki (northern Greece) M6.5 earthquake. *Bulletin of Earthquake Engineering*, 12, pp.2821–2841. doi:10.1007/s10518-014-9599-8.

Pitilakis, K., (2010), Geotechnical Seismic Engineering, Thessaloniki: Ziti.

Proag, V. (2014). The Concept of Vulnerability and Resilience. *Procedia Economics and Finance*, 18(18), pp.369–376. doi:10.1016/s2212-5671(14)00952-6.

Rofooei, F.R., Sangaki, A.H., and Vafai, H. (2021), Probabilistic integrated framework and models compatible with the reliability methods for seismic resilience assessment of structures, *Structures*, [online] 34, pp.4086–4099. doi:10.1016/j.istruc.2021.09.089.

RD-59, Seismic Regulation Royal Decree (1959). Official Gazette 36/A'/19.2.1959, Royal Decree, On the anti-seismic regulation of building works. Retrieved from: http://www.episkeves2.civil.upatras.gr/wp-content/uploads/2015/12/AK-1959.pdf

Skalomenos KA, Morfidis K, Lekidis V, Anagnostopoulos SA (2021), Innovative Eurocode 8-compliant solutions for selection of the optimum retrofitting scheme of buildings with special characteristics, *Earthquake Spectra*, 37(4), 2857-2891, https://doi.org/10.1177/87552930211023519

Shchukin, V. and Skalomenos, K. (2022). Assessing earthquake resilience of urban areas: The 2014 Ludian earthquake. In: *Proceedings of the Partnership Development Workshop on Urbanisation and Resilience against Natural and Man-made Disasters*, University of Wolverhampton, UK, 13–16 December 2022.

Shchukin, V., Skalomenos, K., Stathis, P.-M. and Lin, X. (2023). City-wide macroscopic analysis of seismic building performance in Thessaloniki, Greece. In: *Proceedings of the SECED 2023 Conference*, Cambridge, UK, 14–15 September 2023.

Smerzini, C., & Pitilakis, K. (2018). Seismic risk assessment at urban scale from 3D physics-based numerical modeling: the case of Thessaloniki. *Bulletin of Earthquake Engineering*, *16*, 2609-2631.

Steelman, J. S., & Hajjar, J. F. (2009). Influence of inelastic seismic response modeling on regional loss estimation. *Engineering Structures*, *31*(12), 2976-2987.

Squillacote, A. H., Ahrens, J., Law, C., Geveci, B., Moreland, K. and King, B. (2007). *The ParaView* Guide. Clifton Park, NY: Kitware.

Tsapanos, T.M. (2008), Seismicity and Seismic Hazard Assessment in Greece. NATO Science Series: IV: Earth and Environmental Sciences, pp.253–270. doi:10.1007/978-1-4020-6815-7_17.

USRC (2019). *USRC Building Rating System for Earthquake Hazards: Implementation Manual. Available* at: https://usrc.org/files/technicalresource/USRC%20IMPLEMENTATION%20MANUAL%2010152015.pdf

Wada, A., & Hirose, K. (1989). Building frames subjected to 2D earthquake motion. *Seismic Engineering*, 388-397.

Xiaorui, Z. (2022). Investigation of Financial Loss Caused by Earthquake in a City. MSc dissertation, University of Birmingham.

Xiong, C., Lu, X., Guan, H., & Xu, Z. (2016). A nonlinear computational model for regional seismic simulation of tall buildings. *Bulletin of Earthquake Engineering*, *14*, 1047-1069.

Xiong, C., Lu, X., Lin, X., Xu, Z., & Ye, L. (2017). Parameter determination and damage assessment for THA-based regional seismic damage prediction of multi-story buildings. *Journal of Earthquake Engineering*, *21*(3), 461-485.

Yamada, S., Ishida, T., & Shimada, Y. (2012). Collapse Behavior and Ultimate Earthquake Resistance of Weak Column Type Multi-Story Steel Frame with RHS Columns. In *20th Analysis and Computation Specialty Conference* (pp. 532-541).

Zeqin, L. (2020). Earthquake Damage Visualisation of Building Structures in Urban Areas. MSc dissertation, University of Birmingham.

Zhang Y, Lin X, Wang T, Skalomenos KA (2021), Seismic behavior of masonry walls retrofitted by precast reinforced concrete panels with different connection details, *Engineering Structures*, 242 (112597), https://doi.org/10.1016/j.engstruct.2021.112597

APPENDIX A

Table A1: Building-damage descriptions and corresponding YouSimulator damage-index ranges.

Seismic damage degree	Seismic damage index	Definition
Essentially intact	0.0-0.10	All structural components are intact, although some non-structural components may be slightly damaged. The structure can be used without repair.
Minor	0.10-0.30	Visible cracks occur in some components. The structure can be used without repair or after minor repair.
Moderate	0.30-0.55	Most structural components have slight cracks and a few have more pronounced cracking. Some non-structural components are seriously damaged. The structure can be used after general repair.
Severe	0.55-0.85	Most structural components are seriously damaged, and some non-structural components have partially collapsed. Repair is difficult.
Collapse	0.85-1.0	The structure has collapsed or is on the verge of collapse and is not repairable.

```
REmedium2.txt - Σημειωματάριο
Αρχείο  Επεξεργασία  Μορφή  Προβολή  Βοήθεια
363
Building 192 0.0 0.0 3 6 3
BuiltYear 2003
GMScaleFactor 1.0 1.0
StrengthModificationFactor 2.1
UltimateSDRModificationFactor 1.0
MeasuredT1 0.7
BaseHeight 0
CountryNo 2
Site 0.15 0.6 0.16 1 3.5 0.9
1
ExPolygon 7 18 6
2295313.24 4063256.64
2295319.14 4063262.27
2295329.94 4063257.6
2295327.13 4063252.31
2295328.03 4063249.65
2295315.33 4063246.82
2295313.24 4063256.64
0
Building 193 0.0 0.0 3 6 3
BuiltYear 1965
GMScaleFactor 1.0 1.0
StrengthModificationFactor 1.4
UltimateSDRModificationFactor 1.0
MeasuredT1 0.7
BaseHeight 0
CountryNo 2
Site 0.15 0.6 0.16 1 3.5 0.9
1
ExPolygon 5 18 6
2295360.62 4063253.75
2295367.48 4063262.13
2295383.24 4063254.91
2295376.70 4063246.9
2295360.62 4063253.75
0
Building 194 0.0 0.0 3 5 3
BuiltYear 1953
GMScaleFactor 1.0 1.0
StrengthModificationFactor 1.729
UltimateSDRModificationFactor 1.2
MeasuredT1 0.59
BaseHeight 0
CountryNo 2
Site 0.15 0.6 0.16 1 3.5 0.9
```

Figure A1: Example of a building-data input file.

```
Number of points
5416
Interval [sec]
0.01
Null
0.0
Acceleration X [cm/s/s]
-0.143568369
-0.213870557
-0.308150739
```

Figure A2: Example of a ground-motion input file.

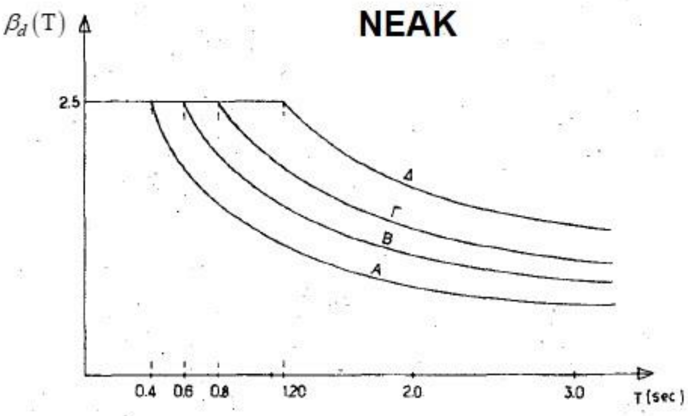

$$\Phi_d(T) = a_g \gamma_1 \frac{\beta_d(T)}{q} \cdot n \cdot \theta$$

$$\beta_d(T) = \begin{cases} 2.5 & \gamma\iota\alpha \quad T < T_2 \\ 2.5(T_2/T)^{2/3} & \gamma\iota\alpha \quad T > T_2 \end{cases}$$

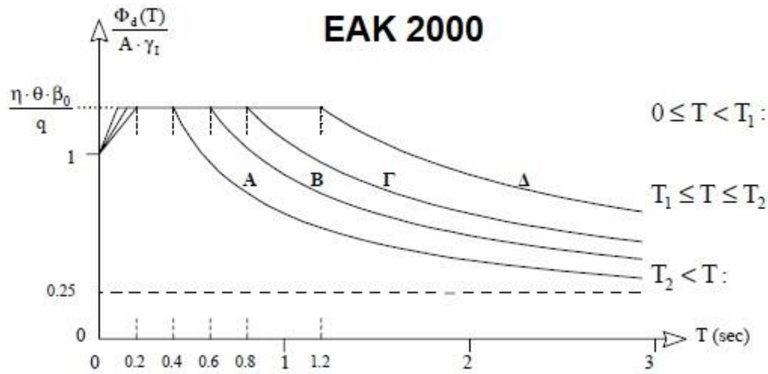

$$0 \le T < T_1: \quad \Phi_d(T) = \gamma_I \ a_g \left[1 + \frac{T}{T_1}\left(\frac{\eta \cdot \theta \cdot \beta_0}{q} - 1\right)\right]$$

$$T_1 \le T \le T_2: \quad \Phi_d(T) = \gamma_I \ a_g \frac{\eta \cdot \theta \cdot \beta_0}{q}$$

$$T_2 < T: \quad \Phi_d(T) = \gamma_I \ a_g \frac{\eta \cdot \theta \cdot \beta_0}{q} \cdot \left(\frac{T_2}{T}\right)^{2/3}$$

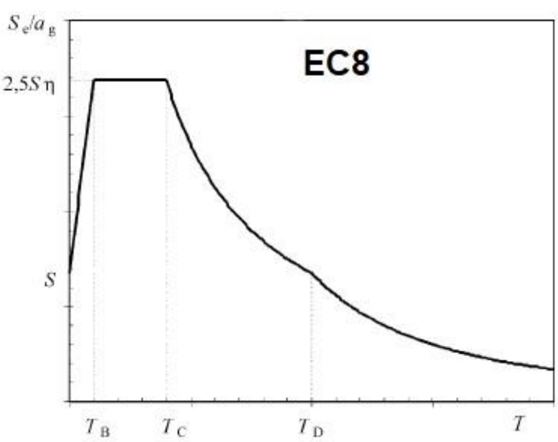

$$0 \le T \le T_B: \ S_d(T) = a_g \cdot S \cdot \left[\frac{2}{3} + \frac{T}{T_B} \cdot \left(\frac{2{,}5}{q} - \frac{2}{3}\right)\right]$$

$$T_B \le T \le T_C: \ S_d(T) = a_g \cdot S \cdot \frac{2{,}5}{q}$$

$$T_C \le T \le T_D: \ S_d(T) \begin{cases} = a_g \cdot S \cdot \frac{2{,}5}{q} \cdot \left[\frac{T_C}{T}\right] \\ \ge \beta \cdot a_g \end{cases}$$

$$T_D \le T: \quad S_d(T) \begin{cases} = a_g \cdot S \cdot \frac{2{,}5}{q} \cdot \left[\frac{T_C T_D}{T^2}\right] \\ \ge \beta \cdot a_g \end{cases}$$

Figure A3: Design spectra from Greek seismic codes integrated into YouSimulator.

Table A2: Overstrength factors, Ω1, adopted for the central Thessaloniki building stock.

Regulation	Height	Frame Type	Code	Ω1
Pre-code	Low-rise	Infilled	RC3.1LN	2.703
		Pilotis	RC3.2LN	1.258
	Mid-rise	Infilled	RC3.1MN	1.729
		Pilotis	RC3.2MN	1.281
	High-rise	Infilled	RC3.1HN	1.289
		Pilotis	RC3.2HN	1.221
Low-code	Low-rise	Infilled	RC3.1LL	2.703
		Pilotis	RC3.2LL	1.258
	Mid-rise	Infilled	RC3.1ML	1.733
		Pilotis	RC3.2ML	1.283
	High-rise	Infilled	RC3.1HL	1.289
		Pilotis	RC3.2HL	1.221
Moderate-code	Low-rise	Infilled	RC3.1LM	3.063
		Pilotis	RC3.2LM	2.300
	Mid-rise	Infilled	RC3.1MM	1.713
		Pilotis	RC3.2MM	1.266
		Infilled	RC4.2MM	2.121
	High-rise	Pilotis	RC3.1HM	1.663
		Infilled	RC3.2HM	1.602
		Pilotis	RC4.2MH	1.985
High-code	Low-rise	Infilled	RC3.1LH	2.632
		Pilotis	RC3.2LH	1.974
	Mid-rise	Infilled	RC3.1MH	2.351
		Pilotis	RC3.2MH	2.071
		Infilled	RC4.2MH	2.100
	High-rise	Pilotis	RC3.1HH	1.486
		Infilled	RC3.2HH	1.475
		Pilotis	RC4.2MH	1.985

Table A3: Extract from HAZUS Table 5-15 (FEMA, 2022), giving landmark IDR thresholds for pre-code buildings.

Building Properties			Inter-storey drift at damage-state threshold			
Type	Height (inches)					
	Roof	Modal	Slight	Moderate	Extensive	Complete
W1	168	126	0.0032	0.0079	0.0245	0.0600
W2	288	216	0.0032	0.0079	0.0245	0.0600
S1L	288	216	0.0048	0.0076	0.0162	0.0400
S1M	720	540	0.0032	0.0051	0.0108	0.0267
S1H	1872	1123	0.0024	0.0038	0.0081	0.0200
S2L	288	216	0.0040	0.0064	0.0160	0.0400
S2M	720	540	0.0027	0.0043	0.0107	0.0267
S2H	1872	1123	0.0020	0.0032	0.0080	0.0200
S3	180	135	0.0032	0.0051	0.0128	0.0350
S4L	288	126	0.0032	0.0051	0.0128	0.0350
S4M	720	540	0.0021	0.0034	0.0086	0.0233
S4H	1872	1123	0.0016	0.0026	0.0064	0.0175
S5L	288	216	0.0024	0.0048	0.0120	0.0280
S5M	720	540	0.0016	0.0032	0.0080	0.0187
S5H	1872	1123	0.0012	0.0024	0.0060	0.0140
C1L	240	180	0.0040	0.0064	0.0160	0.0400
C1M	600	450	0.0027	0.0043	0.0107	0.0267
C1H	1440	864	0.0020	0.0032	0.0080	0.0200
C2L	240	180	0.0032	0.0061	0.0158	0.0400
C2M	600	450	0.0021	0.0041	0.0105	0.0267
C2H	1440	864	0.0016	0.0031	0.0079	0.0200
C3L	240	180	0.0024	0.0048	0.0120	0.0280
C3M	600	450	0.0016	0.0032	0.0080	0.0187
C3H	1440	864	0.0012	0.0024	0.0060	0.0140
PC1	180	135	0.0032	0.0051	0.0128	0.0350

Table A4: EMS-98 building-damage descriptions and classifications based on Panou et al. (2014).

Information from files of repair	
20.	**Infill masonry**
20.1	Infill wall detachment from surrounding frame
20.2	Infill cracking
20.3	Infill wall collapse
21.	**Beams**
21.1	Bending in the opening
21.2	Bending at the upper support
21.3	Bending at the lower support
21.4	Shear cracks
22.	**Columns**
22.1	Concrete crushing at the top or bottom cross section
22.2	Concrete cracking due to bending moments
22.3	Shear cracks (short columns)
23.	**R/C walls**
23.1	Slip cracks
23.2	Shear cracks
23.3	Yielding of reinforcement due to bending moments
23.4	Concrete crushing due to compressive forces
23.5	Failure of coupling beams

EMS-98 Damage Grade	**Type of damage**
0	No damage
1	20.1
2	20.2, 21 22.2, 23.1
3	20.3, 22.1, 23.3, 23.4, 23.5
4	22.3, 23.2
5	Destruction